RICE UNIVERSITY

Surface-immobilized adeno-associated virus nanoparticles for applications in controlled gene delivery and biosensing

by

Kellie Irene McConnell

A THESIS SUBMITTED
IN PARTIAL FULFILLMENT OF THE
REQUIREMENTS FOR THE DEGREE

Doctor of Philosophy

APPROVED, THESIS COMMITTEE:

Junghae Suh, Ph.D.
Assistant Professor Bioengineering

Jennifer West, Ph.D.
Professor, Chair Bioengineering

Jonathan Silberg, Ph.D.
Assistant Professor Biochemistry and Cell Biology

HOUSTON, TEXAS
April 2011

ABSTRACT

Surface-immobilized adeno-associated virus nanoparticles for applications in controlled gene delivery and biosensing

by

Kellie Irene McConnell

Adeno-associated virus (AAV) is a 25 nm replication deficient DNA virus most commonly studied for human gene therapy applications. The work detailed in this thesis investigates the controlled delivery of AAV from surfaces for both transduction and biosensing applications. First, AAV was tested for compatibility with substrate-mediated gene delivery approaches. Two reverse transduction applications were investigated: 1) spatial localization of cells and virus vectors for tissue engineering applications and 2) live cell genetic microarrays. To drive the proper differentiation and assembly of cells within tissue engineering constructs, gene expression patterns may need to be tightly regulated. To localize adhesive proteins and AAV, polydimethylsiloxane stamps and protein adhesive alkanethiols were used. By adsorbing AAV onto adhesive proteins, including human fibronectin, laminin, collagen I, elastin and poly-l-lysine, both cell adhesion and gene delivery were localized to a defined pattern. Gene delivery was efficient on all protein surfaces, with higher expression observed on laminin surfaces. AAV was also patterned using a robotic spotter to create live cell genetic microarrays, creating localized cell islands expressing GFP. This potentially high-throughput technique could be extended to study complex genetic interactions within cells, such as stem cells or induced pluripotent stem cells. Additionally, AAV was explored as a biosensor by modifying virus output functionalities. Wild-type AAV2 externalizes an N-terminus region containing a phospholipase A2 (PLA2) domain during intracellular processing, allowing the virus to escape the endosomal pathway and deliver genetic cargo. This externalization can be replicated outside of cells through heat treatment. AAV2-ΔPLA2-His was created by replacing the PLA2 domain with a nickel binding hexahistidine tag. This replacement allows heat-treated mutant virus to bind a nickel affinity column. Finally, directed evolution was used to 1) improve the ability of AAV to deliver genes into target cells or 2) alter AAV biosensor inputs. Virus libraries were

created using error-prone polymerase chain reaction (EP-PCR) to introduce random amino acid modifications into the protein capsid. The error rate for these libraries was estimated to be between 5-7 errors per *cap* gene. Combining surface immobilization with directed evolution could allow for precise control of AAV for gene delivery and biosensing.

ACKNOWLEDGEMENTS

I would like to thank my thesis advisor, Dr. Junghae Suh, for her assistance and guidance during this process. I am so grateful for this opportunity.

I would also like to thank my committee members, Dr. Jennifer West and Dr. Joff Silberg, for their involvement in this process.

Thank you to the National Science Foundation Graduate Research Fellowship Program for financial support.

Thanks to my friends in the Suh Lab for the Thai Spice and bubble tea. Your friendship and support throughout this process has meant so much to me.

This thesis is dedicated to my wonderful family – Matt, Mama, Daddy, my JT, Nana and Papa, and Grandma and Grandpa. I love you so much.

TABLE OF CONTENTS

LIST OF FIGURES

LIST OF TABLES

CHAPTER ONE

Introduction

1.1 Adeno-associated virus

Adeno-associated virus (AAV) is a replication-deficient dependovirus that requires a co-infection with adenovirus (Ad) or herpes virus for replication. AAV was first isolated as a contaminant in adenovirus stocks in the 1960s and the first AAV serotype 2 infectious clone was isolated in 1982.[1,2] AAV has no known pathogenicity and it is estimated that 90% of the human population is seropositive for AAV2.[3] AAV is a small viral nanoparticle with a diameter of approximately 25 nm. The crystal structure of the virus was determined by Xie et al in 2002 (Figure 1.1A).[4] AAV has a single-stranded DNA genome of ~4.7 kb that consists of two open reading frames flanked by inverted terminal repeats (ITRs) (Figure 1.1B). The two open reading frames of the genome encode for AAV's two genes – *rep* and *cap*. The *rep* gene codes for four non-structural proteins (Rep78, Rep68, Rep52, and Rep40) that aid in the replication of the virus. The *cap* gene codes for three structural proteins and one non-structural protein involved in virus assembly[5] through alternative splicing and alternative start codon usage. VP1, VP2, and VP3 are contained in the capsid at a 1:1:10 ratio, respectively. The virus capsid is composed of 60 subunits and forms through self-assembly.

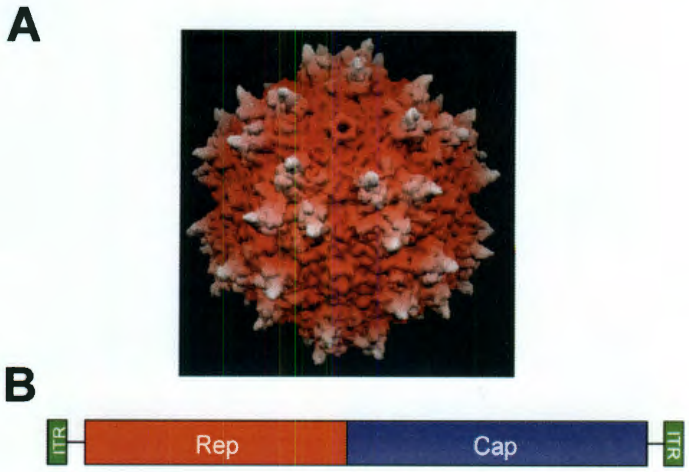

Figure 1.1. Adeno-associated virus. **(A)** Crystal Structure of AAV2 (Adapted from Xie et al).[4] **(B)** Schematic of AAV2 genome, composed of *rep* and *cap* genes flanked by ITRs.

To date, 12 serotypes of AAV have been isolated.[6] Within these serotypes, some capsid regions are conserved and others are notably different. It is known that serotypes have different tropisms and readily transduce different tissues within the body. For example, AAV2 is known to transduce kidney cells readily and AAV4 is known to transduce the central nervous system.[7] These differences in tropisms are mainly due to serotypes binding to different cell surface receptors. AAV2, the most commonly studied serotype, primarily binds heparan sulfate proteoglycans (HSPGs).[8] In contrast, AAV1 and AAV6 both bind sialic acid.[9] In addition to binding tropism, it has also been shown that different serotypes have varying uncoating rates.[10]

1.2 Overview of thesis

While AAV has most commonly been investigated for human gene therapy, this thesis explores the use of AAV for surface-immobilization applications. AAV is a versatile vector capable of delivering genetic cargo to a variety of cell types, both dividing and non-dividing. However, for virus performance to be optimal, we must be able to control the transduction profiles of the virus. By combining surface-immobilization with regulation of virus binding and conformational changes, we may be able to harness AAV delivery for tight control of virus activity. Surface-immobilization allows for spatial control of vectors for both gene expression and biosensing. Further optimization of virus performance could be achieved through combinatorial directed evolution approaches.

An overview of this thesis is outlined in Figure 1.2. We have patterned AAV through 1) microcontact printing using polydimethylsiloxane (PDMS) stamps and alkanethiol solutions and 2) a robotic microarray spotter. Microarray deposition was explored to pattern virus nanoparticles for both live cell genetic microarrays and biosensing. To use AAV as a potential biosensor, we have modified the virus output to allow for the externalization of a nickel ion binding hexahistidine tag. Modification of the virus for both optimal gene delivery and novel biosensing properties was explored through the creation of directed evolution libraries.

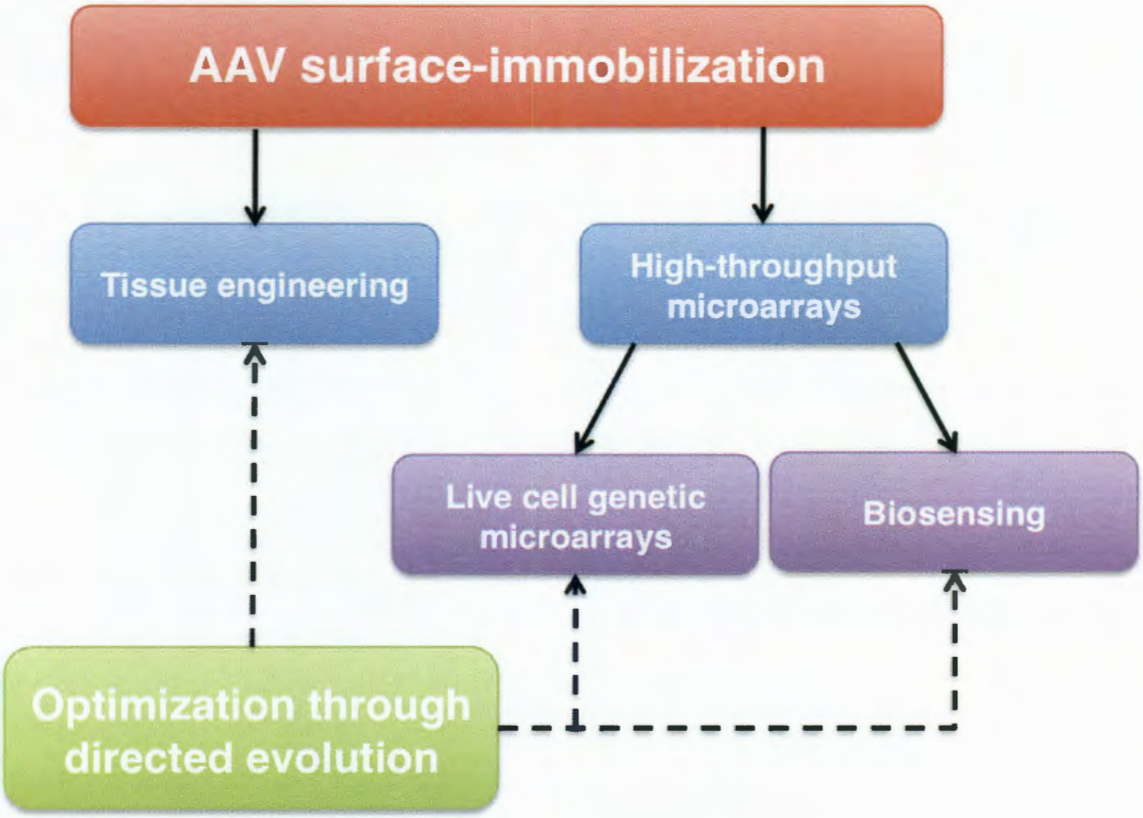

Figure 1.2. Schematic overview of thesis. Immobilization of AAV onto surfaces was investigated for tissue engineering and microarray applications. Directed evolution studies were initiated to tailor AAV for novel gene delivery and biosensing applications.

1.3 Patterned gene delivery for tissue engineering

The creation of more native-like tissues *in vitro* may hinge on the ability to create highly localized gene delivery profiles.[11] The use of AAV for gene delivery in tissue engineering/regenerative medicine applications is a highly attractive choice due to its higher safety profile and ease of manipulation compared to other viral gene delivery systems, and the numerous methods to achieve target cell specificity and efficiency. To begin to address this tissue engineering hurdle, we have used polydimethylsiloxane (PDMS) stamps to create localized regions of protein-adhesive alkanethiols on gold

substrates. Alkanethiols have been extensively used to localize protein and cells.[12-14] These long carbon chains have a sulfur group at one end that can bind to a gold substrate, forming a self-assembled monolayer (SAM) with an exposed functional group. These patterns are backfilled with oligo(ethylene glycol) (-OEG) terminated alkanethiols, creating a protein resistant background. Initial studies, detailed in Chapter 2, explored the use of $-CH_3$, -COOH, $-NH_2$, -OH surface chemistries to localize both human fibronectin (HFN) and AAV2-GFP (delivering the gene for GFP). Alkanethiols were patterned using PDMS stamps displaying 500 micron circular features.

We have demonstrated that this technique can be successfully applied to the localization of HeLa cells. Cells were successfully localized onto three SAM surfaces with minimal adhesion of cells to the passivated background. Additionally, GFP expression was observed on all surface chemistries. Most interestingly, we observed that the presence of a protein mediating layer for AAV adsorption allowed for increased gene expression, in comparison to direct adsorption of virus onto SAMs.

Given the positive results observed with HFN, in Chapter 3 we explored a variety of additional adhesive proteins, including laminin, elastin, poly-l-lysine (PLL) and collagen I. While all four additional proteins are compatible with our patterned reverse transduction platform, we observed that the most efficient gene delivery was observed on laminin surfaces. As it was determined that transcriptional activity was not the reason for the increase in gene expression, additional methods are being used to study the interaction between adhesive proteins and AAV.

1.4 Live cell genetic microarrays

High-throughput manipulation of gene expression may hold the power to elucidating the complex interactions responsible for the differentiation of stem cells and the development of induced pluripotent stem cells. Increased interest in tissue engineering and stem cell lineage development has introduced the need for a high-throughput method for studying the effects of multiple combinations of cells, growth factors, and extracellular matrix components found in stem cell niches.[15,16] Surrounding niche cells have been identified as having particular importance in supporting proper differentiation.[16] However, the exact nature of this interaction is not known. In the past, many classical developmental biology studies have relied on available model organisms such as *Drosophila* and *Caenorhabditis elegans*. Understanding the functionality of stem cells will rely on combining knowledge of different interactions within a niche.[15] In addition to using these important *in vivo* models, valuable information can be obtained by performing high-throughput gene expression screens on mammalian cells. The ability to perform a high number of screens with as few cells as possible is valuable because primary cells required for studies can be difficult to accumulate in large quantities.[17] Moreover, high-throughput screens allow for the delivery of many distinct gene combinations to populations of cells, making this type of experiment a valuable technique for studying downstream cellular effects. In response to the need for patterned gene delivery, both viral[18, 19] and nonviral[20-22] gene delivery methods have been employed to develop an efficient screening technology. In this thesis we have investigated the use of AAV for this technology. AAV offers a number of advantages compared to other virus systems, as AAV is considered to be safer and capable of relatively facile modification to increase gene delivery efficiency and specificity.

In Chapter 4, we explored the use of AAV2 as a gene delivery vector for live cell genetic microarrays. A number of substrates and conditions were tested, and we have determined that nitrocellulose coatings are capable of localizing high levels of non-denatured recombinant AAV when deposited using a robotic spotter. By backfilling these substrates with a blocking agent, we have been able to create localized islands of GFP expressing cells.

1.5 AAV as a potential biosensor

During its natural life cycle, AAV is capable of responding to stimuli located on and within the cell. First, AAV bind ligands on the outside of the cell to initiate cellular infection. For example, AAV2 binds heparan sulfate proteoglycans and AAV1 and AAV6 bind to sialic acid. Post cell binding, the virus is trafficked through the endosomal pathway. Within endosomes, it is proposed that a combination of pH and additional unidentified factors elicits the externalization of a previously internalized N-terminus domain.[23, 24] This region contains a phospholipase A2 (PLA2) domain, facilitating the release of the virus into the cytoplasm[24] and eventual transport of DNA to the nucleus.

In Chapter 5 we have altered this virus "output" by replacing the PLA2 domain with a nickel binding hexahistidine tag, creating a mutant virus (AAV2-ΔP.His). In addition to intracellular factors, the virus N-terminus externalization can be induced outside of the cell by heating the virus to 60-65°C. By heating AAV2-ΔP.His to 63°C, we have shown that we can isolate activated virus particles using a nickel affinity column. Ultimately, we would like to modify the virus input to detect different stimuli. Virus nanoparticles would be modified such that their input would be a desired stimulus (likely a protein or

small molecule of interest) and their output would be a domain that we could efficiently detect (fluorescent particle, enzymatic domain, detectable tag).

1.6 Directed evolution of AAV

A significant amount of work has been done to retarget AAV to increase specificity and transduction efficiency for a desired cell type. The first studies toward retargeting were conducted using rational approaches, attaching antibodies to the capsid to alter virus tropism.[25] Later, rationally determined peptides were added within regions of the capsid that were determined to tolerate small insertions. Generally, these small peptides were inserted to retarget the virus to a known receptor of interest. One such early approach was the insertion of an RGD (arginine-glycine-aspartic acid) motif, known to bind cellular integrins.[26]

In contrast, directed evolution allows us to create large, combinatorial libraries and select for variants with advantageous mutations. To alter the binding properties of AAV, several directed evolution methods, including error-prone polymerase chain reaction (EP-PCR),[27, 28] peptide display,[29, 30] transposon mutagenesis,[31] and DNA shuffling[32-34] have been used to optimize AAV gene delivery. Successful mutants have been found to evade serum neutralization, infect coronary artery cells, infect brain cells, and infect glioma cells, among other applications.[29-36] Directed evolution libraries are generated by creating large ($>10^6$) pools of mutants and selecting for a clone with the desired characteristics. An overview of this process for EP-PCR mutagenesis is shown in Figure 1.3.

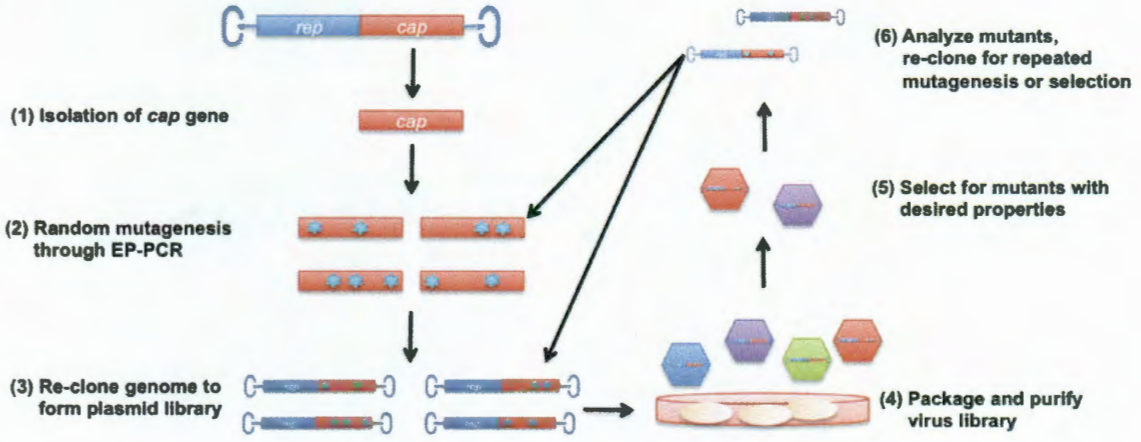

Figure 1.3. Overview of directed evolution process. Large pools of mutant virus are generated using EP-PCR. Selection strategies aim to enrich a pool of mutant virus capable of fulfilling a specified need.

Directed evolution allows us to potentially fine-tune the characteristics of AAV that are critical for optimal performance in our applications detailed in Chapters 2-5. In Chapter 6 we have created two AAV2-based libraries using EP-PCR. One library, based on the wild-type AAV2 genome, contained 5.2 errors per *cap* gene, and has been used to isolate a pool of mutants with increased transduction efficiency for an ovarian cancer cell line. A second library, based on AAV2-ΔP.His, was generated with an error rate of 7.3 errors per *cap* gene. Overall, we show increased efficiency in HeyA8 ovarian cancer cell transduction as well as slight modifications to the temperature responsive properties of our ΔP.His virus. Additional enrichment and mutagenesis should be performed to isolate the "fittest" mutants from these pools. Further studies are needed to fully characterize these mutants and understand the effects that individual mutations have on the change of function observed. By combining spatial localization with modifications through

directed evolution, we can potentially tightly control virus delivery for gene expression and biosensing.

CHAPTER TWO

Microcontact printing for co-patterning cells and viruses for spatially controlled substrate-mediated gene delivery

2.1 Acknowledgements

I would like to thank Dr. John Slater and Dr. Jennifer West for their collaboration on this work. PDMS stamps were created by Jaewon Park in Dr. Arum Han's lab at Texas A&M University. The work presented in this chapter is a modified version of a manuscript accepted for publication in Soft Matter.

2.2 Introduction

A significant hurdle in tissue engineering and regenerative medicine is the difficulty in achieving spatially organized tissue structures.[11] To drive the proper differentiation and assembly of cells, gene expression patterns may need to be tightly regulated. This may entail the expression of certain genes, involved in tissue genesis or repair, to be upregulated or downregulated in a spatially dependent manner. Among the advances in this field has been the incorporation of gene delivery agents, desired to guide the development of more native-like *in vitro* tissues. Pioneering methods of incorporating gene delivery in tissue engineering constructs involved the inclusion of plasmid DNA in polymeric matrices.[21] Since that time multiple groups have worked to create methods to deliver genetic material for tissue engineering applications, based on either the delivery of plasmid DNA or on viral transduction.[19, 22, 37-39]

Viral gene delivery is a promising alternative to the use of plasmid DNA for substrate-mediated gene delivery, also called reverse transfection or reverse transduction when non-viral or viral vectors are used, respectively. Viral particles can be easily modified to deliver a desired genetic cargo of either an overexpression or shRNA cassette. In recent years, several viruses have been used to control the delivery of genes for a variety of substrate-mediated applications, including targeted gene delivery for wound healing, bone remodeling, and prevention of restenosis.[40-42] Lentiviral and adenoviral vectors have been used to create cellular microarrays for upregulation or downregulation of genes of interest.[18, 43, 44] Pirone et al implemented microcontact techniques for patterning adenovirus onto plastic.[19] Retroviruses have also been immobilized using alkanethiol self-assembled monolayers (SAMs), either through direct adsorption or through the use of a protein mediating layer.[37] Previous studies have shown that retrovirus is capable of interacting with extracellular matrix proteins, including fibronectin, to increase gene delivery efficiency in target cell types.[45]

We set out to build upon these previous studies to advance the technology to the next level. First, we envisioned creating a platform where both viral gene delivery vectors and adhesive proteins can be co-patterned to control both cellular attachment and gene expression. This can ultimately enable us to modulate the virus pattern underneath the cell pattern, resulting in the creation of distinct regions of gene expression within the cell pattern. Furthermore, we desired to use a gene delivery vector that can be easily tailored to deliver genes into target cells with high efficiency. AAV is a relatively simple virus to modify, encoding only two viral genes: *rep* and *cap*. Modification of the *cap* gene can substantially improve the specificity and efficiency of AAV-mediated gene delivery.

Numerous advances in AAV targeting have been made recently (reviewed by Schaffer et al[46]), providing us with many potential options to enhance the selectivity of the vectors for specific cells. Eventually, by exploiting different combinations of virus patterns, cell patterns, transgenes, cell types, and AAV capsids (with different capsids targeting different cell types), we may be able to mimic the structure and function of highly complex tissues.

AAV is a small, 25 nm diameter replication deficient parvovirus that is being investigated intensively in 75 gene therapy clinical trials worldwide. AAV is considered to be one of the safest viral vectors for gene delivery, owing to several properties. AAV does not mediate insertional oncogenesis, which has been observed for retrovirus vectors,[47] and immunogenicity against the virus is substantially less than that of adenovirus vectors.[48] AAV is a non-enveloped virus composed of a protein shell encapsidating a 4.7kb single stranded DNA genome. As mentioned above, the simple viral genome contains only two genes: *rep*, coding for non-structural replication proteins, and *cap*, coding for three proteins that self-assemble to form the viral capsid and a fourth protein that aids in this assembly.[5] A number of naturally occurring serotypes with diverse tropism and transduction profiles have been isolated.[7] The most commonly used serotype is AAV2, known to bind negatively charged heparin.[49] The crystal structure of this well-studied virus has been resolved.[4] In addition to the various serotypes, there are a variety of methods to alter the tropism of the virus in order to increase the gene delivery efficiency in a target cell population. These methods range from rationally inserting a targeting moiety into the capsid to using directed evolution to isolate an improved mutant out of a large pool of variants.[26, 27, 29, 34] Lastly, AAV can be altered to deliver various genetic

cargo, including overexpression cassettes as well as shRNA.[50, 51] Collectively, the use of AAV for gene delivery in tissue engineering/regenerative medicine applications is a highly attractive choice due to its higher safety profile and ease of manipulation compared to other viral gene delivery systems, and the numerous methods to achieve target cell specificity and efficiency.

To spatially localize AAV2 vectors and cellular adhesion, we used microcontact printing of alkanethiols to create patterned self-assembled monolayers (SAMs). Microcontact printing techniques use elastomeric stamps with micron scale features to print molecules onto a surface.[52] For this work, we stamped alkanethiols onto gold-coated glass coverslips (Figure 2.1). Alkanethiol molecules are long carbon chains, with a functional group on one end and a gold binding sulfur molecule on the other end. Through Van der Waals forces, the chains self-assemble into a monolayer of 2-3 nm in height at a 30° angle.[52] These SAMs form patterned features and can have either protein adhesive or protein resistive properties. Through this method, we are able to directly control the spatial localization of the virus, as opposed to adding it in a bulk solution and exposing all cells to the same gene delivery agent. In this work, we patterned chemistries that are potentially adhesive to both AAV2 and cellular attachment proteins.

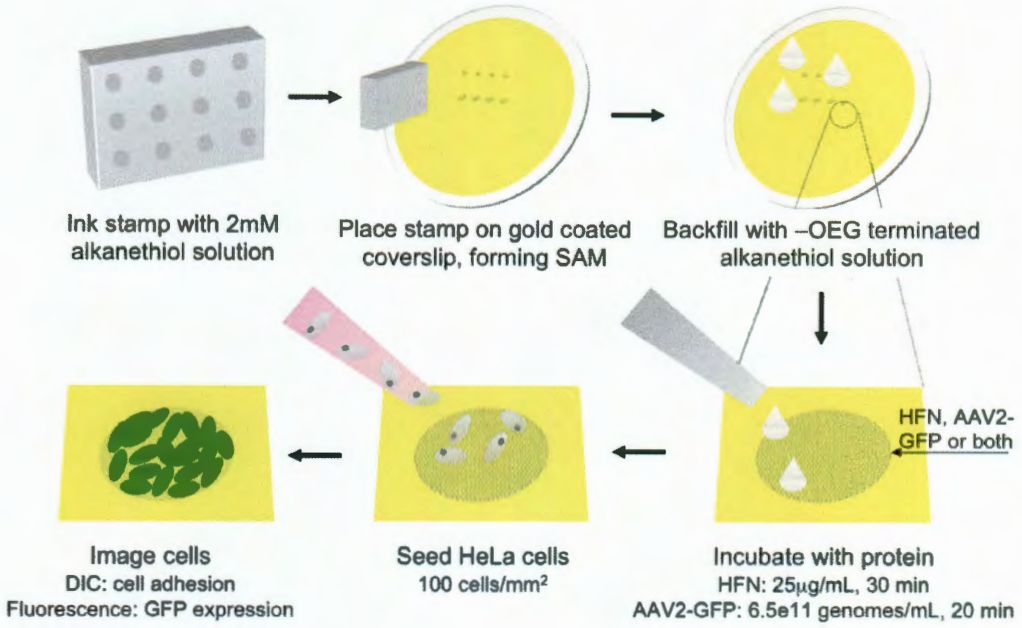

Figure 2.1. Overview of microcontact printing process. PDMS stamps were inked with one of four protein adhesive alkanethiol solutions and placed onto a gold coated coverslip. Samples were backfilled with -OEG and incubated with HFN and AAV2. Samples were seeded with HeLa cells and imaged 72 h later.

We have developed a patterning platform to combine both the patterning of cells as well as AAV2 for gene delivery. Microcontact printing and a variety of alkanethiol surface chemistries have been used to identify a SAM that allows for both the attachment of cell adhesive proteins (human fibronectin, HFN) and reversible immobilization of AAV2. Relative attachment of both fibronectin and AAV2 was visualized and quantified using immunostaining. To test cell adhesion and the efficiency of viral transduction in this system, we used a green fluorescent protein (GFP) reporter gene and HeLa cervical cancer cells, which are known to be highly permissive to AAV2 transduction.[53] At various

times post cell seeding, patterns were analyzed for both cellular attachment as well as efficiency of gene delivery.

2.3 Materials and Methods

Virus preparation. AAV2 was prepared as described previously.[54] Briefly, 293T cells and a triple transfection method were used to produce recombinant AAV2-GFP (AAV2 capsid with a green fluorescent protein (GFP) cassette under the cytomegalovirus (CMV) promoter). Cells were lysed 72 h post-transfection and virus was purified using ultracentrifugation and an iodixanol step gradient. Virus used for these studies remained in a solution of 40% iodixanol. Viral genomic titers were determined using quantitative polymerase chain reaction (QPCR) with primers against the CMV promoter. Virus used in this study was determined to have a concentration of 6.5e11 vector genomes/ml.

PDMS stamp and coverslip preparation. Polydimethylsiloxane (PDMS) stamps were prepared by cast molding PDMS from a mold master that was fabricated by a photolithography process. First, a photoresist (SU-8™, Microchem, Inc., Newton, MA) layer was spin-coated on a 3-inch silicon wafer (SQI, Inc., Santa Clara, CA) and selectively exposed to UV light to transfer stamp patterns on the photomask to the SU-8™ layer. It was then immersed in photoresist developer (Thinner P, Microchem, Inc., Newton, MA) and rinsed with isopropyl alcohol (IPA). To facilitate the release of PDMS stamps from the master after the cast molding process, the mold master was vapor-coated with (tridecafluoro-1,1,2,2-tetrahydrooctyl) trichlorosilane (United Chemical Technologies, Inc., Bristol, PA) for 10 min and briefly rinsed with IPA. The stamps were

replicated by pouring PDMS pre-polymer (10:1 mixture, Sylgard® 184, Dow Corning, Inc., Midland, MI) on the mold master, followed by degassing inside a vacuum connected desiccator for 15-20 min to remove air bubbles and to completely fill the micropatterns with the PDMS. The degassed PDMS device was placed inside a leveled 85°C oven for 1 h for polymerization. The fully polymerized PDMS device was then peeled off from the mold master and used as a microcontact printing stamp.

PDMS stamps presenting 500 micron diameter circles with a 1.2 mm pitch were cleaned by sonication in 100% ethanol. 35 mm diameter gold-coated glass coverslips (100 Å gold over 20 Å titanium, Platypus, Madison WI) were cleaned in dilute TL1 solution (6:1:1 H_2O:NH_4OH:H_2O_2) for 1 min at 80°C, rinsed twice in Millipore purified water (MPH_2O), and dried with ultrapure nitrogen (N_2).

Surface functionalization. Alkanethiol solutions were diluted to 2 mM in 100% ethanol. Stamps were inked with either a $-CH_3$ (1-hexadecanethiol), -COOH (16-mercaptohexadecanoic acid), $-NH_2$ (11-amino-1-undecanethiol hydrochloride), or -OH (11-mercapto-1-undecanol) terminated alkanethiol, all from Sigma Aldrich (St. Louis, MO). Stamps were dried with N_2, placed on a gold coverslip for 20 sec, and gently removed. After printing, coverslips were incubated with 2 mM oligo(ethylene glycol) (-OEG) terminated alkanethiol (HSC_{11}-EG_6, Prochimia, Poland) for 1 h. Samples were rinsed twice with 100% ethanol and dried with N_2.

Protein attachment. Functionalized coverslips were incubated with 1 ml human fibronectin (HFN, Sigma Aldrich) warmed to 37°C at a concentration of 25 mg/ml in phosphate buffered saline (pH 7.0, PBS) for 20 min at room temperature and rinsed dropwise with PBS. To adsorb virus, functionalized coverslips were incubated with 0.75 ml AAV2-GFP at a concentration of 6.5e11 vector genomes/ml in 40% iodixanol for 30 min at room temperature and rinsed dropwise with PBS.

Immunostaining. HFN and/or AAV2 functionalized samples were blocked with 1% BSA in PBS for 1 h followed by gentle dropwise rinsing with PBS. HFN patterns were incubated with sheep anti-FN primary antibody (Abcam, Cambridge, MA) at 0.01 mg/ml overnight at 4°C, rinsed with PBS, and exposed to donkey anti-sheep AlexaFluor 633 (AF633) conjugated antibody (Invitrogen, Carlsbad CA) at 0.02 mg/ml for 1 h at room temperature. Samples were rinsed dropwise with PBS, sterile water, and allowed to air dry. AAV2 patterns were incubated with A20 antibody (mouse anti-AAV2 capsid, American Research Products, Belmont MA) at a concentration of 0.25 mg/ml overnight at 4°C, rinsed with PBS, and exposed to goat-anti-mouse AlexaFluor 532 (AF532) conjugated antibody (Invitrogen) at a concentration of 10 mg/ml for 1 h at room temperature. Samples were rinsed dropwise with PBS and sterile water and allowed to air dry.

Cell studies. HeLa cells were seeded on functionalized surfaces in 60 mm tissue culture dishes at a density of 100 cells/mm^2. Cells were cultured in Dulbecco's Modified Eagle Medium (Invitrogen), supplemented with 10% fetal bovine serum and 1% penicillin/streptomycin (Invitrogen). Cells were maintained at 37 °C with 5% CO_2.

Imaging and image analysis. Images were acquired using a Zeiss 5 LIVE confocal microscope (Carl Zeiss, Munich, Germany). Images within a given sample set (i.e. AAV2 adsorption, HFN adsorption, cell fluorescence) were acquired under identical conditions. GFP images were obtained using a 489 nm excitation at 1.8% power and data was collected for 2 ms pixel dwell time with a bandpass filter between 500-525 nm. Virus immunostaining images were collected using a 532 nm excitation at 50% power and data was collected for 2 ms pixel dwell time using a bandpass filter between 550-600 nm. HFN immunostaining images were collected using a 635 nm laser at 20% power and data was collected for 2 ms using a longpass 650 nm filter. Confocal control experiments were done to ensure no crosstalk between channels. To quantitatively compare the ability of each SAM to adsorb HFN and AAV2, the integrated densities of 15 spots (5 spots from 3 different stamps) were measured with ImageJ (NIH, Bethesda MD). For transduction studies, 5 fluorescence and differential interference contrast (DIC) images were taken at each time point. Integrated densities of fluorescence images were taken and values were normalized to that of $-CH_3$ samples at the 24 h time point. Data is given as mean and standard error of the mean. JMP 9 software was used to determine statistical significance ($p<0.05$) using ANOVA and Tukey's HSD for post-hoc pair comparisons.

2.4 Results

$-CH_3$ and $-NH_2$ surfaces most efficiently immobilize HFN. The ability to spatially control cell attachment to surfaces is an integral component in the creation of patterned cell constructs. We implemented microcontact printing to create 500 μm diameter circular patterns of one alkanethiol SAM, either a $-CH_3$, -COOH, $-NH_2$, or -OH terminated

alkanethiol, surrounded by a biologically inert oligo(ethylene glycol) (-OEG) terminated SAM. Due to the passive nature of the -OEG SAM, HFN preferentially adsorbs to the circular patterns leaving the surrounding background free of protein. Using these alkanethiol molecules, we are able to create hydrophobic ($-CH_3$), hydrophilic (-OH), negatively charged (-COOH), and positively charged ($-NH_2$) surfaces. To study the efficacy of each surface chemistry ($-CH_3$, -COOH, $-NH_2$, and -OH) to mediate HFN binding and hence cell attachment, we used immunostaining and fluorescence microscopy to compare the amount of HFN that adsorbs to each SAM. The patterned surfaces were exposed to HFN, fluorescently immunolabeled, imaged under identical conditions, and the fluorescence integrated density of the patterned regions was measured. The hydrophobic $-CH_3$ SAM adsorbs the highest amount of HFN, displays uniform surface coverage (Figure 2.2A, E) and was, therefore, used to normalize the integrated density values of the remaining surfaces. The $-NH_2$ patterned SAM shows a similar level of high and uniform attachment (Figure 2.2C). The -COOH SAM results in immobilization of less HFN, 47% as compared to the $-CH_3$ SAM, and the patterns contain noticeable defects resulting in non-uniform HFN coverage (Figure 2.2B & E). In these -COOH images, it is interesting to note that the defects appear as though the protein layer is peeling away. We believe that this happens because of the ten washing steps involved with immunostaining and they are seen in additional immunostaining images (Figure 2.3B and 2.4B). In the later studies where cells are seeded on the surfaces, we do not perform these washing steps. The -OH pattern shows minimal HFN attachment and adsorbs only 23% of the HFN compared to the $-CH_3$ SAM (Figure 2.2D, E). Previous studies that used non-patterned alkanethiol SAMs with varying functional groups showed similar results in protein adsorption and observed both surface wettability- and charge-dependent protein adsorption behavior.[55] The finding that HFN adsorbs to all of the

SAMs tested indicates the potential of each SAM to support cell attachment. However, SAM-dependent differences in the amount of HFN adsorbed and in the uniformity of coverage could lead to differences in initial cell attachment, cellular proliferation, AAV2 adsorption, AAV2 transduction, and ultimately gene expression.

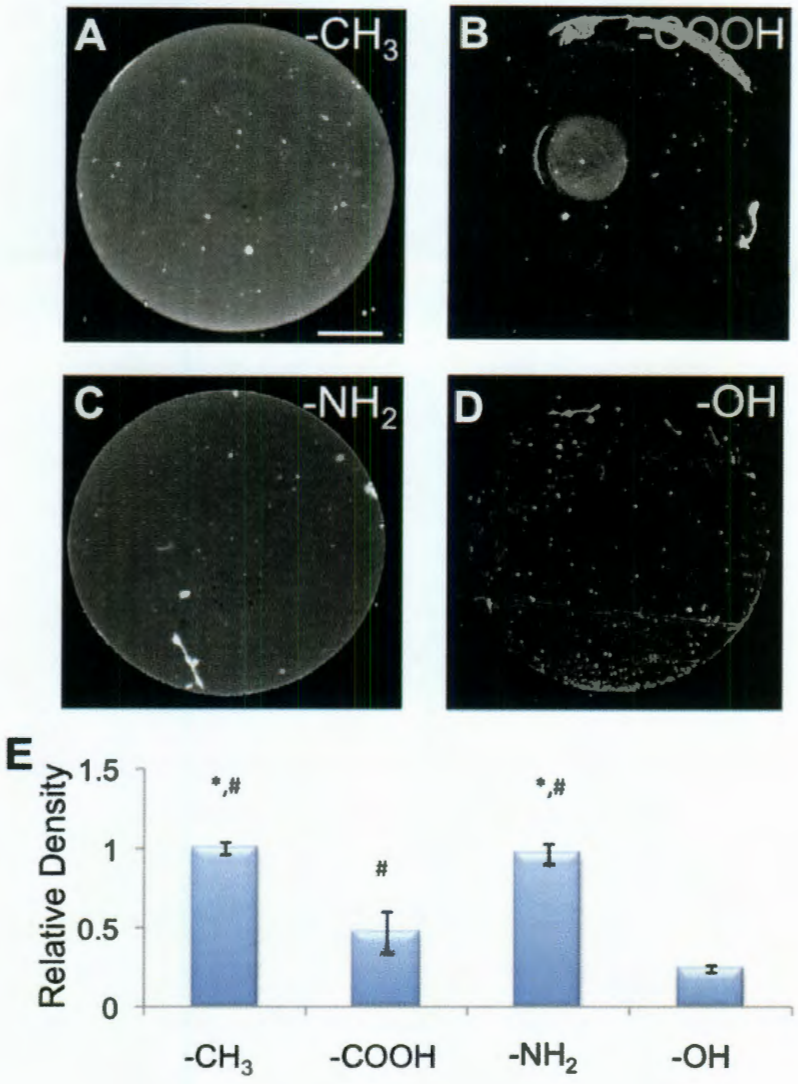

Figure 2.2. Adsorption of HFN to micropatterned SAMs with varying functional groups. $-CH_3$ (**A**), -COOH (**B**), $-NH_2$ (**C**), and -OH (**D**) terminated alkanethiol SAMs were microcontact printed in 500 μm diameter circles, backfilled with an -OEG terminated SAM, exposed to HFN, fluorescently immunostained, imaged, and the integrated density of the patterns measured (**E**). The $-CH_3$ and $-NH_2$ terminated alkanethiol patterns (**A&C**) show a similar amount of adsorbed HFN. The -COOH (**B**) and -OH (**D**) surfaces show significantly less adsorption. Scale bar is 100 µm. (**E**) Relative amounts of HFN adsorbed to the various SAMs were determined by comparing the integrated densities (as quantified with ImageJ) of the circular patterns. Values were normalized to that of the $-CH_3$ spots. Error bars indicate standard error of the mean. Statistical significance ($p<0.05$) is indicated with * for comparison against -COOH and # against -OH.

-CH_3 surfaces most efficiently immobilize AAV2. Similar to how spatial control of HFN adsorption is important for effective cell patterning, spatial control of AAV2 vector adsorption is crucial in spatial regulation of gene expression. To determine the efficacy of the four previously tested surfaces on AAV2 attachment, we repeated the adsorption analysis procedure used to quantify HFN adsorption. Micropatterned surfaces of the various functional group SAMs were exposed to AAV2, fluorescently immunolabeled, imaged under identical conditions, and the integrated densities measured. The various alkanethiol terminal groups yield different AAV2 immobilization patterns as well as variable amounts of virus attachment (Figure 2.3). As with HFN attachment, the -CH_3 surface results in the highest adsorption of AAV2 with the most uniform coverage (Figure 2.3A, E). The patterned -COOH, -NH_2, and -OH SAMs result in heterogeneous, non-uniform, punctate AAV2 coverage (Figure 2.3B-D) with each SAM immobilizing 43%, 46%, and 41% of the amount adsorbed to the -CH_3 SAM, respectively (Figure 2.3E). Overall, it appears that HFN and AAV2 both have similarly high affinities for the hydrophobic -CH_3 patterned SAMs. Interestingly, surface charge seems to have little influence here on AAV2 adsorption as the -COOH and -NH_2 have similar levels of attachment. Furthermore, the antibody used in the immunostaining detects intact virus capsids only. Thus, the immobilized virus appears structurally intact and not denatured.

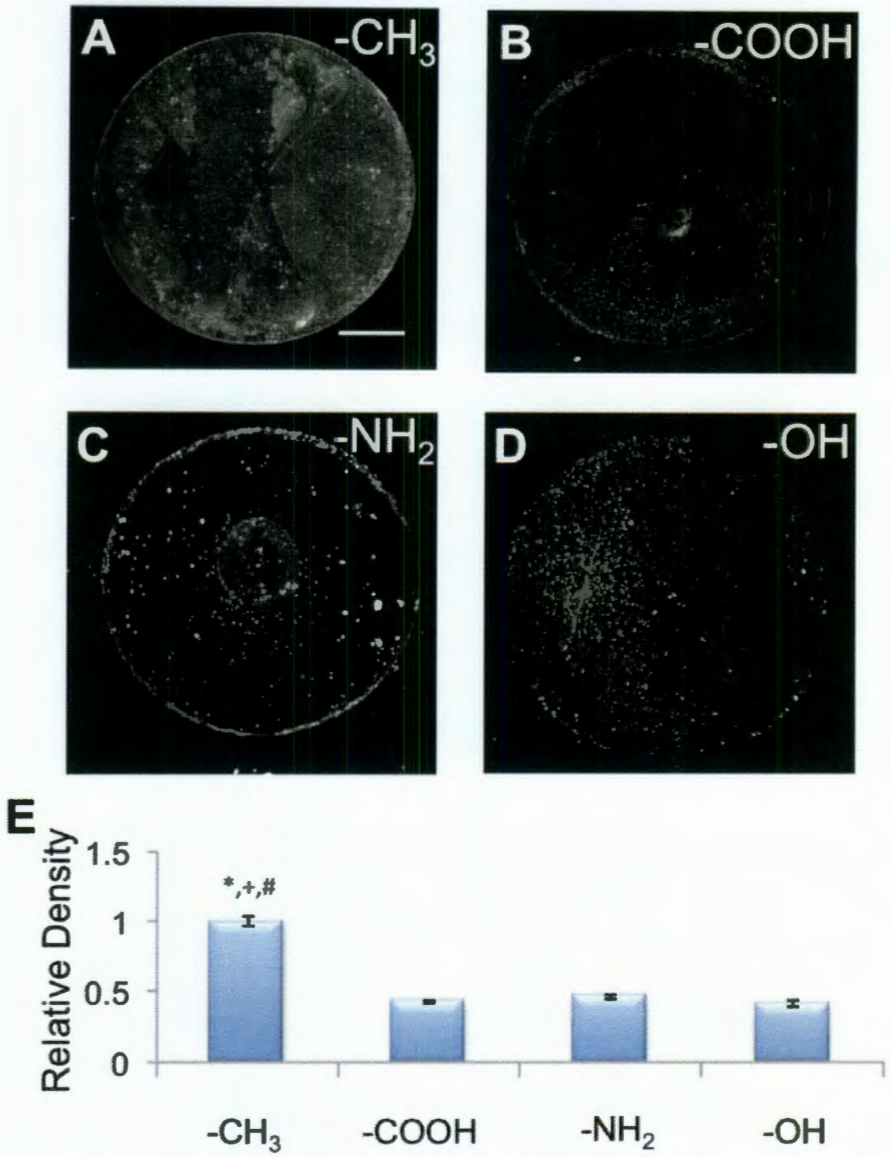

Figure 2.3. Adsorption of AAV2 to micropatterned SAMs with varying functional groups. $-CH_3$ (**A**), -COOH (**B**), $-NH_2$ (**C**), and -OH (**D**) terminated alkanethiol SAMs were microcontact printed in 500 μm diameter circles, backfilled with an -OEG terminated SAM, exposed to AAV2, fluorescently immunolabeled, imaged, and the integrated density of the patterns measured (**E**). The $-CH_3$ terminated alkanethiol patterns (**a**) adsorb more AAV2 than -COOH (**B**), $-NH_2$ (**C**) or -OH (**D**) terminated alkanethiols. Scale bar is 100 µm. (**E**) Relative amounts of AAV2 adsorbed to the various SAMs were determined by comparing the integrated densities (as quantified with ImageJ) of the circular patterns. Values were normalized to that of the $-CH_3$ spots. Error bars indicate standard error of the mean. Statistical significance ($p<0.05$) is indicated with * for comparison against -COOH, + against $-NH_2$, and # against -OH.

-CH_3 and -NH_2 surfaces most efficiently immobilize AAV2 and HFN. Patterned gene expression requires the attachment of both cell adhesive protein (HFN) and gene delivery vectors (AAV2) to the same micropatterned region. To achieve this, we patterned HFN and viral vectors together on one surface. For our studies, micropatterned SAM surfaces were exposed to HFN followed by incubation with AAV2. We rationalized that immobilizing HFN first will prevent this layer from sterically impeding the virus from gaining access to cells. The four different functional group SAMs were investigated and the samples were immunostained, imaged, and analyzed as described above. In this co-patterned case, the -CH_3 and -NH_2 (Figure 2.4A and 2.4C) spots show qualitatively high, homogenous levels of attachment. Again, -COOH and -OH patterns display incomplete pattern coverage (Figure 2.4B and 2.4D). As with Figure 2.2B, we see a similar staining pattern for the -COOH surface that suggests washing away of the protein layer. The image shown in Figure 2.4B is one example from the images taken, all of which showed a similar phenomenon. Quantitative measurements show that the -CH_3 and -NH_2 spots have statistically similar levels of AAV2 adsorption while the -COOH (42%) and -OH (18%) spots show significantly less (Figure 2.4E). Since adsorption of both HFN and AAV is important for the viability of this technique, these qualitative and quantitative results for all surfaces suggest that AAV2 can successfully attach to a layer of HFN. In particular, homogenous coverage of AAV2 on the HFN pre-incubated -CH_3 and -NH_2 SAMs suggests that these surfaces will be particularly effective in supporting viral transduction, as seen previously with retrovirus.[37]

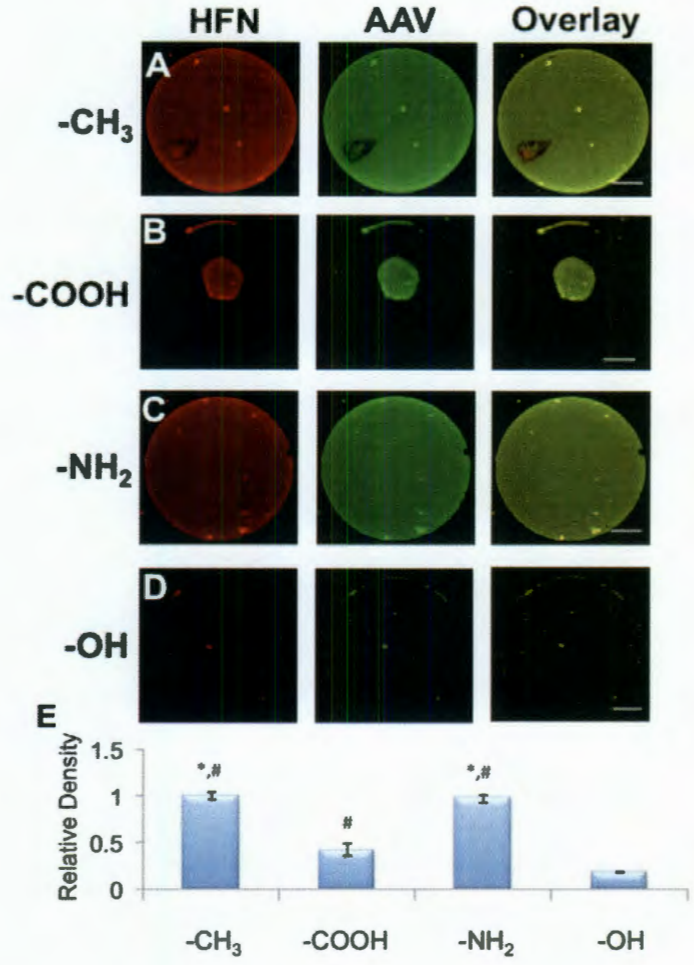

Figure 2.4. Adsorption of AAV2 to pre-adsorbed HFN on micropatterned SAMs with varying functional groups. $-CH_3$ (**A**), -COOH (**B**), $-NH_2$ (**C**), and -OH (**D**) terminated alkanethiol SAMs were microcontact printed in 500 μm diameter circles, backfilled with an -OEG terminated SAM. Samples were pre-incubated with HFN and then exposed to AAV2, fluorescently immunolabeled, imaged, and the integrated density of the patterns measured (**E**). Images are pseudocolored for visualization of overlay. The left column shows HFN staining, the middle column shows AAV2 staining, and the right column is an overlay of the two channels. The $-CH_3$ and $-NH_2$ terminated pre-incubated patterns (**A&C**) adsorb more AAV2 than -COOH (**B**) or -OH (**D**) terminated alkanethiols. Scale bar is 100 µm. (**E**) Relative amounts of AAV2 adsorbed to the various SAMs were determined by comparing the integrated densities (as quantified with ImageJ) of the circular patterns. Values were normalized to that of the $-CH_3$ spots. Error bars indicate standard error of the mean. Statistical significance ($p<0.05$) is indicated with * for comparison against -COOH and # against -OH.

-CH_3, -COOH, and -NH_2 surfaces support cell adhesion and efficient gene delivery. The goal of this platform technology is to precisely pattern cells of interest and deliver desired genes via immobilized viral vectors. To determine the efficacy of both of these goals, we conducted cell studies using HeLa cells as a model. Cells were added to HFN and AAV2 co-patterned substrates to determine cell attachment and transduction. For the construct to be maximally successful, the pattern should be uniformly covered with cells and all cells should be expressing the virus encoded transgene, GFP. Alkanethiol patterns were incubated with HFN, then AAV2-GFP, and finally seeded with HeLa cells at a density of 100 cells/mm^2. Samples were imaged at 24, 48, and 72 h post-seeding and cell coverage and GFP expression were qualitatively observed. Minimal background cell attachment is seen in each case, indicating that the -OEG terminated alkanethiol surfaces provide an effective block to protein and cell attachment (Figure 2.5). Three surfaces, -CH_3, -COOH, and -NH_2 (Figure 2.5A-C), yield homogenous coverage of cells throughout the pattern. The -COOH surface may better retain the protein layer in this experiment, in comparison to immunostaining studies (Figures 2.2& 2.4), since we do not perform the ten washing steps when we seed cells. Cell attachment on the -OH patterned surface yields incomplete spot coverage (Figure 2.5D). The viral vectors immobilized on the surfaces retain their infectivity, as seen by the robust GFP expression in the patterned cells for all four surfaces. This implies that vectors are able to efficiently release from the surfaces and are not denatured by immobilization.

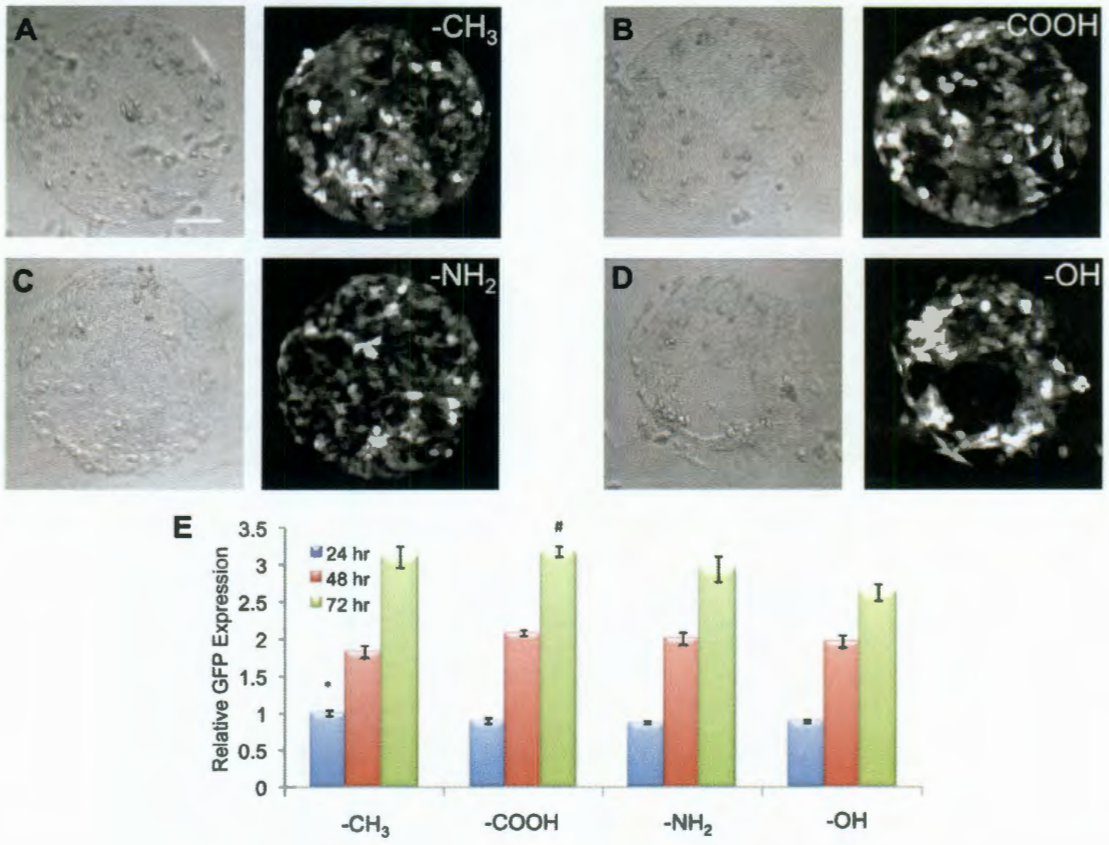

Figure 2.5. Attachment and transduction of HeLa cells. Gold coated coverslips were patterned with -CH_3, -COOH, -NH_2, or -OH terminated alkanethiols in a spot pattern **(A-D).** Patterns were pre-incubated with HFN and then exposed to AAV2. Samples were rinsed and seeded with HeLa cells at a density of 100 cells/mm^2. Cells were imaged under DIC conditions to evaluate cell deposition (left image) and fluorescence to evaluate GFP expression (right image). Images shown are at 72 h time point. Scale bar is 100 μm. Fluorescence intensity was measured at 24, 48, and 72 h post-cell seeding **(E).** Values were normalized to the -CH_3 spot intensity at 24 h. Error bars indicate standard error of the mean. At 24 h, -CH_3 is significantly higher (*) than the other three surfaces ($p<0.05$). At 48 h, all surfaces are similar. At 72 h, statistical significance ($p<0.05$) is indicated with # for comparison against -OH.

At each time point, gene expression was quantified. Fluorescence for each time point was normalized to that of the -CH_3 samples at the 24 h time point. GFP expression increases over time for all four SAMs (Figure 2.5e). At the 24 h time point, GFP

expression is significantly higher for -CH_3 compared to the other 3 surfaces. All samples are similar at the 48 h time point. By the final 72 h time point, the -COOH spots have significantly higher overall GFP expression only when compared to the -OH surface. The -OH surface has a lower cell density compared to the other surfaces (73% average cell coverage). If the -CH_3 normalized integrated density at 72 h is adjusted to match the cell density of the -OH surface, the density will drop to 2.3 – a value lower than the -OH integrated density of 2.6. This result suggests that cells on the -OH pattern have a slightly higher fluorescence per cell.

2.5 Discussion

The ability to localize cells and deliver genes efficiently is a favorable outcome for this study. For three of the chemistries, pattern features are completely covered with cells, with almost no background or extension off the spots. As expected from immunostaining data, both the -CH_3 and -NH_2 surfaces support cell attachment and efficient gene delivery. However, the same cellular result is also true for the -COOH SAMs, a result that seems inconsistent with immunostaining data. From analyzing the images in Figure 2.2B and Figure 2.4B, we believe that the flaws in these patterns are due to the removal of protein during the successive wash steps in immunostaining. For cell studies, fewer washes are conducted, likely resulting in more protein remaining attached to the surface. Additionally, it is possible that even on surfaces adsorbing significantly less AAV (-COOH and -OH), there is still enough virus to transduce the overlying cells. If we assume that there is a complete monolayer of viral vectors on the HFN coated -CH_3 surfaces, this would equate to a multiplicity of infection (MOI) of $4x10^8$ viral vectors per cell, based on the average cell density. Even with the lower amount of viral vectors seen

on other surfaces, this would still lead to an MOI of $8x10^5$ and $4x10^5$ viruses per cell on the -COOH and -OH SAMs, respectively. These MOIs are substantially large and could lead to the high levels of expression observed on these surfaces. More quantitative analytical methods are currently under investigation to validate these hypotheses. Overall, gene expression is robust on all four SAMs, indicating that there are a variety of surface chemistries that can support this technique.

Cell transduction studies show high transduction of the patterned cell population. By transducing a large percentage of cells, we have the ability to efficiently modulate the behavior of the whole cell population. Ultimately, this process can be extended to the creation of more complex tissues using various cells, adhesive proteins, and gene delivery cassettes. Since cellular attachment and viral transduction are compatible with -CH_3, -NH_2, and -COOH surfaces, this may allow for the use of other adhesive proteins besides HFN. Other cell types may require different proteins for proper attachment and guidance, so this platform will be versatile for a number of systems. Additionally, AAV2 vectors are easily modifiable to include overexpression cassettes and shRNA cassettes, leading to the efficient upregulation and downregulation of many combinations of genes that may be of interest for tissue engineering applications. Moreover, AAV is an attractive viral platform because there are currently 12 identified serotypes, each serotype having the ability to deliver genetic cargo to different cell types within the body. The virus can also be modified through the introduction of a targeting ligand into the virus capsid.[26, 56] Finally, there are a number of directed evolution procedures that can be implemented to increase tropism to a desired cell type.[27, 29, 32-34, 57] Overall, our

versatile platform allows for the facile creation of different patterns, as well as the attachment and potential targeting of many cell types.

Interestingly, when AAV is adsorbed to an HFN layer, there are a variety of surface chemistries that are capable of supporting the surface immobilization needed for successful reverse transduction. Previous studies on retrovirus or adenovirus have suggested that virus adsorbed directly on $-CH_3$ terminated alkanethiol surfaces may denature or fail to release these viruses.[19, 37] Similar to these results, we do not see acceptable transduction levels using AAV incubated directly onto SAMs. When analyzed on a $-CH_3$ SAM, we find that without the use of a mediating HFN layer, gene expression is only 13% of that seen with the HFN layer (Figure 2.6A). Our immunostaining with an antibody that detects intact capsids only indicates the presence of undenatured AAV capsids on the $-CH_3$ surface (Figure 2.3A). Therefore, inefficient release of AAV from the $-CH_3$ surface may be the more likely explanation for the poor reverse transduction. Most surfaces show an increase in virus attachment when HFN is present (Figure 2.6B). HFN pre-adsorption on $-CH_3$ and -COOH SAMs yields an 80% increase in AAV2 attachment while pre-adsorption on $-NH_2$ surfaces yields an almost 300% increase. As seen with a previous retrovirus study, successful transduction is observed from $-CH_3$, -COOH, and $-NH_2$ surface chemistries when HFN is used as a protein mediating layer.[37] This was a surprising result given that retroviruses and AAV have substantial structural and functional differences between the two virus particle surfaces. Retroviruses are ~100 nm enveloped viruses, where the embedded envelope proteins mediate interactions of the virus with extracellular factors.[58] AAV, in contrast, are 25 nm non-enveloped viruses, where patches of amino acid residues displayed on capsid surfaces allow the virus to

interact with extracellular factors.[49] These structural differences in conjunction with the knowledge that retroviruses and AAV infect different target cell types *in vivo*[7, 59], in part due to differences in virus particle surface-target cell surface interactions, we did not predict similar behavior of AAV and retroviruses on HFN. Further studies are necessary to determine more precisely how AAV is binding HFN.

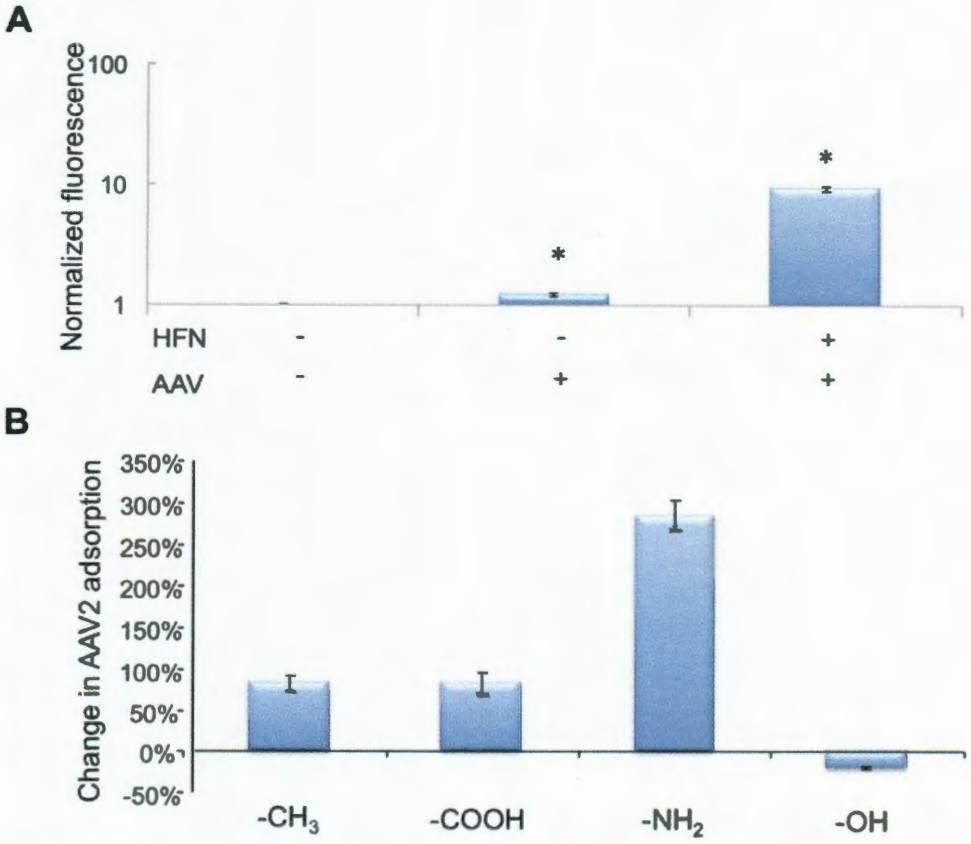

Figure 2.6. AAV2 and HFN have a synergistic relationship. GFP expression was analyzed with or without the use of an HFN mediating layer on $-CH_3$ SAMs **(A)**. When compared to autofluorescence of HeLa cells alone, fluorescence intensity measurements (as determined using ImageJ) are significantly higher ($p<0.05$). However, AAV2 alone yields only 13% of the fluorescence measured in the HFN pre-incubated sample. To help explain this result, we compared the integrated density values from immunostaining AAV2 on SAMs alone versus AAV2 on HFN pre-incubated SAMs **(B)**. When compared, HFN preincubation yields an 80% increase on $-CH_3$ and -COOH surfaces. For the $-NH_2$ surface, HFN pre-incubation yields an almost 300% increase in attachment. Pre-incubation leads to no improvement on the -OH SAM, instead causing a 20% decrease in attachment. Error bars represent standard error of the mean (A) and propagation of error (B).

An interesting outcome from this study was the discovery of a synergistic relationship between AAV2 and pre-adsorbed HFN. Specifically, presence of HFN significantly improves the ability of AAV to reverse transduce cells. The quantity of virus that

attaches to the substrate surface is higher when HFN is used to mediate adsorption. More interestingly, gene expression is nearly 8 times higher on surfaces pre-adsorbed with HFN. A possible explanation for this result is that AAV2 is able to bind HFN through electrostatic interactions. Previous reports have taken advantage of the negative charge of HFN in forming assembled layers.[60, 61] AAV2 binds its natural receptor heparan sulfate, a negatively charged extracellular biomolecule, via patches of positively charged amino acids on the virus capsid.[49] It is possible that AAV2 is able to bind negatively charged HFN using a similar electrostatic mechanism. Different conformations of HFN exist when adsorbed on different surfaces, potentially exposing variable binding regions of the protein.[62, 63] This variation in exposed HFN domains could yield changes in attachment and detachment of the virus to and from HFN that is adsorbed onto different chemistries. Previous reports have identified interactions between fibronectin and retrovirus[45], suggesting binding to fibronectin may be a common feature between these two viruses. To our knowledge, no reports exist of AAV2 binding HFN, therefore, more in-depth quantitative investigations are necessary to support this potential explanation.

Microcontact printing is a versatile technique that has previously been applied to cellular localization studies.[12-14] Pattern formation for this method is simply controlled by the features on the elastomeric stamp and can easily be tailored to a desired size and pattern for a particular application. Additionally, various chemical surfaces can be created using different terminated alkanethiols. For this work we chose to test the efficacy of four different potentially protein adhesive groups: $-CH_3$, -COOH, $-NH_2$, and -OH. These various surfaces allowed us to test a spectrum of conditions, including hydrophobic/hydrophilic and negatively/positively charged surfaces, to determine the

optimal conditions for HFN and virus attachment. It is imperative to create an efficient, reversible immobilization. To prevent protein from attaching to the non-patterned regions of the substrate, we utilized an oligo(ethylene glycol) terminated alkanethiol solution to create a protein resistant layer. This layer successfully provided a crucial barrier to background protein attachment.

As tissue engineering strategies continue to develop, incorporation of gene delivery vectors presented in spatially meaningful ways may become increasingly important. Here, we have demonstrated the ability to spatially localize both cells and gene delivery vectors. Importantly, we overcame the concern of virus localization - viral vectors must be tightly localized, but also be able to release efficiently to transduce cells. By being able to control the deposition of extracellular matrix proteins and gene delivery vectors, we are able to control both cell localization and spatial gene delivery. In the future extension of this work, we will endeavor to create complex virus patterns underneath the cell patterns. This will lead to a clear advantage over creating cell patterns and adding gene vectors suspended in the bulk media. In this latter approach, all of the cells will be transduced by the viral vectors, yielding no formation of a gene expression pattern. In our approach, we should be able to pattern multiple different gene vectors, each encoding different transgenes, underneath a cell pattern. By combining variable virus patterns with cell patterns, complex blueprints for tissue genesis can be designed. Studies are underway to separate virus patterning from cell patterning so that these features can be controlled independently.

2.6 Conclusions

We have demonstrated the ability to precisely localize the immobilization of both extracellular matrix proteins and viral gene delivery vectors. Patterns were isolated to the desired area without background attachment. Through the use of microcontact printing, we have shown there are a variety of surface chemistries capable of immobilizing both HFN and AAV, and allowing for efficient viral transduction and gene expression. This effective approach has been shown for HeLa cells and a model reporter gene but can be translated to other cell types and multiple AAV vectors delivering either overexpression or shRNA cassettes. In the future, more complicated structures can be created by patterning different combinations of adhesive proteins and viral vectors. Approaches such as this should support the future generation of structurally and functionally complex tissues.

CHAPTER THREE

Investigating the effect of adhesive proteins on substrate-mediated virus gene delivery

3.1 Acknowledgments

I would like to thank Dr. Lisa Biswal, Jinghui Wang, and Dr. Joff Silberg for helpful discussions regarding protein binding studies.

3.2 Introduction

The creation of realistic *in vitro* tissue engineered constructs has yet to become a reality. A crucial hurdle in this development is the ability to efficiently localize and deliver genes in necessary spatial orientations. In Chapter 2 we have shown that microcontact printing and adeno-associated virus could be used synergistically with human fibronectin to localize high efficiency gene delivery. In this chapter we have investigated the ability of other adhesive proteins to be used in this platform technique.

We have previously demonstrated in Chapter 2 that microcontact printing is an effective method for spatially localizing gene delivery using AAV. Using PDMS stamps and protein adhesive alkanethiol solutions, we are able to create patterns of both human fibronectin (HFN) and AAV2-GFP (recombinant virus encoding the gene for GFP) to modulate both cellular adhesion and gene delivery. Interestingly, we discovered there was a synergistic relationship between the pre-adsorption of HFN and both virus attachment and efficient gene delivery. The use of an HFN mediating layer not only

allows for cellular adhesion, but also increases the amount of virus adsorbed as well as the efficacy of delivery.

In this chapter, we have explored additional adhesive proteins (collagen I, laminin, elastin, and poly-l-lysine) to determine if they are 1) capable of working within our platform technology and 2) display any synergistic relationship with AAV2. PDMS stamps were prepared by inking in 2 mM of various protein adhesive alkanethiol solutions and were then placed on a gold-coated substrate. Samples were backfilled with an -OEG terminated alkanethiol to passivate the coverslip background. Coverslips were then incubated with adhesive protein, followed by AAV2-GFP. Finally, samples were either immunostained to observe virus deposition or seeded with HeLa cells for analysis of cell adhesion and gene expression. By examining a variety of adhesive proteins, we have determined that pre-adsorption of laminin leads to significantly increased AAV2 transduction efficiency. This effect cannot be explained by changes in transcription rate due to cell-ECM interactions.

3.3 Materials and Methods

Virus preparation. AAV2-GFP was prepared as described previously in Chapter 2. Viral titers were determined using quantitative polymerase chain reaction (QPCR) with primers for the CMV promoter of the cassette. Virus used in this study was determined to have a concentration of 1e12 vector genomes/ml in 40% iodixanol.

PDMS stamp preparation and surface functionalization. PDMS stamps were prepared as described in Chapter 2. PDMS stamps displaying 500 μm diameter circles with a 1.2 mm pitch were cleaned by sonication in 100% ethanol. Gold-coated glass coverslips (35 mm diameter, 100 Å gold over 20 Å titanium, Platypus, Madison WI) were cleaned in dilute TL1 solution (6:1:1 H_2O:NH_4OH:H_2O_2) for 1 min at 80°C, rinsed twice in Millipore purified water (MPH_2O), and dried with ultrapure nitrogen (N_2). Alkanethiols were diluted to 2 mM in 100% ethanol. Stamps were inked with either a -CH_3 (1-hexadecanethiol), -COOH (16-mercaptohexadecanoic acid), or -NH_2 (11-amino-1-undecanethiol hydrochloride) terminated alkanethiol, all from Sigma Aldrich (St. Louis, MO). Patterns were created by inking PDMS stamps, placing them gently on the substrate for 20 sec, and then carefully removing. Coverslips were then incubated with 2 mM oligo(ethylene glycol) (-OEG) terminated alkanethiol (HSC_{11}-EG_6, Prochimia, Poland) for 1 h to passivate the background. Samples were rinsed with 100% ethanol and dried with N_2.

Protein attachment. Functionalized coverslips were incubated with 1 ml protein warmed to 37°C diluted in phosphate buffered saline (PBS, pH 7.0) for 30 minutes. Human fibronectin (HFN, Sigma Aldrich, Franklin Lakes, NJ) was used at a concentration of 25 µg/ml. Bovine collagen I was used at a concentration of 50 µg/ml (Becton Dickinson). Human laminin was used at a concentration of 25 µg/ml (Sigma Aldrich). Soluble elastin was obtained from Spectrum Chemical (Gardena, CA) and was used at a concentration of 100 µg/ml. Poly-l-lysine (PLL) from Sigma Aldrich was used at a concentration of 50 µg/ml. Coverslips were rinsed twice with 5 ml of PBS using a

platform rocker. Virus was incubated with protein pre-adsorbed coverslips for 30 min at room temperature. Samples were again rinsed twice with PBS.

Immunostaining. Samples were blocked with 1% BSA in PBS for 1 h and rinsed twice with PBS. Patterns were incubated with A20 antibody (mouse anti-AAV2 capsid, American Research Products, Belmont MA) diluted 1:200 in PBS overnight at 4°C. Samples were rinsed with PBS and incubated with goat-anti-mouse AlexaFluor 532 conjugated antibody (Invitrogen) diluted 1:100 in PBS for 1 h at room temperature. Coverslips were rinsed with PBS and mounted using Fluromount (SouthernBiotech, Birmingham, AL).

Cell studies. Coverslips were placed in 60 mm tissue culture dishes and HeLa cells were seeded at a density of 100 cells/mm^2. Cells were seeded in Dulbecco's Modified Eagle Medium (Invitrogen) supplemented with 1% penicillin/streptomycin (Invitrogen). After 8 h, media was exchanged to Dulbecco's Modified Eagle Medium supplemented with 1% penicillin/streptomycin and 10% fetal bovine serum (Invitrogen). Cells were maintained at 37 °C with 5% CO_2. At 72 h post-seeding, cells were fixed in 4% PFA-PBS and stained with 2 µg/ml Hoechst 33342 stain (Invitrogen). Coverslips were mounted using Fluoromount. For BrU studies, cells were incubated with 2 mM BrU (Sigma Aldrich) for 1 h and permeabilized with 0.25% Triton X in PBS. Cells were blocked with BSA and rinsed with PBS. Primary anti-BrdU antibody (Sigma Aldrich) and secondary antibody (goat-anti-mouse AF532 conjugated, Invitrogen) were incubated for 1 h each at a 1:200 dilution in PBS. Samples were mounted using Fluoromount.

Imaging and image analysis. Images were acquired using a Zeiss 5 LIVE confocal microscope (Carl Zeiss, Munich, Germany). Images within a given sample set (immunostaining, GFP expression, Hoechst staining, BrU analysis) were acquired under identical conditions. Virus immunostaining images were collected using a 532 nm excitation at 50% power and data was collected for 2 ms pixel dwell time using a bandpass filter between 550-600 nm. GFP images were obtained using a 489 nm excitation at 1.8% power and data was collected for 2 ms pixel dwell time with a bandpass filter between 500-525 nm. BrU immunostaining images were collected using a 532 nm excitation at 3% power and data was collected for 2 ms pixel dwell time using a bandpass filter between 550-600 nm. To quantify virus attachment, 10 images were taken and integrated densities were measured with ImageJ (NIH, Bethesda MD). For cellular studies, ten fluorescence and DIC images were taken of each sample (five images from two independent replicates). For BrU analysis, the integrated density of 20 cell nuclei per sample were determined. Data is given as mean and standard error of the mean. Statistical testing was performed using JMP 9. Significance was determined using ANOVA and post-hoc testing using Tukey's HSD with a $p < 0.05$.

3.4 Results

Localization of AAV2 onto protein surfaces. We have previously shown in Chapter 2 that HFN is capable of increasing the efficiency of AAV2 adsorption to an alkanethiol surface. Here, we have examined the effect of using bovine collagen I, poly-l-lysine (PLL), laminin, and elastin as both cellular adhesion molecules and as aids for AAV deposition. We also included analysis of HFN at a higher concentration of AAV2-GFP. First, alkanethiol surface patterns were created by using PDMS stamps with 500 μm

circular patterns using chains with $-CH_3$, -COOH, or $-NH_2$ terminal groups. Samples were backfilled with an -OEG terminated alkanethiol. Adhesive protein was first adsorbed to the patterns in order to form a protein monolayer, followed by incubation with AAV2-GFP. Samples were rinsed, blocked, and incubated with an anti-AAV2 primary antibody (A20) and a fluorescently tagged secondary antibody (AF532). Integrated density measurements of individual spots were determined for each protein and surface chemistry (Figure 3.1). A20 antibody only recognizes intact AAV2 particles, indicating that the signal we observe is from undenatured virus particles. When each protein is compared, we observe that HFN is capable of localizing significantly more AAV2, when $-CH_3$ surfaces are compared. Elastin is capable of adsorbing the next highest amount of virus, and laminin immobilizes the least. It is also important to note that for each case, significantly more protein is immobilized onto the $-CH_3$ SAM surface.

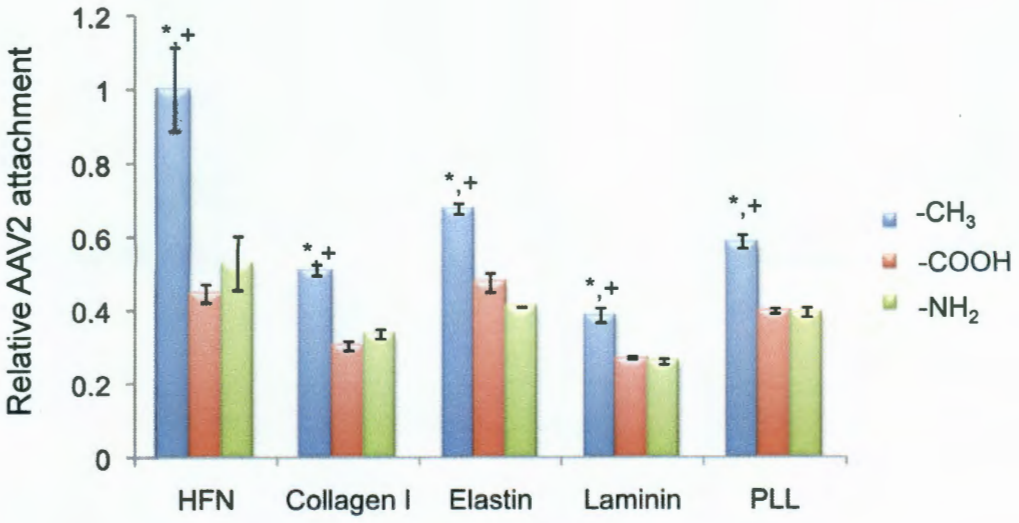

Figure 3.1. AAV deposition varies on adhesive protein surfaces. AAV deposition was determined through immunostaining and quantified using ImageJ. Ten images of each condition (alkanethiol surface and adhesive protein combination) were taken for quantification. For each adhesive protein, the $-CH_3$ surface yields the highest levels of AAV2 attachment. When comparing individual proteins, HFN yields the highest levels of attachment over other proteins. Within each protein, significance over -COOH surfaces is indicated by * and over $-NH_2$ is indicated by + ($p<0.05$).

Gene delivery from protein surfaces. Ultimately, we are interested in the effect of different proteins on the gene delivery efficiency of AAV. To test this, we again created patterns with both adhesive protein and virus adsorbed in circular patterns. HeLa cells were seeded on these patterns and samples were incubated for 72 h. Coverslips were then fixed and stained with Hoechst. Figure 3.2 displays DIC and fluorescence images of cells on different adhesive proteins, each adsorbed to $-CH_3$ SAMs. For all protein surfaces, the greatest levels of cellular coverage are seen on $-CH_3$ surfaces. All three surface chemistries yield high transduction levels.

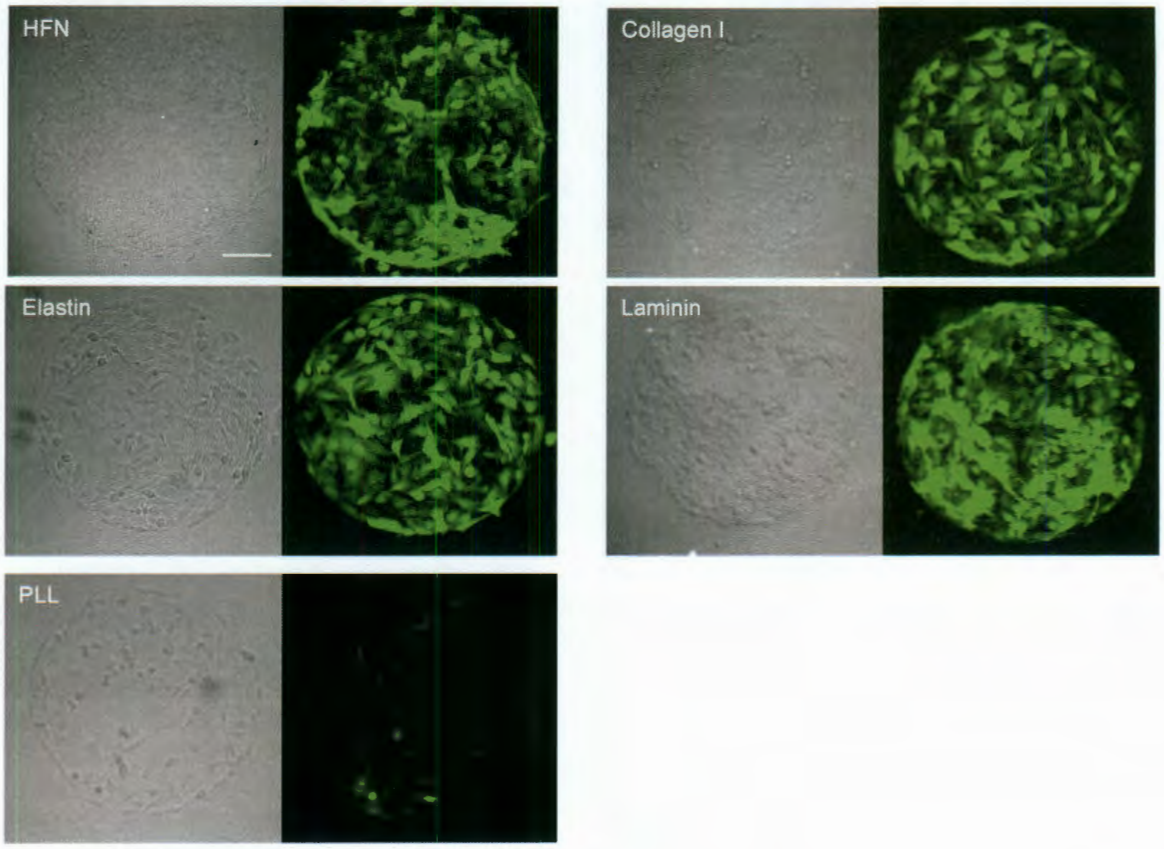

Figure 3.2. Cell adhesion and gene expression on various protein surfaces. HeLa cells were seeded at a density of 100 cells/mm^2 and fixed 72 hours post seeding. Proteins are adsorbed to -CH_3 SAMs. Successful gene expression is observed on all protein surfaces. Scale bar is 100 microns.

For each sample, the integrated density of both the GFP signal and Hoechst signal were determined using ImageJ. The GFP signal was normalized to the nuclear signal in order to normalize expression to the number of cells on the pattern (Figure 3.3). When individual proteins are compared, laminin and HFN led to significantly higher GFP expression ($p<0.05$). When SAM surfaces for each protein are compared, HFN, elastin, and laminin surfaces all show significantly higher GFP expression on the -CH_3 surfaces. For HFN and laminin surfaces, the -COOH surfaces have higher gene expression than

the $-NH_2$ surfaces. Gene expression levels on collagen and PLL surfaces are statistically similar. From this analysis, we observe the highest level of gene expression when AAV2 is adsorbed onto laminin pre-coated patterns. As seen previously, HeLa cells seeded onto HFN and AAV2 surfaces also yields high levels of gene expression.

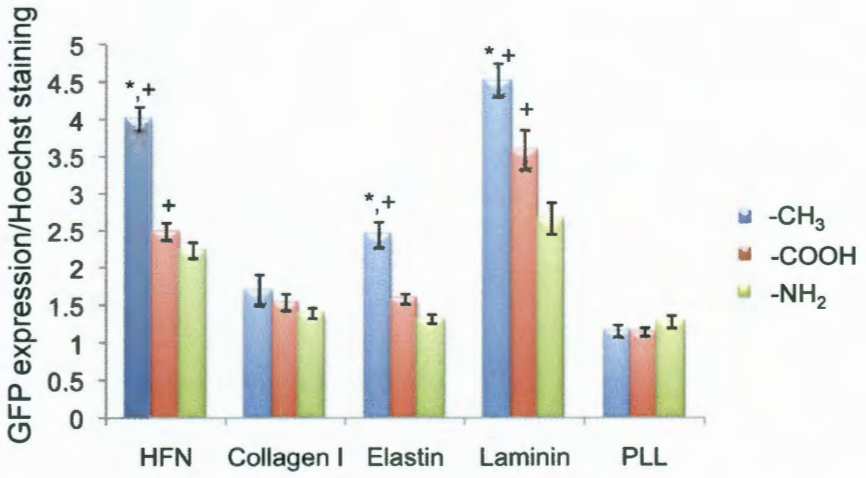

Figure 3.3. Quantification of GFP expression. HeLa cells were seeded onto adhesive protein and AAV2-GFP co-patterned samples. Cells were fixed and Hoechst stained 72 h post cell seeding. HFN and laminin pre-adsorption leads to significantly higher levels of GFP expression. Five images each from two experiments were quantified for gene expression and nuclear staining using ImageJ. GFP expression was normalized to nuclear staining. Within each protein, significance over -COOH surfaces is indicated by * and over $-NH_2$ is indicated by + ($p<0.05$).

Ultimately, we would like to know the relationship between immobilized virus and gene delivery efficiency. To relate these values, we normalized the gene expression levels to the relative amount of virus adsorbed, as measured by immunostaining (Figure 3.4). Again, laminin pre-adsorption yields dramatic results with a much higher ratio of gene expression: virus adsorption. The ratio of gene expression to virus adsorption for laminin is approximately twice as high as HFN. When we compare the GFP/A20 ratio for each

protein -COOH surface, laminin surfaces show significantly higher gene expression over all four other proteins. HFN and collagen I gene expression is higher than both elastin and PLL gene expression.

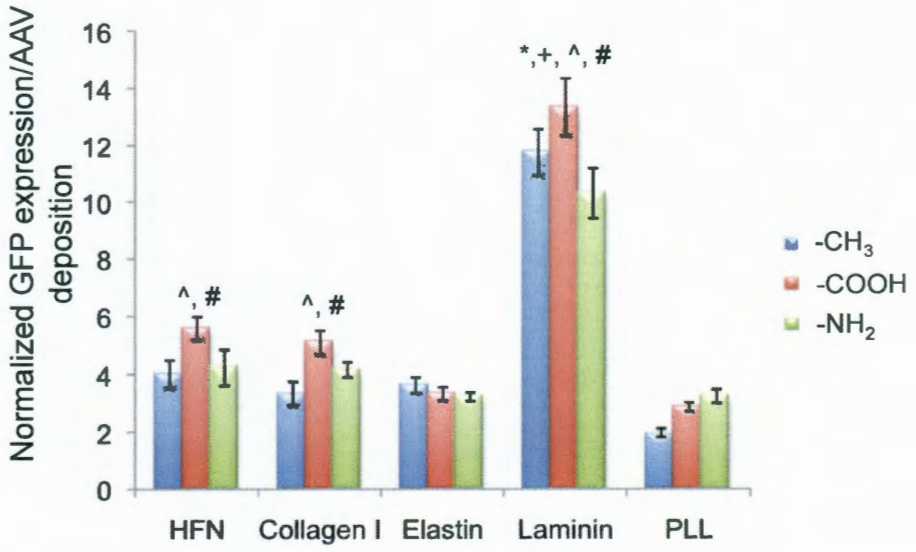

Figure 3.4. GFP expression normalized to virus deposition. Gene expression from laminin surfaces is more than twice that from HFN, and significantly higher than all four other protein surfaces. -COOH surfaces for each protein were compared. Significance over HFN surfaces is indicated by *, over collagen I is indicated by +, over elastin is indicated by ^, over PLL is indicated by # ($p<0.05$).

To determine the reason for the dramatic gene expression increase on laminin surfaces, we hypothesized that the gain in expression could be due to two possible reasons. First, HeLa cells could be inherently more transcriptionally active on laminin surfaces, making the expression of all gene products (including GFP) higher than on other surfaces. Second, there could be differences in the disassociation properties between the viral

particles and various protein surfaces that make laminin a more optimal substrate for gene delivery.

Transcriptional analysis. We sought to first test the transcriptional activity of HeLa cells on each of our surfaces using bromouridine (BrU) incorporation to compare the relative transcriptional activities on the surfaces (Figure 3.5). BrU incorporation levels were compared using ANOVA, and it was determined that $p<0.05$. We observe differences in cellular activity on different surfaces, as HeLa cells are nearly twice as active on PLL-COOH surfaces as compared to HFN-CH_3 surfaces. It is most interesting to note that transcriptional activity on laminin-CH_3 surfaces is not significantly higher than cellular activity on any of the other protein-CH_3 surfaces. This lack of increased activity on laminin surfaces suggests that the increase in transduction levels seen on these surfaces is due to a laminin-AAV specific interaction.

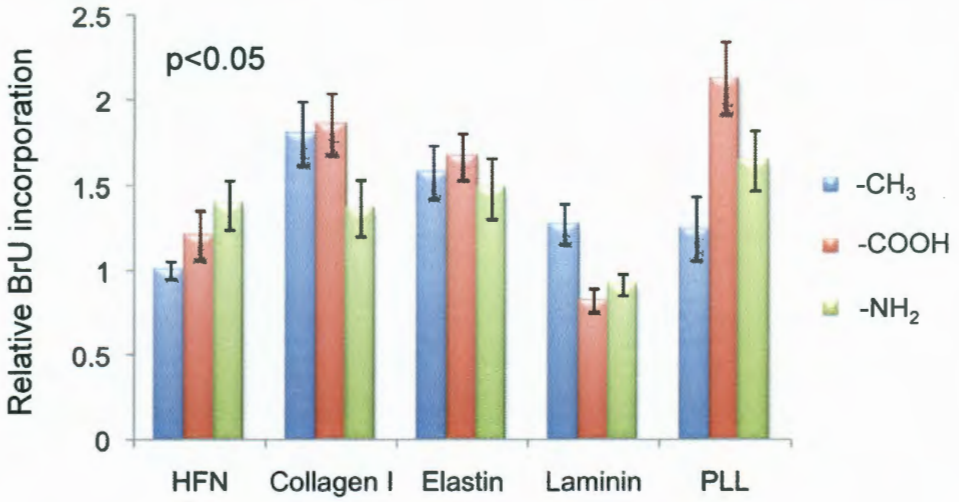

Figure 3.5. Relative transcriptional activity for HeLa cells seeded on various adsorbed proteins. HeLa cells were seeded onto adhesive protein adsorbed onto SAMs. Cells were treated with BrU 24 h later and immunostained to observe BrU incorporation. The integrated densities of 20 cell nuclei per condition were quantified. Values were normalized to the HFN-CH_3 surface. It was determined by ANOVA that the cases were significantly different ($p<0.05$).

3.5 Discussion

We have previously shown that HFN is capable of supporting AAV2 patterning by localizing both cells and gene expression. Our reverse transduction format allows us to modulate the spatial organization of gene delivery. Viral vectors are immobilized onto a substrate and cells are seeded on top, which allows us to control gene expression by controlling the underlying pattern. This is in contrast to a bulk delivery system, which would lead to a uniform transduction of cells. Surprisingly, we have found that AAV2 is capable of interacting with a variety of adhesive proteins. This is a very important idea to note as we work to expand this technology. As we create more complicated structures,

we will integrate additional cell types into our constructs. Each cell type used may need to be supported by particular adhesive proteins, thus more flexibility in our system will be important.

Interestingly, we have identified that laminin surfaces are most effective for AAV2 gene delivery. Laminin pre-adsorption yielded nearly twice as high transduction efficiency per immobilized virus capsid. We rationalized that this dramatic increase in transduction efficiency could be due to increased transcriptional activity of HeLa cells on laminin surfaces. However, since BrU studies indicated that these cells are no more transcriptionally active on laminin surfaces as compared to other proteins, we believe that the interaction, particularly the release of virus from laminin, must be more efficient on laminin surfaces compared to other ECM proteins. This hypothesis is currently being explored using quartz crystal microbalance (QCM) and surface plasmon resonance (SPR) to more quantitatively study the deposition of virus on these proteins and the binding and release kinetics on these surfaces.

The interaction of AAV with extracellular matrix proteins has not been studied extensively. While we know the primary cell receptors for several serotypes (e.g. AAV2 binds heparin sulfate proteoglycans, AAV1 and AAV6 bind sialic acid[64]), very little is known about the interaction of AAV with ECM proteins. As various serotypes are known to transduce selected tissues within the body, the specific interactions that lead to these transduction events has not been identified. While it is presumed that these transduction effects are based on cell-binding interactions, the information we are learning about AAV-protein interactions creates additional questions about the interaction of these vectors with the surrounding supporting structures.

In addition to *in vitro* gene delivery studies, this work has implications for *in vivo* gene delivery. As targeting strategies for *in vivo* gene delivery continue to advance, it will likely be important that vectors are capable of transversing extracellular boundaries. Currently, little is known about the interaction between AAV serotypes and ECM proteins within the body. These interactions could be crucial for efficient gene delivery, as it has previously been shown that co-injection of heparin with AAV2 vectors in the brain allowed vectors to travel farther into the brain.[65] It has also been shown that retinal transduction is increased with the digestion of the inner limiting membrane by protease.[66] AAV5, for example, is unable to delivery genes efficiently to the inner retinal cells unless this membrane is digested.[66] The authors suggested that this was due to a lack of appropriate receptors for this membrane.

Other viral vectors have been shown to interact with protein. Fibronectin has been shown to localize retroviral vectors to target cells as retrovirus is capable of associating with a heparin binding domain on fibronectin. This interaction can be blocked by addition of heparin.[67] Cell binding domains on fibronectin allow the protein to interaction with cells, while retrovirus is brought in contact to cells through interaction with the heparin binding domain. RetroNectin (Takara Bio Inc, Madison, WI) is a fibronectin-based technology developed based on these interactions. Plates coated with RetroNectin can be incubated with retrovirus or lentivirus, and then seeded with cells to increase virus-cell interactions and increase gene delivery within cells.[68, 69]

3.6 Conclusions

In this chapter we have explored the efficacy of adsorbing AAV2 to a number of adhesive proteins. We have used PDMS stamps and protein adhesive alkanethiols to localize HFN, laminin, collagen, elastin, and PLL. AAV2 particles were immobilized to the pre-adsorbed protein. While all proteins facilitate cell adhesion and successful gene delivery, we observe that laminin pre-adsorption leads to the most successful gene delivery. We hypothesize that this could be due to 1) increased AAV2 transcriptional activity on laminin surfaces or 2) advantageous interactions between AAV2 and laminin that allow for more efficient virus release. BrU incorporation suggests that HeLa cells are no more transcriptionally active on laminin surfaces, suggesting that AAV2 release from laminin surfaces could be the reason for increased transduction efficiency. Currently, quartz crystal microbalance with dissipation (QCM-D) and surface plasmon resonance (SPR) studies are being developed to further explore this possibility.

CHAPTER FOUR

Live-cell microarray surface coatings supporting reverse transduction by adeno-associated viruses

4.1 Acknowledgements

I would like to thank Ryan Schweller and Dr. Michael Diehl for assistance with robotic spotting and Jerry Leu for schematic creation assistance.

4.2 Introduction

Live cell genetic microarray technology is a potentially powerful approach to investigating the cell behavioral effects of expressing or knocking down various combinations of genes.[70] Each spot of the microarray can contain a different combination of genes or RNAi cassettes, and live target cells are seeded on top of the spots. Through the process of reverse transduction (when viral vectors are used) or reverse transfection (when nonviral vectors are used), the cells will internalize the genes/RNAi cassettes resulting in the overexpression or knockdown of specific genes. Different gene expression profiles in each of the microarray spots may lead to phenotypic changes in the cells. Detecting these changes via automated imaging and image processing will provide a high-throughput combinatorial screening method that can help identify key gene expression profiles that yield a desired cellular outcome.

Live cell genetic microarrays have previously been generated using both viral and nonviral gene delivery methods.[18, 20, 43, 71] Non-viral gene delivery methods have been used to generate single cell microarrays to study up to 600 cell spots on a single chip.[72]

siRNA lipoplexes mixed with matrigel have been successfully arrayed onto poly-l-lysine coated slides for high-throughput siRNA silencing.[73] The success of any live cell genetic microarray approach hinges upon the ability of vectors to deliver nucleic acids with high efficiency to cells of interest. Although nonviral delivery systems are promising, viral vectors in general still have significantly higher gene delivery efficiencies, supporting their continued development for genetic microarray technology. In terms of viral vectors, both adenovirus and lentivirus have been spotted under various conditions to create genetic microarrays. For example, lentivirus was spotted with a robotic spotter to create alternating patterns of overexpression and shRNA cassettes, and phenotypic changes in target cells were analyzed.[18] Fibrin hydrogels have been used to help immobilize lentiviruses in spot patterns, suggesting a difficulty in maintaining lentivirus spots without such an approach.[74] Adenovirus microarrays have been created using a manual spotting device and 25 mg/ml nitrocellulose coated slides.[43] Notably, a synthetic blocking agent was used to localize cell adhesion to areas of virus deposition, creating distinct cell islands. These previous studies have made great strides towards the creation of versatile, high-throughput genetic microarray technology, and we sought to improve upon the successes through the use of an alternate, potentially more advantageous gene delivery vector.

Specifically, additional improvements in delivery efficiency and safety would enhance the potential for virus-based live cell genetic microarrays. A virus vector capable of being modified relatively easily to increase transduction specificity and efficiency would increase the power of this technology. Thus, we chose to investigate the potential of AAV for the creation of genetic microarrays.

AAV is an appealing alternative to the other viruses due to its increased safety profile and the relative ease with which its delivery efficiency can be improved. AAV is able to deliver genes into both dividing and nondividing cells. A number of naturally occurring serotypes of AAV have been identified, with each serotype displaying variable tropism.[7] Numerous rational[26, 56] and combinatorial[27, 29, 75] methods have been developed to enhance gene delivery efficiencies into target cells. Furthermore, AAV is non-pathogenic, meaning it is not known to cause any human disease. Recombinant AAV does not integrate effectively into the human chromosome, alleviating concerns over insertional oncogenesis. Due to the numerous positive features of AAV, we have initiated the development of AAV-based live cell genetic microarrays.

To create AAV-based microarrays, a custom-built robotic spotter was used to deposit AAV serotype 2 (AAV2) encoding GFP (AAV2-GFP) onto glass slides (Figure 4.1). For the microarray to be successful, AAV must be localized into spots but retain the ability to release from the surface and transduce target cells. If virus affinity to the surface is too low, the virus patterns may dissipate quickly upon addition of cell seeding media, resulting in a lack of localized gene expression profiles. Conversely, if affinity to the surface is too high, vectors may adsorb irreversibly or possibly even denature, resulting in suboptimal gene delivery efficiencies. No previous reports exist testing AAV for microarray development; therefore, we screened several commonly used surface coatings for their ability to adsorb AAV. Specifically, three different glass slide coatings (gamma amino propyl silane [GAPS], amine silane, and nitrocellulose) were investigated to determine an optimal substrate for AAV immobilization and reverse transduction.

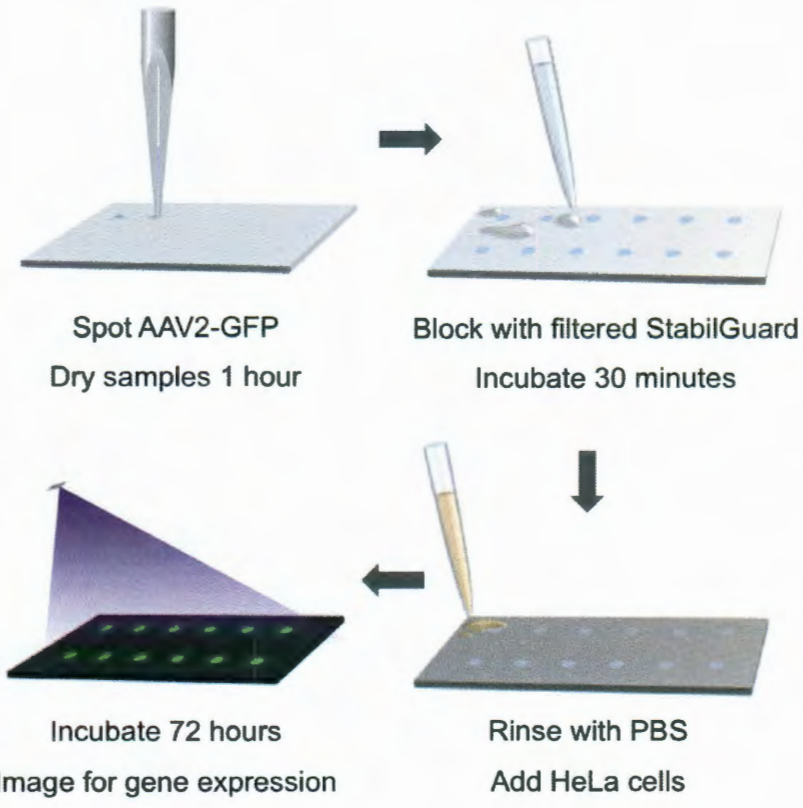

Figure 4.1. Schematic of patterning process. Recombinant AAV is spotted onto coated glass slides. Slides are backfilled with microarray stabilizer and then seeded with cells. Arrays are imaged three days later for gene expression.

4.3 Materials and Methods

Virus production. HEK 293T cells and a triple transfection method were used to create AAV2-GFP as described previously.[54] Virus was purified using ultracentrifugation and a step iodixanol gradient. Virus used in these experiments was purified using a heparin affinity column and dialysis against DPBS, as virus in iodixanol inhibited deposition from the array pin. Virus solution (1 ml) was added to a heparin column (GE Healthcare, Piscataway, NJ), rinsed with column buffer (150 mM NaCl, 10 mM Tris, 10 mM $MgCl_2$)

and eluted with elution buffer (1 M NaCl, 10 mM Tris, 10 mM $MgCl_2$). Eluted virus was added to a 10,000 molecular weight cut off dialysis cassette (Pierce, Rockford, IL) and dialyzed against three changes of DPBS over nine hours. Virus was titered using real time quantitative polymerase chain reaction (RT-QPCR) with primers against the CMV promoter in the recombinant virus cassette.

Virus spotting. GAPS coated slides (Corning, Corning NY) and amine silane functionalized slides (CEL Associates, Pearland TX) were used as is. These slides should yield similar surfaces. Nitrocellulose (Sigma Aldrich, St. Louis MO) was dissolved in methanol at concentrations of 2-4 mg/mL. Glass slides were rocked for 1 h with nitrocellulose solutions at room temperature and then allowed to dry at room temperature for 1 h. Spotting was conducted using an in-house fabricated microarray robot and an SMP15 pin (7 nl delivery volume) from Arrayit (Sunnyvale CA). Slides were allowed to dry for 1 h and then backfilled with StabilGuard (Surmodics, Eden Prairie MN) for 30 min. Slides were then rinsed with PBS.

Immunostaining. Slides were blocked with 1% BSA-PBS for 1 h, rinsed with PBS and then incubated with a 1:200 dilution of A20 antibody (American Research Products, Belmont MA) at 4°C overnight. Microarrays were then rinsed with PBS and incubated with a 1:100 dilution of a goat-anti-mouse AlexaFluor 532 (AF532) conjugated antibody (Invitrogen, Carlsbad CA) for 1 h. Samples were washed with PBS and mounted using Fluoromount. Intensity plots were created using ImageJ. Lines were drawn through an image of 4 spots and the fluorescence intensity profile was plotted as a function of distance in microns.

Cell culture. Slides were seeded with HeLa cells in a 10 cm tissue culture dish. GAPS and amine functionalized slides were seeded at a confluency of 95% and nitrocellulose slides were seeded at a confluency of 20%. Cells were cultured in DMEM supplemented with 10% FBS and 1% penicillin/streptomycin (Invitrogen). Slides were moved to a new dish the next day and supplemented with fresh media. Slides were fixed with 4% PFA in PBS 72 h post cell-seeding.

Imaging and analysis. Microarrays were imaged using a Zeiss LSM 5 LIVE confocal microscope (Carl Zeiss, Munich, Germany). Integrated densities were determined using ImageJ (NIH, Bethesda MD). Data is reported as average with standard error of the mean. Statistical significance was determined using ANOVA and Tukey's HSD for post hoc pairwise testing ($p<0.05$, JMP 9 software).

4.4 Results

Virus immunostaining. Deposition of AAV on the three different surfaces was visualized via immunostaining with an antibody that detects nondenatured AAV2 capsids only (Figure 4.2A-C). Spot diameter for all three cases is approximately 400 microns with a pitch of 800 microns, as expected. Although GAPS and amine silane coatings allow for localized AAV deposition, the density of nondenatured virus deposition is low, highlighted by low fluorescence values on the intensity plots (Figure 4.2D-E). Low levels of AAV2 adsorption on amine surfaces is consistent with our previous studies.[76] An edge effect can be observed, where more virus is deposited along the edges of the spots. In contrast, the nitrocellulose coating yields bright virus staining, indicating a greater amount of nondenatured AAV is immobilized in the spotted area (Figure 4.2F).

Our previous work indicates a hydrophobic methyl (-CH_3) surface is able to mediate high levels of AAV2 adsorption,[76] suggesting the hydrophobic character of nitrocellulose may be responsible for effective AAV immobilization in this study. Interestingly, a higher distribution of AAV is observed along the center axis of the spot, likely attributable to the geometry of the microarray pin. The pin used in this study has a linear slit opening positioned at the center of the tip. The sample presumably flows out of the slit opening and spreads along the shape of the tip.

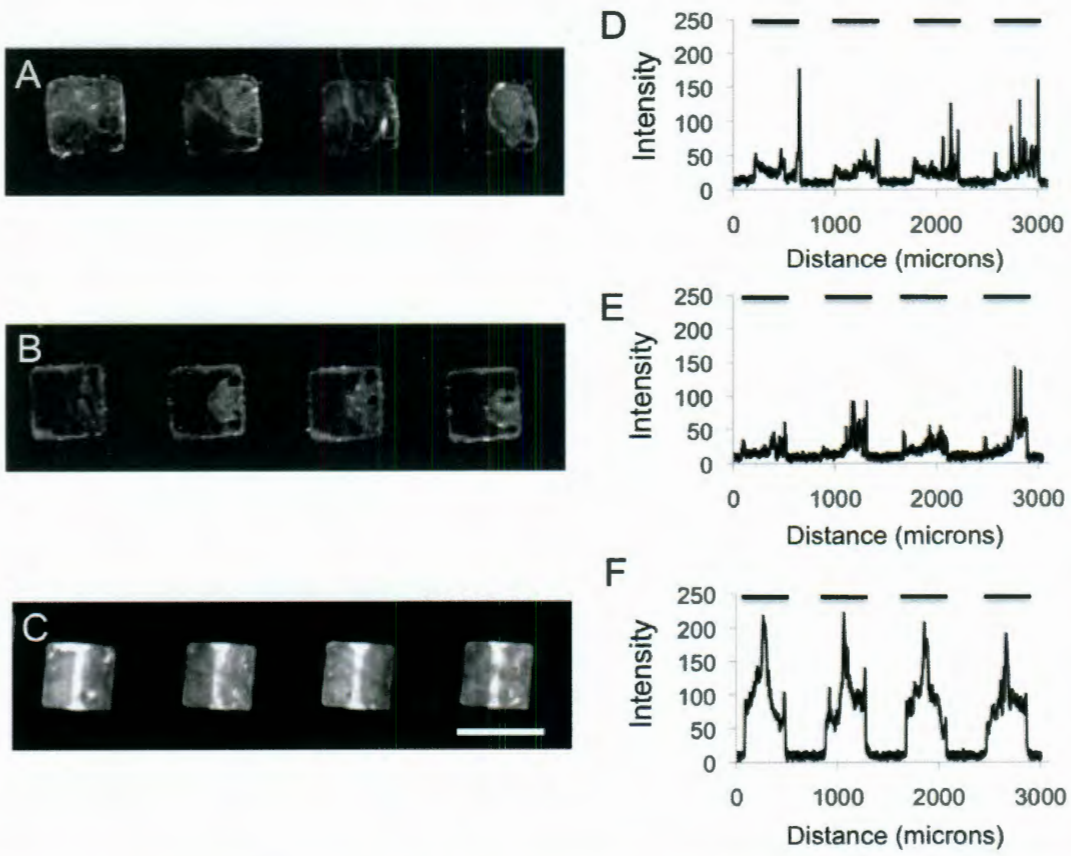

Figure 4.2. Immunostaining of AAV deposition on three different coated glass slides. Virus was spotted onto (**A**) GAPS slides, (**B**) amine silane slides, or (**C**) 3 mg/mL nitrocellulose coated slides. Samples were immunostained with an anti-AAV antibody and an AF532 conjugated secondary antibody. Scale bar is 500 microns. Images **D-F** are intensity plots generated over 4 spots using ImageJ. Bars at top of graphs indicate locations of virus patterns. While patterned deposition is observed on all surfaces, the most intense staining is seen with the nitrocellulose coated slides.

Cell adhesion and gene expression. We next seeded cells on top of the virus patterns to test for reverse transduction. The immobilized AAV must release from the surface and be internalized by the cells in order to mediate successful gene delivery. This release cannot happen too quickly, otherwise virus patterns will be dispersed as they come into contact with cell media. Although GAPS and amine silane coated slides result in

positively transduced cells, the GFP-expressing cells are scattered and do not yield distinct patterns (Figure 4.3). The nonspecific affinity of AAV to these surfaces may not be strong enough to resist disassociation in media prior to cell attachment. In other words, as soon as cells and media are added to the virus patterned slides, the viruses may lift off and drift away from the established patterns. The nitrocellulose coated slide, however, successfully yields a pattern of GFP-expressing cells (Figure 4.4A), indicating AAV is able to release effectively off the surface. Cells are attached only to these discrete spot regions, with no cells adhering to the background (Figure 4.5). Interestingly, we observe a series of linear cell islands reflective of the higher AAV deposition along the center axis of the microarray pins (Figure 4.2C). We hypothesize that cells may be able to utilize specific receptor-ligand interactions to adhere to this region displaying higher amounts of AAV. AAV2 is known to bind heparan sulfate proteoglycans on target cell membranes.[49] At sufficient concentrations, immobilized AAV2 may be able to mediate cell binding to the surface, as previously demonstrated.[77] In future optimizations, adding cell adhesive proteins to the virus solution could help generate complete spot formation. Alternatively, we may use a different shaped pin to obtain a more uniform virus deposition. In future optimizations, adding cell adhesive proteins to the virus solution could help generate complete spot formation. Alternatively, we may use a different shaped pin to obtain a more uniform virus deposition.

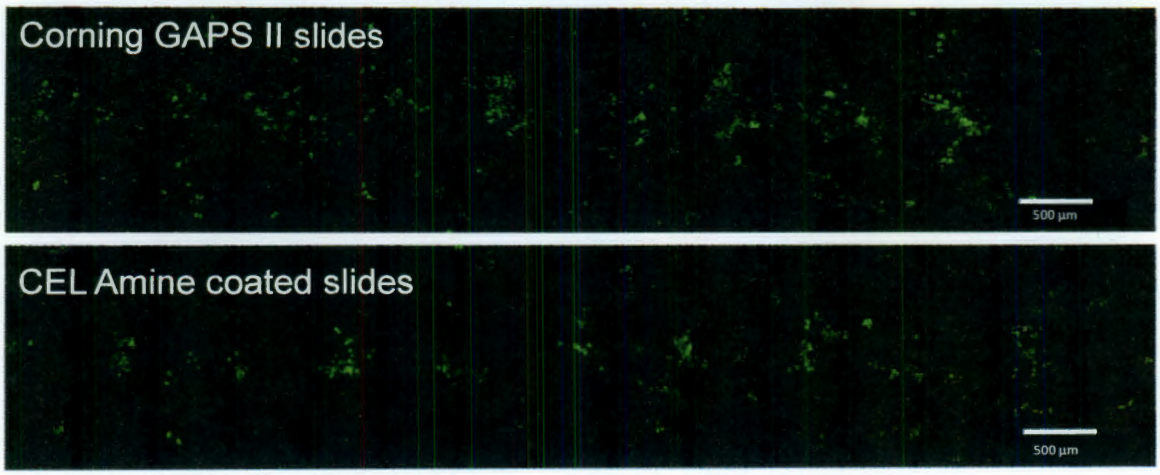

Figure 4.3. Cell adhesion and gene expression on amine slides. As suggested in Figure 4.2, virus deposition onto GAPS II (top) and amine silane functionalized slides (bottom) leads to semi-localized gene expression with an undesirable level of spreading.

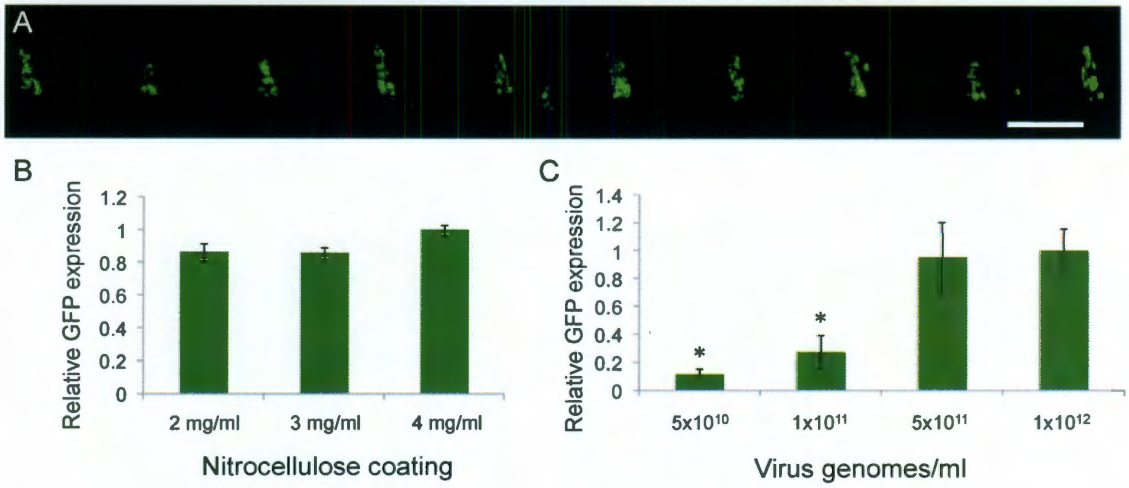

Figure 4.4. Cell adhesion and gene expression on nitrocellulose coated slides. AAV was printed on nitrocellulose coated glass slides and HeLa cells were seeded on top of the virus patterns. (**A**) Pattern of GFP-expressing cells can be observed on 3 mg/ml nitrocellulose coated slides at 72 h post cell seeding. Cells are located only within the patterns. Scale bar is 500 microns. (**B**) 2-4 mg/ml nitrocellulose coatings yield similar levels of reverse transduction. The differences are not statistically significant. (**C**) Different concentrations (virus genomes/mL) of AAV were used in the spotting and efficiency of reverse transduction quantified. A dose-dependent response in gene expression is observed, with significantly less gene expression observed with virus at concentrations of $5x10^{10}$ and $1x10^{11}$ vg/ml ($p<0.05$).

Figure 4.5. DiC image of localized spot. DIC image of HeLa cell spot on 3 mg/ml nitrocellulose slide.

We next sought to optimize the promising nitrocellulose coating by testing different nitrocellulose concentrations (Figure 4.4B). Preliminary tests indicated coatings with higher than 4 mg/ml nitrocellulose are not efficient for gene delivery and less than 1 mg/ml leads to undesirable virus spreading (Figure 4.6). In the concentration range of 2-4 mg/ml nitrocellulose, we observe similar levels of GFP expression in the cells. We also investigated the minimum concentration of virus needed to obtain significant gene expression from the nitrocellulose surface (Figure 4.4C). Using a 3 mg/ml nitrocellulose coated substrate, we spotted $5x10^{10}$ to $1x10^{12}$ viral genomes (vg)/ml AAV solutions. A sharp decrease in gene expression is observed when a virus solution under $5x10^{11}$ vg/ml is used. Based on a spot size of 400 microns and a pin deposition volume of 7 nl, we estimate a virus concentration of $3x10^{11}$ vg/ml is required to create a monolayer of virus.

Due to inefficiencies in the system, we likely do not have a monolayer and not all AAV that is bound is able to release effectively and deliver genes into target cells.

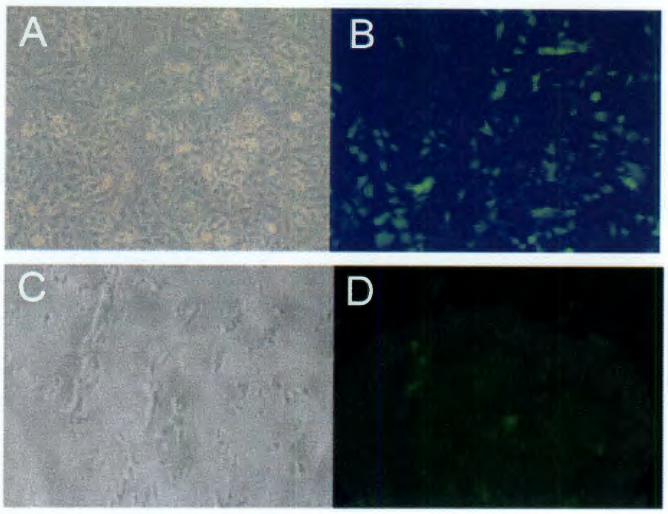

Figure 4.6. GFP expression on additional nitrocellulose concentration surfaces. 1 mg/ml nitrocellulose coating leads to spread cell adhesion (**A**) and non-localized gene expression (**B**). 5 mg/ml nitrocellulose coating leads to low levels of gene expression within a spot (**C** & **D**).

4.5 Conclusions

In summary, our AAV-based live cell genetic microarray platform is a promising alternative to platforms using other viruses. AAV has a demonstrated track record of being readily modified to improve gene delivery efficiencies and specificities. Moreover, AAV has a greater safety profile compared to other viruses, supporting its continued use and investigation in gene delivery applications. We have demonstrated that AAV can be patterned using a robotic spotter. The immobilized AAV is capable of releasing from the nitrocellulose surface and mediating effective reverse transduction. Further optimizations

of our method will take us closer to the development of a microarray technology for high-throughput combinatorial genetic screening that may help identify unique gene expression profiles necessary for reprogramming iPS cells or differentiating stem cells. For example, combinatorial gene expression screening in induced pluripotent stem cells (iPS) may reveal improved gene combinations for more efficient stem cell reprogramming. Current iPS technology, relying on the delivery of genes encoding four transcription factors, has a success rate of less than 1%.[78] Substantial enhancements to iPS reprogramming may be made by identifying improved combinations of genes to deliver. Investigations into stem cell differentiation can also benefit from a live cell genetic microarray technology. Stem cell differentiation is a complicated multi-step process involving an array of genetic changes, cell interactions, as well as additional factors.[11] To better understand the effects of genetic factors on differentiation, the effects of these genes must be tested in combination and analyzed for downstream implications. An improved high-throughput genetic microarray technology would allow researchers to conduct these experiments in an efficient manner to analyze the interplay of genes responsible for complex cell behaviors.

CHAPTER FIVE

Reprogramming virus nanoparticles to bind metal ions upon activation with heat

5.1 Acknowledgements

This work was conducted in collaboration with Dr. Matthew Musick and Jerry Leu. I would like to thank Clive Chen for initial molecular biology work. The work detailed in this chapter is a modified version of a manuscript accepted for publication in Biomacromolecules.

5.2 Introduction

In this chapter we will re-program the virus output in order to study AAV as a potential biosensor. Instead of using the virus to infect cells, we will take advantage of virus capsid conformational change dynamics in order to modify the output of our virus vectors. Modified vectors could then be patterned using a high-throughput approach to assay for biomolecules of interest.

We are focused on investigating whether the dynamic functionalities of the AAV capsid can be reprogrammed in pursuit of our goal to develop novel, intelligent, genetically encoded nanoparticles. In particular, our proof-of-concept study endeavored to exploit the stimulus-responsive conformational change behavior of the virus capsid in order to externalize metal-binding motifs upon activation. Such virus nanoparticles (VNPs) can be interfacial building blocks, guiding the organization and creation of higher order structures using metals as assembly center.[79] Ideally, we would like to employ the

conformational change dynamics exhibited by AAV to function as a biosensing device (Figure 5.1). Virus nanoparticles would be modified such that their input would be a desired stimulus (likely a protein or small molecule of interest) and their output would be a domain that we could efficiently detect (fluorescent particle, enzymatic domain, detectable tag).

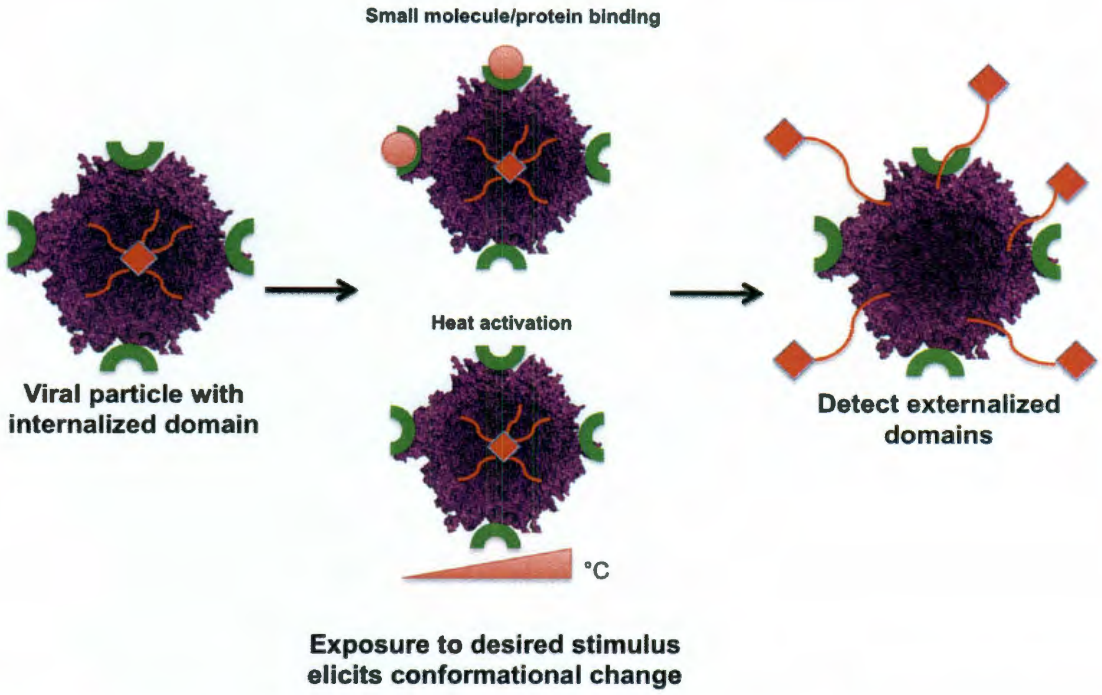

Figure 5.1. Alteration of AAV VNPs for biosensing. To use AAV as a biosensor, we envision replacing the PLA2 domain on the VP1 N-terminus with a detectable domain (left) which would be internalized until activation. VNPs could be activated through the binding of a small molecule or protein (center, top) or through a current stimulus, heat activation (center, bottom). Treatment with stimuli would lead to externalization of these residues and detection of the inserted domains (right).

The end goal of this work would be to create arsenals of different VNPs, each capable of activation under different stimuli. VNPs would then be patterned unto a suitable substrate using a high-throughput microarray spotter (Figure 5.2). Viral particles

recognizing biomolecules of interest would be arrayed, dried, and the patterned chip would be blocked with a microarray stabilizer. Sensor chips would then be exposed to a solution containing potential biomolecules of interest. After activation of virus particles and externalization of N-terminus residues the sensor chip would be imaged. Viral particles detecting molecules within the solution would be activated, while those not responding to any of the present molecules would remain in the native state.

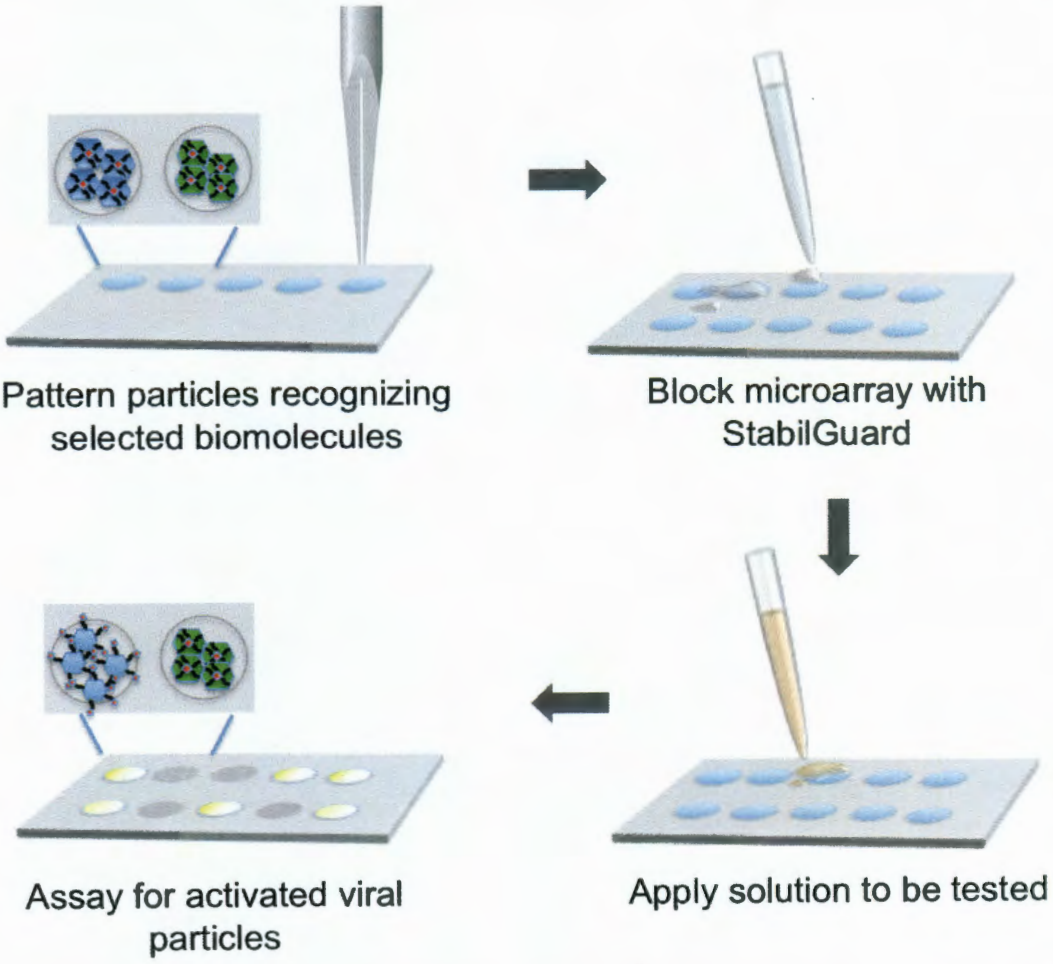

Figure 5.2. High-throughput patterning of AAV biosensors. We envision patterning modified VNPs using a microarray spotter. VNPs sensing selected biomolecules will be patterned into individual spots and blocked using StabilGuard. Solution containing biomolecules to be tested will be applied to the array. VNPs responding to molecules in the solution will be activated.

Viruses have gained considerable interest as genetically encoded nanoscale structures that can be harnessed to create novel materials with unique properties and functionalities. For example, the rod-like M13 bacteriophage has been used to generate semiconductor nanowires[80] and to create cell substrates for the guidance of neuronal progenitor cells,[81] while MS2 bacteriophage has been investigated as a taxol drug delivery scaffold.[82] Plant viruses, such as cowpea mosaic virus[83] and cowpea chlorotic mottle virus[84] have been used as protein scaffolds for biomineralization of heavy metals. Cowpea mosaic virus has also been investigated as a nanoparticle for the imaging of *in vivo* vasculature,[85] as an MRI contrast agent,[86] and for potential use as electroactive biomaterials or biosensors.[87] Brome mosaic virus, another plant virus, has been studied as an encapsulation agent for negatively charged gold or iron oxide nanoparticles to be potentially utilized as imaging and tracking agents.[88, 89] Tobacco mosaic virus has been used to create thin film surfaces for the detection of methanol and ethanol vapors.[90] Each virus system has a unique set of characteristics, thus providing a diverse range of structures and functions that can be leveraged for the creation of new nanostructures for human application.

Adeno-associated virus (AAV) has so far mainly been used for gene therapy applications, with at least 75 human clinical trails underway. The biology pertaining to AAV structure and function is an area of intense investigation by numerous groups.[7] We are focused on investigating whether the dynamic functionalities of the AAV capsid can be reprogrammed in pursuit of our goal to develop novel, intelligent, genetically encoded nanoparticles. In particular, our proof-of-concept study endeavored to exploit the stimulus-responsive conformational change behavior of the virus capsid in order to externalize metal-binding motifs upon activation. Such virus nanoparticles (VNPs) can be

interfacial building blocks, guiding the organization and creation of higher order structures using metals as assembly centers.[79]

The simple genome of AAV is composed of two genes: *rep* and *cap*. The *rep* gene encodes for four non-structural proteins that are integral in virus replication. The *cap* gene encodes for three structural proteins, VP1, VP2, and VP3 (Figure 5.3A). The VPs share a common C-terminus and self-assemble in a 1:1:10 ratio to form a 60 subunit icosahedral capsid. A fourth protein also encoded by *cap*, assembly activating protein (AAP), activates this self-assembly process.[5] When assembled, the capsid contains twelve pore structures at the five fold axes of symmetry.

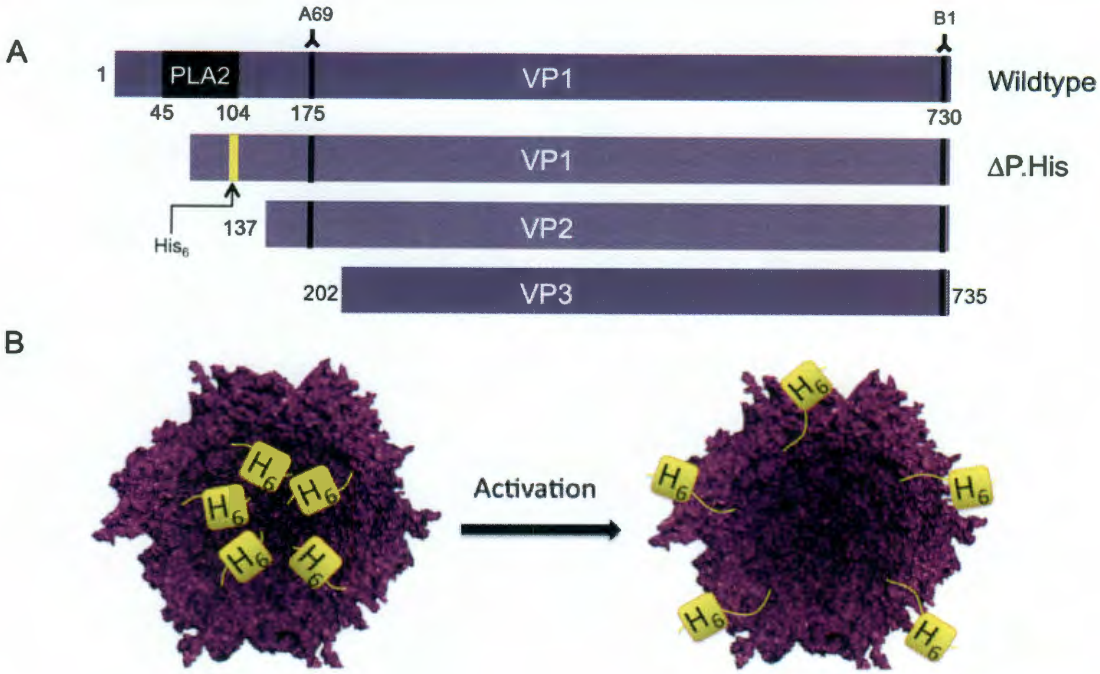

Figure 5.3. Overall design of metal-binding virus nanoparticles (VNPs). (**A**) The PLA2 region of VP1 in the wildtype (wt) virus was excised and replaced with a hexahistidine tag (His_6) in order to create the AAV2-ΔPLA2-His (ΔP.His) construct. The first amino acid residue number corresponding to the antibody binding sites for A69 and B1 are indicated. Plasmid constructs are used to generate VNPs by transfecting into 293T cells along with pXX6. Wt virus contains an internalized PLA2 domain and ΔP.His virus contains the His_6 tag. (**B**) Viruses are exposed to heat to activate the capsid conformational change. Upon stimulation, ΔP.His VNP surface exposes His_6 tags.

Notably, the AAV capsid is capable of undergoing a dynamic conformational change upon exposure to specific stimuli - low pH and additional unknown endosomal factors in cells and heat or urea shock in the laboratory.[23, 24] Exposure to low pH alone is not sufficient to induce this conformational change.[91] Upon stimulation, the N-termini of VP1 and VP2, which have been identified as globules located inside capsid lumens prior to activation,[24] become externalized on the capsid surface. This externalization is hypothesized to occur through the pores at the five fold axes of symmetry. The

conformational change requires the presence of encapsidated viral genome[24] and specific amino acid residues at certain locations.[23] The externalized VP1 N-terminus contains a catalytic phospholipase A2 domain (PLA2), hypothesized to enable AAV to escape from endosomes and avoid lysosomal degradation. Externalization of these protein domains can be detected using antibodies, namely A69 (epitope located on both VP1 and VP2) (Figure 5.3a).

While externalization of the PLA2 domain *in vivo* is crucial for virus infectivity, for our goal of developing novel nanoscale materials we sought to reprogram this functionality by replacing the domain with other functional motifs. As the first proof-of-concept demonstration that the AAV capsid is amenable to such alteration and retains its dynamic behavior, we have created VNPs that develop the ability to bind metal upon external activation. To achieve this function, we replaced the PLA2 domain with a hexahistidine (His_6) tag (Figure 5.3). We show the VNPs maintain wild-type (wt) like dynamic behavior and, upon exposure to heat, develop the ability to bind nickel (Figure 5.3b).

5.3 Materials and Methods

Mutant plasmid construction. Plasmid AAV2-ΔPLA2-His was constructed using the AAV2 wild-type genome. Genes *rep* and *cap* were excised from plasmid pSub201 using an XbaI restriction digest and cloned into vector pBluescript II SK (+) (Agilent, Santa Clara, CA). Using site-directed mutagenesis (Agilent), an EagI site in the multiple cloning site of pBluescript was silenced. An EagI site was introduced directly upstream of the PLA2 domain and consecutive EagI and MluI sites were introduced directly

downstream. The vector was digested with EagI and religated, removing the PLA2 domain and allowing for the insertion of a hexahistidine tag through directional cloning. The *cap* fragment was then excised and cloned back into the AAV2 genome flanked by ITRs.

Virus production. Virus was produced as described elsewhere.[54] Briefly, plasmid AAV2-ΔPLA2-His or pSub201 were co-transfected with pXX6 (to create mutant or wild-type virus, respectively) into 293T cells using polyethylenimine. Virus was isolated using ultracentrifugation and an iodixanol step gradient. Virus titers were determined by quantitative real-time PCR (QPCR) using SYBR Green PCR Master Mix (Applied Biosystems, Foster City, CA) with primers directed against *rep*.

Western and dot blots. For Western blot analysis of capsid proteins, wild-type AAV2 and AAV2-ΔPLA2-His were denatured in NuPAGE LDS buffer for 30 minutes at 75°C. Samples were electrophoresed in NuPAGE 7% Tris-acetate gels according to manufacturer protocol (Invitrogen, Carlsbad, CA). Protein was then wet transferred to Hybond ECL nitrocellulose membrane (GE Healthcare, Piscataway, NJ) and blocked in 5% skim milk in PBS-T (137 mM NaCl, 2.7 mM KCl,10 mM Na_2HPO_4, 2 mM KH_2PO_4, 0.1% Tween-20). Membranes were probed for VP capsid proteins and His_6 tag using mouse monoclonal B1 and α-His antibodies, respectively (both 1:50 dilution; American Research Products), followed by incubation with HRP-conjugated goat anti-mouse IgG antibody (1:2000 dilution; Jackson Immunoresearch, West Grove, PA). Lumi-Light Western blotting substrate (Roche Diagnostics, Indianapolis, IN) was added to each membrane and the resulting stains digitally visualized.

For immuno-dot blot detection of externalized N-termini and His_6 tags, virus was diluted in PBS (137 mM NaCl, 2.7 mM KCl,10 mM Na_2HPO_4, 2 mM KH_2PO_4) and transferred to nitrocellulose membrane using a Bio-Dot microfiltration apparatus according to manufacturer protocol (Bio-Rad, Hercules, CA). Membranes were incubated with monoclonal mouse A20, A69, B1, or α-His antibodies (American Research Products) and visualized as above.

Heparin binding assay. Wild-type and AAV2-ΔPLA2-His VNP heparin binding profiles were determined by using HiTrap Heparin HP columns (GE Healthcare). The column was loaded with 500 µL of 1-5e12 virus genomes/ml and eluted with increasing concentrations of NaCl solution. Fractions from each elution were collected and titers were determined by using QPCR with primers against *rep*.

Nickel column purification. Binding of VNP to nickel affinity columns was quantified using QPCR. Wild-type and AAV2-ΔPLA2-His VNP (1-5e12 virus genomes/ml) was incubated at 37°(n=2), 60°(n=5), 63°(n=3), 65°(n=9), or 75°C (n=2) for 30 min and loaded onto His SpinTrap nickel affinity columns (GE Healthcare). Columns were washed with 20 mM imidazole and eluted with three applications of 500 mM imidazole solution. Fraction titers were determined using QPCR as above.

Statistical analysis. Statistical analysis was performed using SPSS v11.5 (IBM). One-way ANOVA calculations were performed to compare the various groups and Bonferroni post-hoc analysis was utilized to find differences. P values less than 0.05 were reported as statistically significant.

5.4 Results

Successful replacement of PLA2 domain with His_6 tag. We have created a virus variant, named AAV2-ΔPLA2-His, where the PLA2 domain has been replaced with a His_6 tag. Utilizing site-directed mutagenesis, we replaced the native PLA2 domain located on the N-terminus of VP1 subunit with nucleotides encoding for a His_6 tag. After verification of correct plasmid sequence (data not shown), we used the triple transfection method followed by ultracentrifugation on an iodixanol step gradient to obtain the VNPs. The titer of AAV2-ΔPLA2-His, as quantified with real-time quantitative PCR (QPCR), is equivalent to wild-type capsid AAV2 (wtAAV), ranging from 4.3×10^{12} to 2.9×10^{13} virus genomes/ml depending on the batch. To confirm proper expression of the His_6 tag in the VP1 capsid subunit, Western blots were performed using B1 and anti-His_6 (α-His) antibodies (Fig. 5.4). The B1 antibody binds to the C-terminus of all three capsid subunits. The B1 blot confirms a smaller VP1 subunit in AAV2-ΔPLA2-His due to replacement of the 60 amino acid (aa) PLA2 domain with the 6 aa His_6 tag (Fig. 5.4, left). The VP2 and VP3 proteins are of equal size, as expected, in comparison between the AAV2-ΔPLA2-His and wt virus. In addition, AAV2-ΔPLA2-His qualitatively has the proper 1:1:10 stoichiometric ratio of the three capsid subunits. Utilizing the α-His antibody, we confirm that only VP1 in AAV2-ΔPLA2-His contains the desired His_6 tag (Fig 5.4, right).

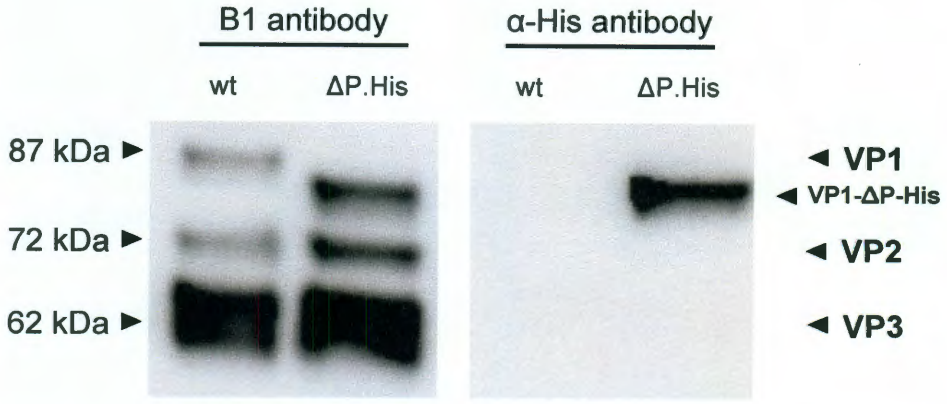

Figure 5.4. Successful generation of AAV2-ΔPLA2-His VNP. (Left) Western blot of wt and AAV2-ΔPLA2-His (ΔP.His) VNPs using B1 antibody that binds to the C-terminus of all three capsid proteins. Blot demonstrates smaller VP1 of AAV2-ΔPLA2-His VNP due to replacement of PLA2 domain with a substantially shorter His_6 tag. Sizes of VP2 and VP3 are unchanged. (Right) Western blot of wt and AAV2-ΔPLA2-His VNPs using α-His antibody. Positive signal is observed only for VP1 of ΔP.His, demonstrating subunit specific insertion of the His_6 tag. VP markers corresponding to different subunits is indicated left of blot.

Temperature reactive properties of AAV2-ΔPLA2-His capsid similar to wt. Next, we performed a dot blot assay to demonstrate the His_6 tag is both internal to the capsid in the unactivated state and is properly externalized upon external stimulation, similarly to wt virus. AAV2-ΔPLA2-His and wtAAV were incubated at different temperatures for 30 minutes, applied to a nitrocellulose membrane, and probed with various antibodies (Fig 5.5). A20 detects intact AAV2 capsids and B1 detects a buried C-terminal epitope common to all 3 VPs that becomes exposed upon capsid denaturation. A69 detects an N-terminal epitope present in VP1 and VP2 that becomes exposed upon VNP activation (or denaturation), and α-His detects the His_6 tag.

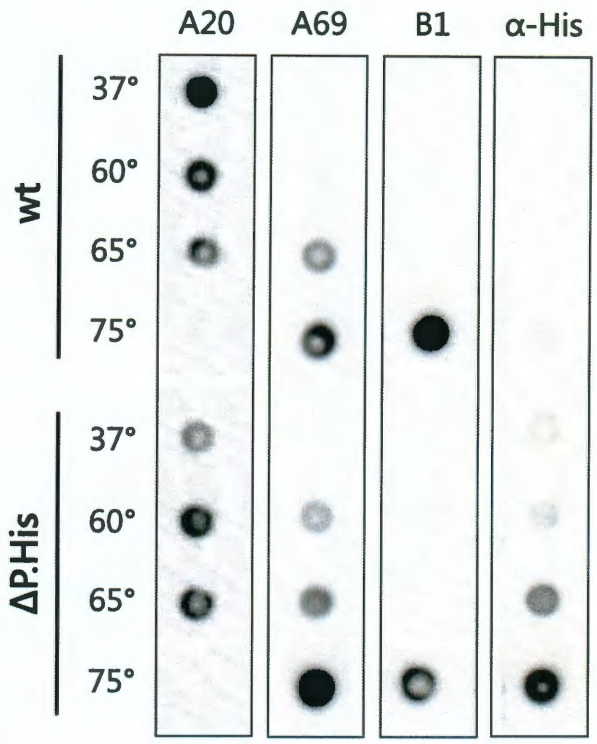

Figure 5.5. Dot blot of wt and AAV2-ΔPLA2-His (ΔP.His) VNPs after 30 minute exposure to various temperatures. A20 binds intact virus capsids, A69 binds N-termini of VP1 and VP2, and B1 binds C-terminus of all three VPs (only accessible when capsid has been denatured). α-His binds to His_6 tag. The blot demonstrates intact capsids at 37°, 60°, and 65°C for both wt and ΔP.His. N-termini externalization occurs at 65°C for both VNPs and His_6 tag is evident only for ΔP.His. Heating to 75°C results in capsid denaturation and all epitopes, except for A20, are accessible.

At 37°C, both wtAAV and AAV2-ΔPLA2-His VNPs are positive for A20 and negative for B1, indicating capsids are intact. Importantly, no staining is evident for A69 or α-His for the mutant virus, indicating these residues are internal to the capsid. The capsid structure remains intact at 65°C, but externalization of the N-termini is evident by the presence of positive A69 staining. Faint A69 and α-His staining are observed at 60°C in our AAV2-ΔPLA2-His virus, representing the accepted temperature range of N-termini externalization. When exposed to 75°C, both samples show a negative A20 staining and

a positive B1 staining, indicating the capsids are denatured. Lastly, utilizing an α-His antibody, we demonstrate that the His_6 tag externalizes upon stimulation of AAV2-ΔPLA2-His at 65°C and that no His_6 tag is present on wtAAV. Collectively, we have shown that insertion of the His_6 tag does not appear to interfere with the supramolecular assembly of the capsid or modify its conformational change dynamics. The His_6 tag is buried inside the VNP until it becomes externalized upon stimulation at approximately 65°C.

Heparin binding properties of AAV2-ΔPLA2-His capsid similar to wt. An affinity assay was performed to determine if AAV2-ΔPLA2-His maintained the wt ability to bind heparin (Fig. 5.6). WtAAV2 binds heparan sulfate proteoglycans as its natural receptor in humans.[49, 92] Here, we are interested in modifying a specific functional output of the VNPs (e.g. externalization of active peptide domains) while maintaining all other virus features, such as binding properties of the capsid. Virus samples from either wt or AAV2-ΔPLA2-His populations were added to a heparin-agarose affinity column. The column was subsequently washed with buffer containing increasing salt concentrations, and the concentration of virus genomes in each fraction was determined using QPCR. The elution profiles of the two virus samples are similar, sharing a characteristic peak elution at 500 mM NaCl. The result suggests that insertion of the His_6 tag in the VP1 N-terminus does not affect heparin binding properties of the VNP.

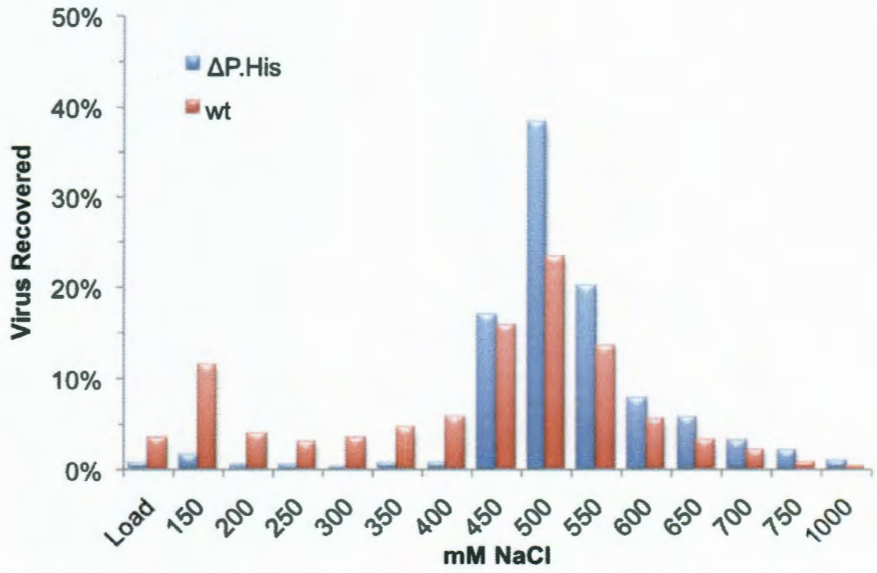

Figure 5.6. Heparin affinity assay demonstrates similar binding of wt and AAV2-ΔPLA2-His VNPs. Both wt and AAV2-ΔPLA2-His (ΔP.His) VNPs display similar peak elutions at 500 mM NaCl. Results from one representative experiment are shown.

AAV2-ΔPLA2-His binds nickel upon activation with heat. We next investigated the ability of AAV2-ΔPLA2-His to externalize His_6 tags and bind nickel upon stimulation with heat. If successful, this would be the first proof-of-concept demonstration of reprogramming the dynamic externalization of functional motifs on the AAV capsid. AAV2-ΔPLA2-His and wt viruses were incubated at 60° or 65°C and then loaded onto nickel columns (Figure 5.7). After washing and eluting with an imidazole buffer solution, virus genomic content in the collected fractions was analyzed using QPCR. When heated to 65°C, only 12% of wtAAV is recovered in the elution. In contrast, approximately 39% of the AAV2-ΔPLA2-His viral load is recovered when the mutant is activated at 65°C. The 3.2-fold enhancement in recovery is statistically significant ($p < 0.005$). Activation at 60°C also increases the amount of AAV2-ΔPLA2-His recovered in the elution compared to wt, but the difference is not statistically significant. This result

corresponds well to our dot blot results (Figure 5.7), suggesting the His_6 tags on the AAV2-ΔPLA2-His VNPs are both externalized and functional at 65°C.

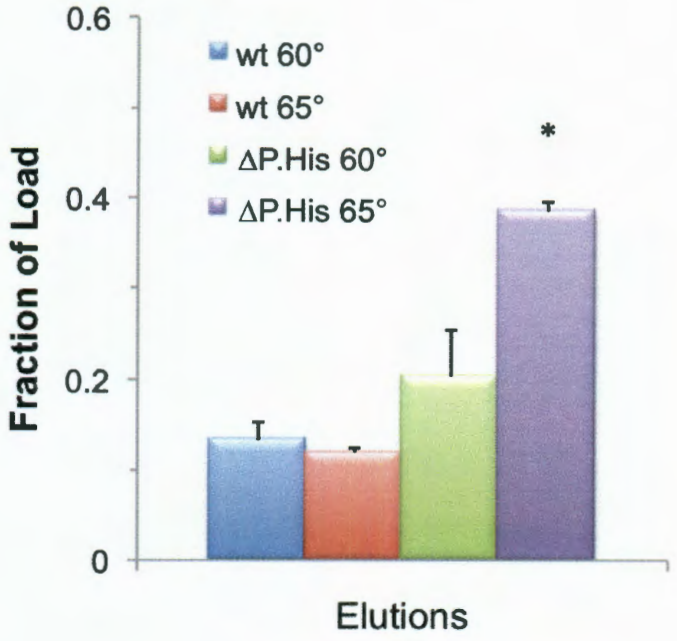

Figure 5.7. AAV2-ΔPLA2-His VNP binds nickel upon activation with heat. AAV2-ΔPLA2-His (ΔP.His) and wt VNPs were exposed to 60° and 65°C for 30 minutes, loaded onto Ni affinity spin columns, and eluted with an imidazole buffer. Activation of ΔP.His at 65°C results in significantly greater amount of VNP captured and eluted from the column, suggesting not only that the His_6 tag is functional but also that this activity can occur at a range of temperatures. Amount of virus in elutions was determined by QPCR and data represent mean values (error bars represent standard error of the mean). Asterisk indicates $p < 0.05$ for comparison to all other groups.

Optimal activation temperature exists for AAV2-ΔPLA2-His binding nickel. We sought to further narrow down the optimal activation temperature for externalizing the His_6 tags. We exposed the intact mutant virus to 37°, 60°, 63°, 65°, and 75°C prior to

loading onto nickel affinity columns (Figure 5.8). Virus genomes in elution fractions were again quantified using QPCR. Compared to the 20% recovered with 60°C activation, exposing the viruses to 63°C increases the amount recovered to 44%. A similar improvement of VNP recovery was seen at 65°C as well. These values are statistically significant when comparing the 63° and 65°C groups to the other temperatures. The difference between 63° and 65°C groups is not statistically significant. The control treatment of AAV2-ΔPLA2-His at 37°C is not expected to yield high recovery since N-terminus externalization does not occur at this temperature (Figure 5.5). Furthermore, exposure of the virus to 75°C fully denatures the capsid (Figure 5.5); therefore the released virus genomes are expected to pass through the column during the loading and washing steps, resulting in little recovery in the elutions. Indeed, the expected outcomes for 37°C and 75°C treatments are observed.

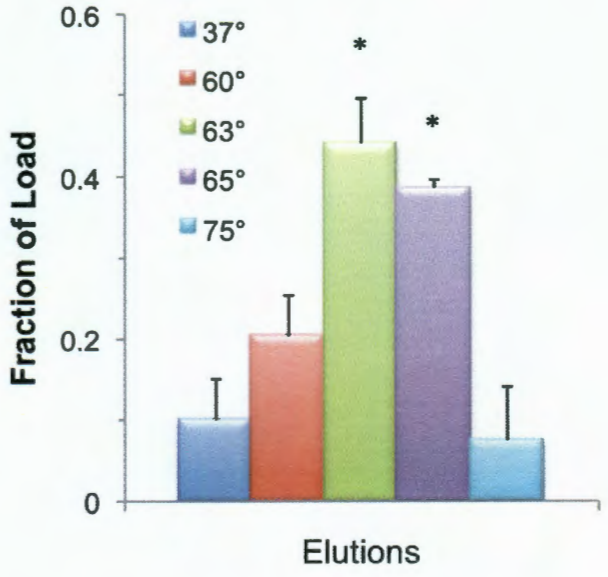

Figure 5.8. Binding of AAV2-ΔPLA2-His VNP to nickel is modulated by temperature. AAV2-ΔPLA2-His VNP was exposed to 37°, 60°, 63°, 65°, and 75°C for 30 minutes, loaded onto Ni affinity spin columns, and eluted with an imidazole buffer. AAV2-ΔPLA2-His stimulated at 63° or 65°C yields the greatest binding to nickel. Virus capsid denatures at 75°C and, therefore, elution is not above the 37°C control. Amount of VNP in elutions was determined by QPCR and data represent mean values (error bars represent standard error of the mean). Asterisk indicates $p < 0.05$ for 63° and 65°C samples in comparison to the 37°, 60°, and 75°C groups. There was no statistically significant difference between the 63° and 65°C groups.

Verification of capsid properties after temperature activation and nickel binding. To confirm VNP integrity and interrogate capsid conformational status after elution from the nickel column, we performed dot blots on VNPs in the elution fractions. After heating VNP samples to 65°C, we evaluated AAV2-ΔPLA2-His and wt capsids both prior to column loading and after elution (Figure 5.9). Appropriately, the wtAAV has strong A20 (intact capsid) and there is no signal for the α-His antibody in the preload fraction. A weak A20 signal is present in the elution fraction. As 65°C is close to the upper limit of capsid stability, we have a faint B1 signal in the wt sample. The AAV2-ΔPLA2-His VNP

sample demonstrates that both the pre-load and the elution fraction demonstrate a strong positive signal for A20, and α-His. This result is expected and further supports the hypothesis that externalization of His_6 tags upon heating confers metal-binding functionality to the AAV2-ΔPLA2-His VNPs.

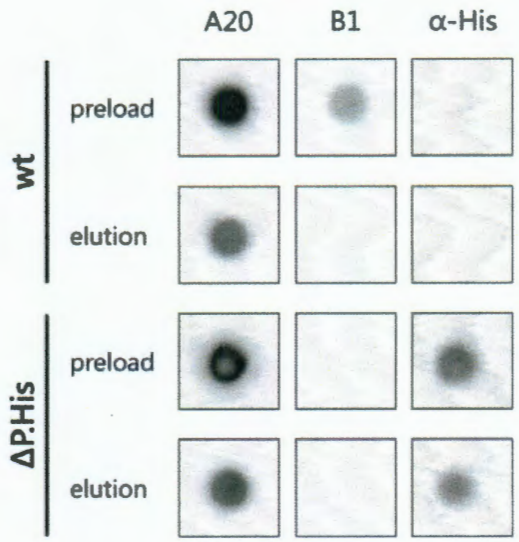

Figure 5.9. AAV2-ΔPLA2-His VNP capsid remains intact after Ni column. AAV2-ΔPLA2-His (ΔP.His) and wt VNPs were exposed to 65°C for 30 minutes, loaded onto Ni affinity spin columns, and eluted with an imidazole buffer. The preload VNPs and the elution fraction were evaluated using dot blot. A20 binds intact virus capsids, B1 binds C-terminus of all three VPs (only accessible when capsid has been denatured), and α-His binds to His_6 tag. The blot demonstrates intact capsids for both wt and ΔP.His (with minimal denaturing for wt preload) both before and after Ni column. The His_6 tag is evident only for ΔP.His virus.

5.5 Discussion

To reprogram the functional output of the AAV capsid conformational change behavior, we replaced the PLA2 domain in the N-terminus of VP1 with a His_6 tag. As demonstrated by Western blot (Figure 5.4), the His_6 is appropriately expressed only on

VP1. The virus variant capsid successfully self-assembles similarly to wt, with N-termini inaccessible to antibodies at 37°C (Figure 5.5). Furthermore, the temperature-induced conformational change behavior, predominantly characterized by the surface display of VP1 and VP2 N-termini, occurs under similar conditions between the mutant and wt VNPs. Specifically, incubating both VNPs at 65°C for 30 minutes results in N-termini externalization while maintaining the integrity of the intact capsid. These results, combined with the maintenance of heparin binding by the mutant (Figure 5.6), strongly support our conclusion that we have only modified the functional output of the capsid conformational change, leaving capsid assembly, binding properties of the capsid exterior, and conformational change dynamics of the capsid unaltered.

We next demonstrated that the inserted His_6 tag is not only functional, but is externalized only upon external stimulation with heat. This was observed through immunoblotting and nickel affinity column assays (Figure 5.7 & 5.8). Upon activation at 63° or 65°C, His_6 tags previously internal to the VNP become surface-exposed and the VNP is able to bind nickel at levels significantly greater than before activation. This temperature range appears to yield maximum N-terminus externalization while maintaining capsid integrity. Additional studies are necessary to improve the amount of mutant virus bound and eluted from the nickel columns and decrease the amount of wt virus found in elution fractions. Optimizing imidazole concentrations in the wash and elution steps may help increase virus yield and differentiation.

Theoretically, each AAV particle will only externalize five His_6 tags, underscoring the importance of each binding event in holding the almost 4 MDa virus capsid in place during the column washing steps. Furthermore, a distribution of capsid subunit

stoichiometries per VNP likely exists, generating a subset of capsids with greater than five His_6 tags per VNP and some with less. Recently, Koerber et al. and Zhang et al. inserted His_6 tags into surface exposed regions on the AAV capsids.[92, 93] These insertions resulted in the presentation of 50-60 nickel binding sites per VNP, leading to a substantial increase in virus binding to a nickel column. In our investigation, however, lower binding is not unexpected given the ten-fold lower number of potential binding motifs. Whether this lower binding efficiency is acceptable will be determined in future studies and will likely be dependent on the particular conferred functionality and ultimate application. Any potential reversibility of the N-termini externalization process would also decrease the number of His_6 tags available for nickel binding. There is no evidence to suggest that this process is reversible, but further studies are required to conclusively answer this crucial question.

5.6 Conclusions

We present the first proof-of-concept demonstration that the functional output of the AAV-based VNP, in response to a specific external stimulus, can be reprogrammed. In particular, we exploited the intrinsic property of the VNP to dynamically externalize peptide domains upon stimulation with heat in order to create genetically encoded nanoparticles that possess the potential to bind a variety of metal ions (Ni, Cu, Zn, or Co) upon heat exposure. Utilizing AAV's unique ability to externalize a previously hidden protein domain is an innovative approach to designing supramolecular switches. Incorporation of other functional domains should enable the VNP to carry out more sophisticated tasks.

Furthermore, our studies have revealed insights into the process of VP1 N-terminus externalization. We demonstrated that the PLA2 domain is not required for N-terminus externalization. Additionally, since mutant VNPs with His_6 tags can be isolated with nickel columns, the insertion location is sufficiently accessible for binding to external surfaces.

Overall, the studies presented here lay the groundwork for developing intelligent, genetically encoded nanoparticles with novel functions. Further advancements to nanoparticle design will help broaden and strengthen the application of virus based nanoscale materials for human use.

CHAPTER SIX

Directed evolution of adeno-associated virus for modification of tropism and capsid dynamics

6.1 Acknowledgements

I would like to thank Kelly Horn for her contributions to preliminary EP-PCR troubleshooting and Chris Dempsey for running flow cytometry studies for serotype analysis.

6.2 Introduction

In Chapters 2-5 we have explored the use of AAV virus particles for non-conventional applications. We have shown that AAV can be efficiently immobilized for tissue engineering applications as well as for high-throughput microarray studies. We have also shown that the virus output of AAV can be altered for the presentation of alternative domains. However, for AAV to be most effective in these and other applications, the virus must be specific in either its tropism or stimuli that it detects. To address these needs, we are using directed evolution to create tailored AAV vectors with the efficiency and specificity required for our applications.

AAV viral vectors are currently being tested in over 75 human clinical trials. The ultimate efficiency and success of *in vivo* gene delivery is highly dependent on effective virus localization and transduction efficiency. Bottlenecks to delivery include antibody neutralization and binding to and being processed in the target cells. To address these concerns, several directed evolution methods, including DNA shuffling,[32-34] error-prone

polymerase chain reaction (EP-PCR),[27, 28] peptide display,[29, 30] and transposon mutagenesis[31], have been used to optimize AAV gene delivery. Successful mutants have been found to evade serum neutralization, infect coronary artery cells, infect brain cells, and infect glioma cells, among other applications.[29-36]

We are interested in using directed evolution to generate vectors for 2 applications: 1) improved transduction efficiency in target cells, and 2) altered activation temperature threshold.

A promising new strategy for cancer treatment involves the delivery of apoptotic shRNA. For these strategies to be successful, we must have a vector capable of efficiently delivering these cassettes to cancer cells. In our lab, we are interested in targeting ovarian cancer cells. First, to determine the native efficacy of AAV serotypes on ovarian cancer cells, we tested the transduction efficiency of AAV1-9 and AAV12 on a panel of ovarian cancer cells, using an MOI of 1000 virus particles per cell (Figure 6.1A-G). HeLa cells were used for comparison, as they are highly permissive to AAV2 infection. Very low levels of transduction are seen in most ovarian cancer cell types. To create viral vectors capable of delivering nucleic acids with high efficiency to ovarian cancer cells, we have decided to use directed evolution. This approach involves the generation of large, diverse virus libraries and the application of appropriate selection strategies to isolate improved variants. AAV2 transduces HeyA8 cells with at a modest 34% at this relatively low MOI. Because of this pre-existing level of transduction, we have selected these cells as the target cells for our selection strategy. It will be our first goal to isolate a pool of mutants with increased efficiency in transducing this cell line.

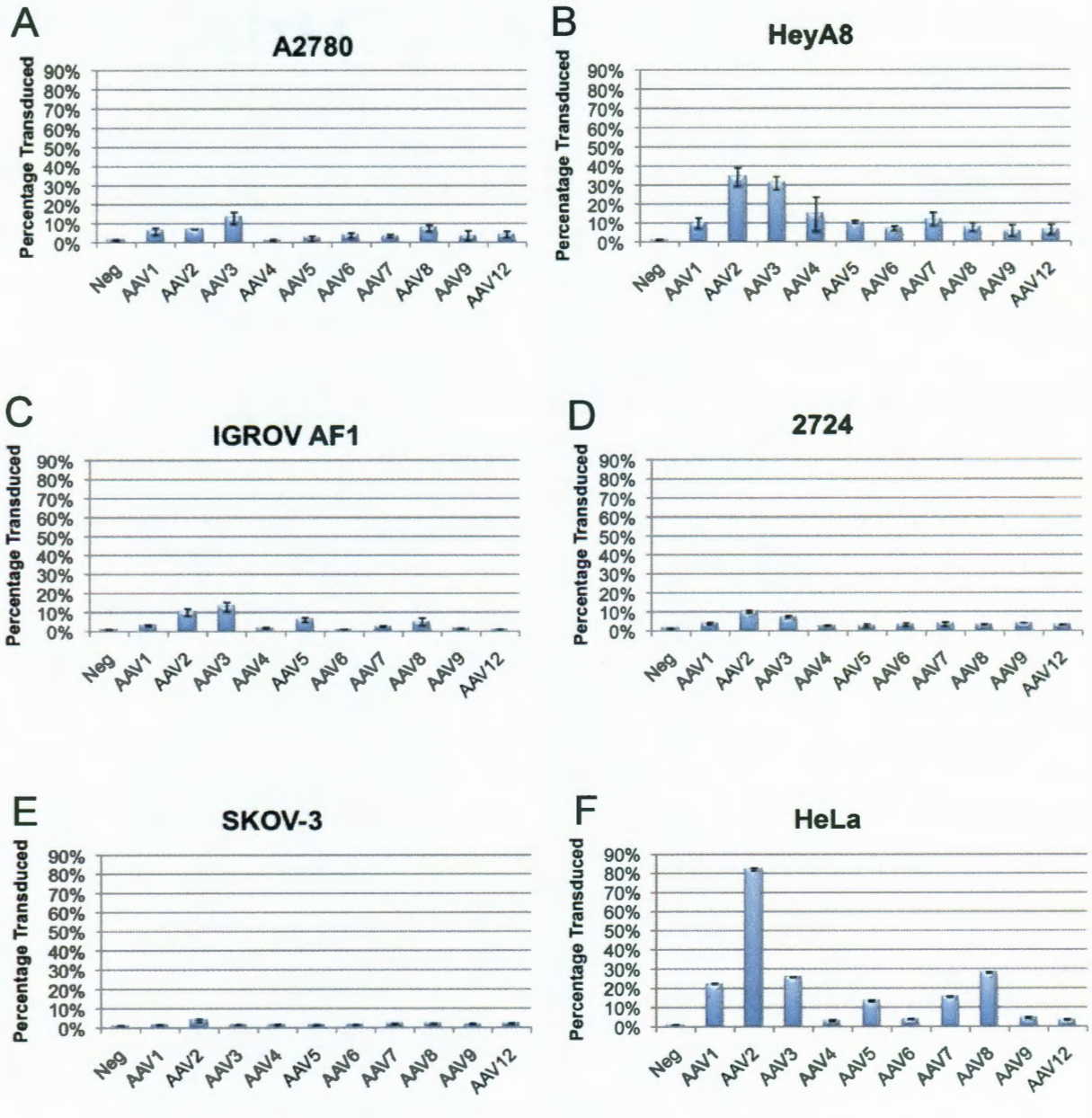
A
A2780
B
HeyA8
C
IGROV AF1
D
2724
E
SKOV-3
F
HeLa
Percentage Transduced
90%
80%
70%
60%
50%
40%
30%
20%
10%
0%
Neg
AAV1
AAV2
AAV3
AAV4
AAV5
AAV6
AAV7
AAV8
AAV9
AAV12

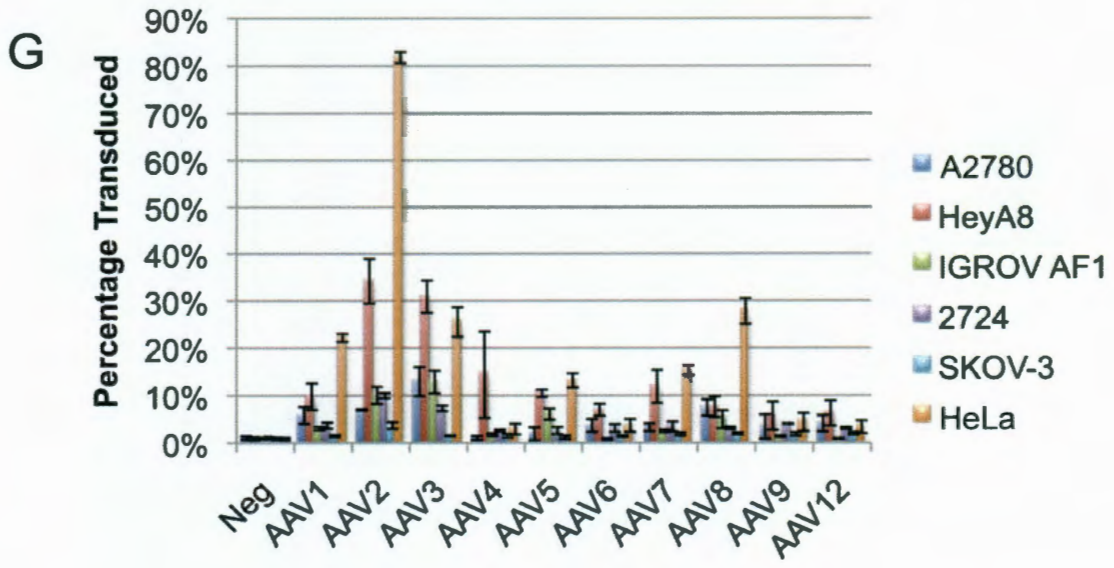

Figure 6.1. Transduction of ovarian cancer cell lines by ten AAV serotypes. **(A)–(F)** Ovarian cancer cells (and HeLa cells as an AAV2 control) were infected with AAV serotypes at an MOI of 1000. **(G)** Ovarian cancer cells show very limited permissivity to AAV, as compared to HeLa cells. Cells were fixed 72 h post infection and GFP expression was quantified with flow cytometry.

In the second use of directed evolution, we are interested in modifying the activation temperature of AAV. In Chapter 5 we explored the use of AAV as a potential biosensor by modifying the N-terminus output upon temperature activation. As the ultimate goal of this work is to control the virus "input" and "output", it is crucial that we gain more information about the 'input' properties of the virus particles. Currently, response to heat is being investigated as a potential proof-of-concept input. We are developing libraries of mutant virus to isolate clones with modified temperature response profiles. As a first step, we are looking to isolate clones that externalize their N-terminal residues at temperatures lower than 60°C. In other words, we hope to identify less thermostable AAV variants.

The library creation process is similar for both applications. First, we used the wild-type AAV2 *cap* as a template for mutagenesis (Figure 6.2). DNA was mutagenized using an EP-PCR procedure and cloned into a *cap*-free vector to reform the virus genome.[28] Libraries were generated using Taq polymerase, $MgCl_2$, an unbalanced dNTP ratio, and $MnCl_2$. Taq polymerase is reported to have an error rate of $2.4x10^{-4}$ mutations per base for each amplification cycle.[94] Taq's natural bias for AT to GC mutations will be mitigated using an unbalanced dNTP ratio including a lower concentration of dATP and dGTP relative to dTTP and dCTP.[95] An increased concentration of $MgCl_2$ further facilitates error incorporation by stabilizing non-complementary base pair binding.[96] Increased concentrations of $MnCl_2$ lead to an increased occurrence of point mutations, due to the interaction of Mn^{2+} with DNA.[97] Re-ligated vectors were transformed into and propagated in E.Coli. DNA was isolated from these cells and transfected (along with helper plasmids) into 293T packaging cells. Virus mutants will be isolated and selection strategies will be applied. Potential mutants of interest will be studied via QPCR, western blot, and sequencing. Mutant DNA can then be subcloned into the original vector to create new virus libraries to be further enriched through additional rounds of selection.

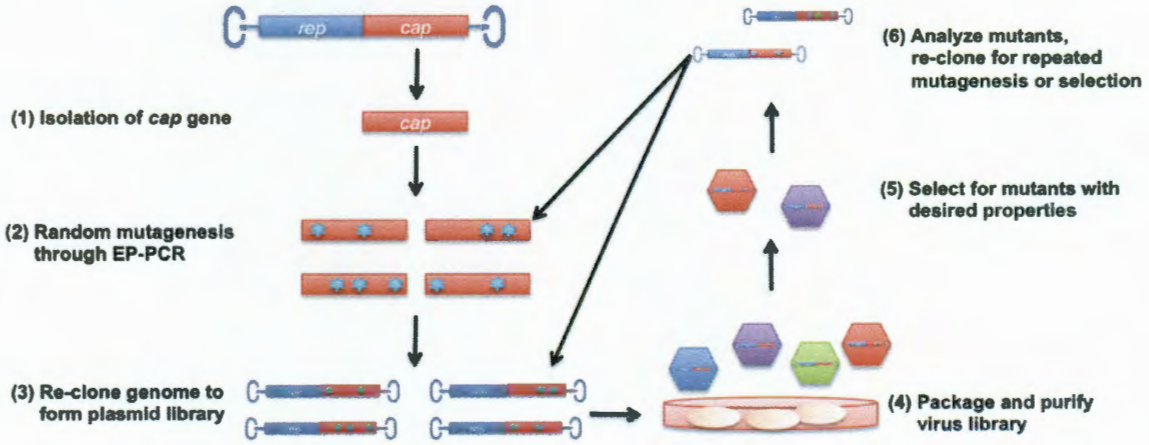

Figure 6.2. Overview of directed evolution procedure. AAV *cap* genes are isolated, mutagenized, and cloned into the remaining AAV2 genome to create mutant vectors. These plasmids are used to package virus in HEK 293T cells. Virus particles are harvested, purified, and applied to a selection strategy. Successful mutants are isolated and characterized, then subjected to additional mutagenesis and selection.

Our first library, AAV2-EP, will be used to isolate virus mutants with increased transduction efficiency in ovarian cancer cells. Diversity in this library has been confirmed and the final error rate is 2/1000bp of *cap* gene, or approximately 5 errors per *cap* gene. Preliminary selection studies have been conducted to begin isolating mutants with increased gene delivery efficiency.

Our ΔPLA-His externalization library (ΔP.His-EP) is based on the AAV-ΔPLA-His construct developed in Chapter 5. A virus library with 2.8/1000bp of *cap* gene, or approximately 7 errors per *cap* gene has been generated based on AAV-ΔPLA-His. Initial selection schemes involve the isolation of mutants with temperature responsive properties that are slightly different from the wild-type virus. In particular, we are

isolating pools of mutants that are capable of N-terminus externalization at a sub-optimal temperature (58°C). Nickel-NTA columns used in Chapter 5 have been used to capture mutants with this capability. After further enrichment, amino acid changes in these mutants will be studied in order to draw conclusions about the mechanism for N-terminus externalization, as this phenomenon is very poorly understood.[23, 24, 98] Once we have a better understanding of this dynamic property of the virus, we can begin to engineer alternative inputs. These novel stimuli may be small molecules or proteins present in a sample of interest.

6.3 Materials and Methods

Cell transduction assays. Ovarian cancer cells were cultured at 37 °C with CO_2. 2774 cells (cultured in MEM supplemented with 5% FBS, 1x L-glutamine, 1x Sodium Pyruvate, 1x MEM-NEAA, and 1% penicillin/streptomycin), A2780 (RPMI1640 supplemented with 15% FBS and 1% penicillin/streptomycin), HeyA8 (RPMI1640 supplemented with 15% FBS and 1% penicillin/streptomycin), IGROV-AF1 (RPMI1640 supplemented with 10% FBS and 1% penicillin/streptomycin), and SKOV-3 (DMEM supplemented with 10% FBS and 1% penicillin/streptomycin) were tested for their permissivity to ten AAV serotypes. HeLa cells (cultured in DMEM with 10% FBS and 1% penicillin/streptomycin) were used as a positive control for AAV2 transduction. Cells were passed to 24 well plates and transduced the next day at a confluency of ~75-80%. Cells were transduced with AAV1-9 and AAV12 at an MOI of 1000. Cells were harvested 72 hours post infection, were fixed with 4% PFA-PBS, and added to FACS tubes with cap filters. Samples were performed in triplicate using a FACSCantoII (Becton Dickinson, Franklin Lakes, NJ), with 1e4 cells analyzed for each sample.

Error-prone PCR. pSub201 and AAV2-ΔPLA2-His were used as templates for EP-PCR. Primer C (5'-GCGGAAGCTTCGATCAACTACGF-3') and Primer K (5'-GGGACTAGTAATTACAGATTACGAGTCAGGTATCTGGTG-3') were used to amply the *cap* sequence from the 5'- and 3'- end and introduce HindIII and SpeI sites, respectively. Primers were used at a concentration of 50 µM. Reaction conditions were used as those by Koerber et al.[28] Mutagenic buffer (70mM $MgCl_2$, 500 mM KCl, 100 mM Tris (pH 8.3), 0.1% (wt/vol) gelatin) and Taq polymerase (NEB, Ipswitch, MA) were used to introduce mutations. An unbalanced 10X dNTP mix (2mM dATP, 2 mM dGTP, 10 mM dCTP, 10 mM dTTP, Invitrogen) was also used. Final reaction conditions were: mutagenic buffer (5 µl), 5 mM $MnCl_2$ (1.5 µl), 10X dNTP mix (5 µl), 50 µM Primer C (1 µl), 50 µM Primer K (1 µl), template DNA (10 ng/µl, 1 µl), Taq polymerase (5U/µl, 1 µl), and ultrapure water (34.5 µl). Samples were amplified by 24 rounds of PCR.

Vector creation. Plasmid vector pSub2SpeIStuff, a variation of that used by Koerber, et al[28], was used to create mutant virus libraries. This *cap*-free vector contains the virus ITRs and *rep* with adjacent restriction enzymes to directionally clone in the mutant *cap* genes. A SpeI restriction site was introduced instead of a NotI site. Between HindIII and SpeI restriction sites, a 1000bp non-coding region of the LacZ gene was introduced to confirm vector digestion.

Plasmid library creation. Amplified *cap* genes were isolated on 1% agarose gels. The approximately 2.6kb bands were purified using a Zymo Gel Extraction kit (Irvine, CA). Samples were digested for 1 hour at 37°C using HindIII and SpeI (NEB) and run on 0.8% agarose gel. Modified *cap* genes were cloned into pSub2SpeIStuff at a 1:3 ratio using T4 DNA polymerase (NEB). For each ligation, 100 ng of vector plasmid was used and

samples were ligated at room temperature for 1 h. Samples were purified into 10 µl water using a Zymo Clean and Concentrate kit. The full volume was then transformed into electrocompetent DH5α E.Coli cells (~1e9 cfu/1ug). Samples were allowed to recover 20 minutes and were plated onto LB plates containing ampicillin. To determine library diversity, 1 µL of the library was placed on a plate and colonies were counted the next day. Plasmid was harvested using a Zymo Miniprep kit or an Invitrogen PureLink Maxi prep kit.

Sequence verification. Clones were selected from each library for sequencing. Ten plasmid clones were sequenced using a primer upstream of the AAV2 heparin binding domain. Sequencing was performed by Lone Star Labs (Houston, TX). Sequences were aligned to the wt AAV2 sequence using VectorNTI 10 software (Invitrogen).

Virus library production. Virus was produced as describe by Koerber et al.[28] 293T cells were used to produce virus and were transfected using polyethyleneimine (PEI). Cells were transfected with 7 ng library plasmid, 25 µg pBluescript (stuffer plasmid to ensure that each cell only receives one library plasmid), and 25 µg pXX6. Cells were harvested 72 h post transfection and purified as in Chapters 2 and 3.

Western blot verification. Virus production was further verified using western blotting. Blots were performed on virus samples as in Chapter 5. ΔP.His-EP samples were probed with both B1 and anti-His_6 antibodies. AAV2-EP samples were probed with B1.

Virus library sequence verification. Virus library diversity was determined by sequencing ten virus mutants. Purified virus samples were lysed using heat and NaOH

treatment. Sequences were amplified using PCR and Primers C and K. Mutant *cap* genes were subcloned into pSub2SpeIStuff and transformed into electrocompetent DH5α cells. Ten clones were miniprepped, sequenced, and analyzed as above.

Virus selection on target cells. The AAV2-EP library was used for selection on HeyA8 ovarian cancer cells. Cells were seeded onto a 10 cm tissue culture dish. The next day, cells were transduced at a density of 75%. AAV2-EP was added at an MOI of 1000 and Ad5 was added at an MOI of 20. Cells were harvested 48 hours post infection, resuspended in buffer, and lysed using three cycles of freeze/thaw. Samples titers were quantified using QPCR. Mutant virus was re-applied using decreasing MOIs.

ΔP.His dot blot. Virus samples were diluted 1:40 and heat treated for 30 minutes at either 37, 58, 60, 63, 65, 70, or 75 °C. Dot blots were performed as in Chapter 5.

Nickel column selection. ΔP.His-EP library samples were activated at 58°C for 30 minutes and applied to a nickel spin column as in Chapter 5. Fractions were collected and virus concentrations were quantified using QPCR with primers against the *rep* gene. Virus *cap* genes were amplified using Primer C and Primer K and cloned back into pSub2SpeIStuff. Virus libraries were then created as listed earlier.

6.4 Results

Effect of $MnCl_2$ on AAV2 cap gene error rate. It is difficult to predict the amount of error that we must introduce to create virus mutants with our desired properties. In order to create the diversity that we need, it might be necessary to test libraries with varying

levels of mutations. Error rates can be modified by a number of factors. Polymerases can have variations in their native error rates, adding varying amounts of diversity. In these studies, we have used Taq polymerase, which has a native error rate of ~3 errors per 10,000 bp. However, by adding additional co-factors such as $MnCl_2$, we are able to further increase the error rate of our mutant product. We have shown that by using a constant concentration of Taq polymerase and template DNA we are capable of drastically altering the error rate of our product simply by modifying the amount of $MnCl_2$ added to our amplification reaction (Figure 6.3). This regulation of error rate will allow us to potentially modulate the conservative nature of our library. Too many errors can possibly lead to destabilization concerns, while too few errors may not give us the change in virus properties needed to achieve our goals. If the initial libraries do not yield our desired results, we can create additional libraries using more or less conservative amplification strategies, yielding lower or higher error rates. If we have introduced too much diversity and the capsid is destabilized, it would be possible to create libraries with lower levels of mutations. However, if virus particles are too close to wild-type and their phenotype has not been sufficiently altered, we can use more $MnCl_2$ to introduce higher levels of diversity.

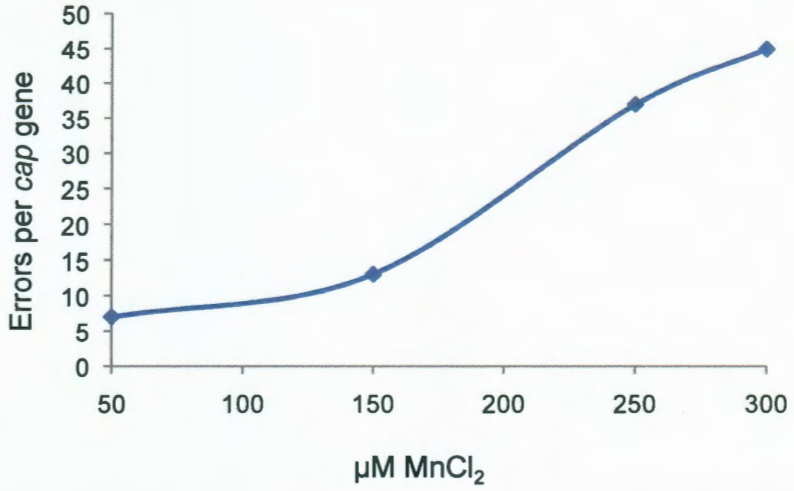

Figure 6.3. Effect of $MnCl_2$ on *cap* gene error rate. Increasing the concentration of $MnCl_2$ increases the observed error rate on the AAV2 *cap* gene.

Creation and verification of AAV2-EP virus libraries. Error-prone PCR libraries were created using Taq polymerase and $MnCl_2$. Mutant *cap* genes were purified on an agarose gel and cloned into a *cap*-free vector containing the remainder of the AAV2 genome. AAV2-EP (EP-PCR library based on wild-type AAV2 *cap* gene) plasmid library diversity was estimated at 1e6 library members (Table 6.1). After sequencing isolated clones, the error rate of the plasmid library was determined to be ~2.6errors/1000bp. The transition rate was determined to be 42%, while there were 58% transversions. There were no insertions or deletions, which is important as these could cause gene truncation and inhibit capsid formation.

Table 6.1 AAV2-EP Plasmid Library Analysis

Transitions	42%
Transversions	58%
Insertions/deletions	0%
Error rate	2.6bp/1000bp
Diversity	1e6

AAV2-EP virus libraries were created by transfecting 293T cells with 7 ng libray DNA per 15 cm tissue culture dish. Cells were co-transfected with helper plasmid pXX6 and pBluescript. Plasmid pBluescript was used as a filler to help ensure that only one library member would enter each cell. Multiple *cap* sequences in one cell could lead to mosaic capsids, since the supramolecular structure of the virus self-assembles. Virus titer was determined to be 1.57e11 vg/mL, a reasonable titer as most are in the range of 1e11-1e12 vg/mL (Table 6.2).

Table 6.2 AAV2-EP Virus Library Analysis

Transitions	64%
Transversions	36%
Insertions/deletions	0%
Error rate	2bp/1000bp
Titer	1.57e11 vg/ml

AAV2-EP virus library error rate was determined to be 2bp/1000bp, slightly less than that of the plasmid library. This is reasonable as variants with higher error rates might be less likely to form viable capsids. In contrast to the plasmid library, the virus library had 64% transitions and 36% transversions, a shift towards more transitions. There were no

observed insertions or deletions, as these mutations would be expected to yield incomplete capsids.

Western blot analysis shows that the appropriate virus subunit sizes and ratios are maintained in the virus library (Figure 6.4). As compared to wt AAV2, AAV2-EP has the same VP1, VP2, and VP3 subunit sizes (87, 72, and 62 kDa, respectively). The characteristic stoichiometic 1:1:10 virus subunit ratio is also preserved.

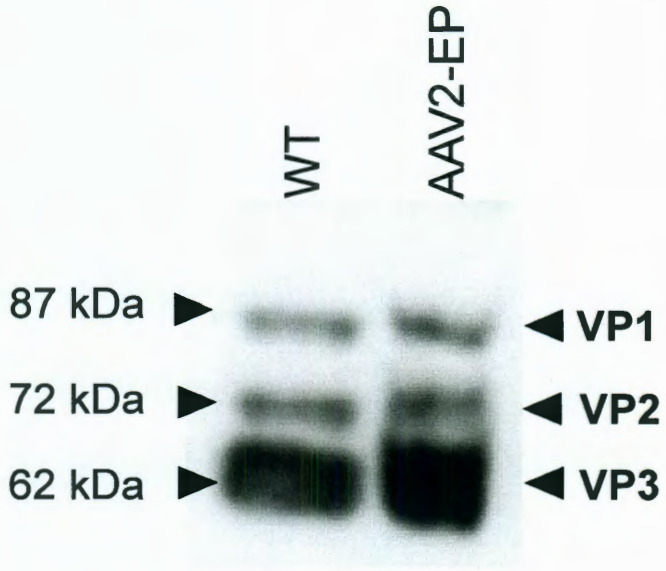

Figure 6.4. Western blot of wt AAV2 and AAV2-EP. Similar band sizes and stoichiometric ratios are observed when wt AAV2 and AAV2-EP are probed with B1 antibody, indicating that no significant change in virus capsid structure has occurred.

Selection of mutants with increased HeyA8 transduction efficiency. Our first selection goal is to isolate an AAV2 mutant with increased capacity to transduce HeyA8 ovarian cancer cells for shRNA therapy. We applied our AAV2-EP virus library to cells at an MOI of 1000. Cells were co-infected with adenovirus at an MOI of 20, as adenovirus is required for the replication of AAV. After 48 h, cells were scraped and resuspended in buffer. After three cycles of freeze-thaw to lyse the cells, cell debris was spun down and viral content in the supernatant was quantified using QPCR. This pool of mutant virus was applied to cells for the next round of selection. Overall, five rounds of selection were performed with decreasing MOIs (Figure 6.5).

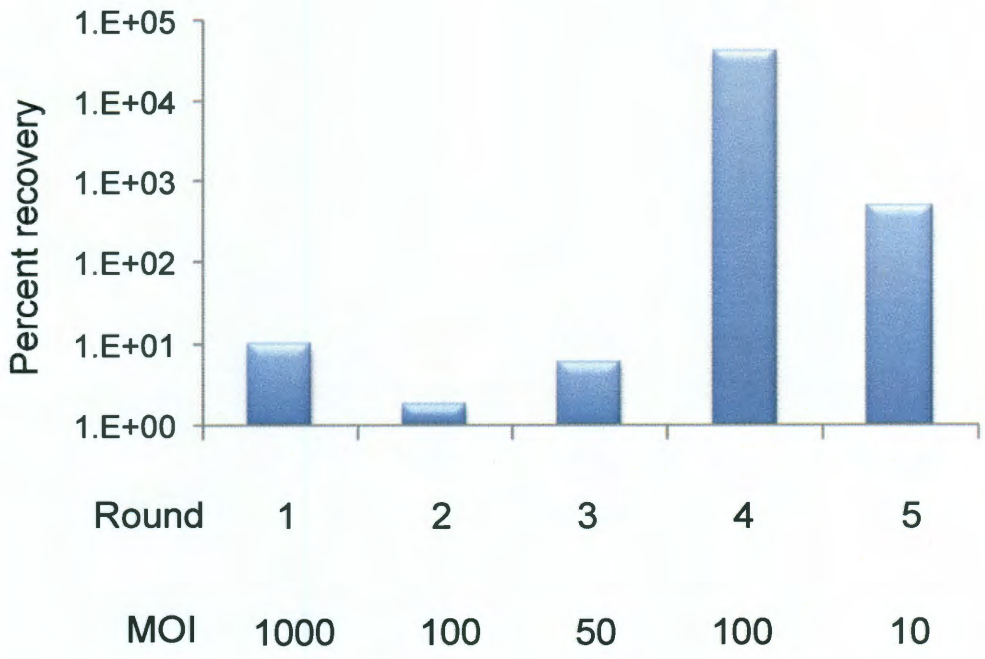

Figure 6.5. Mutant virus recovery over five rounds of selection. AAV2-EP was applied to HeyA8 cells at decreasing MOIs. Virus was co-infected with adenovirus to allow for replication. Virus titers were quantified after each round using QPCR.

Analysis of isolated virus pool. After five rounds of selection, virus *cap* genes were isolated by lysing the viral capsids. Genes were amplified using primers outside of the mutant *cap* genes and sublconed into the previously used pSub2Spelstuff vector for sequencing and virus production. Mutant pool transduction efficiency was directly compared to that of the wild-type by conducting a side-by-side transduction analysis. HeyA8 cells were either infected with wild-type AAV2 or our enriched pool at an MOI of 1000. Cells were co-infected with adenovirus at an MOI of 20. Cells were lysed 48 h post-infection and viral content was quantified using QPCR (Table 6.3). The enriched pool yields a 8700% increase in recovery over the wild-type virus. To analyze clones in this enriched pool, ten sequences were analyzed to determine mutations in the successful clones (Table 6.3). However, no clones tested yielded similar mutations. This suggests that we may not have found the "fittest" mutant in our pool. Additional, tighter selection conditions might help isolate the most successful clones.

Table 6.3 HeyA8 Selected Library Analysis

Increase over wt	~8700%
Transitions	86%
Transversions	14%
Insertions/deletions	0%
Error rate	1.4bp/1000bp

Response of capsids to temperature change. In addition to modifying virus particles for altered tropism, we aim to modify the virus conformational dynamics of the virus. Specifically, we are creating libraries to isolate mutant vectors capable of externalizing their N-termini at slightly lower than optimal temperatures. By analyzing mutations that

led to these changes, we hope to determine relevant residues that can be altered to allow the virus capsids to respond to additional stimuli.

We first determined the effect of temperature on wt AAV-like capsid conformation. ΔP.His virus was exposed to temperatures ranging from 37-75°C and stained with A20 (intact capsids), A1 (N-terminus externalization), and B1 (disassembled virus subunits) (Figure 6.6A). At 37°C, a strong A20 signal is observed, indicating almost all virus is intact. A small amount of B1 signal is observed, indicating that a subset is denatured. When heated to 58°C, we begin to see a small amount of A1 signal, indicating the beginning of the N-terminus externalization processes. Stronger A1 signaling is observed from 60°C-65°C. When heated from 70°C-75°C, capsid disassociation is complete, with strong A1 and B1 signaling observed.

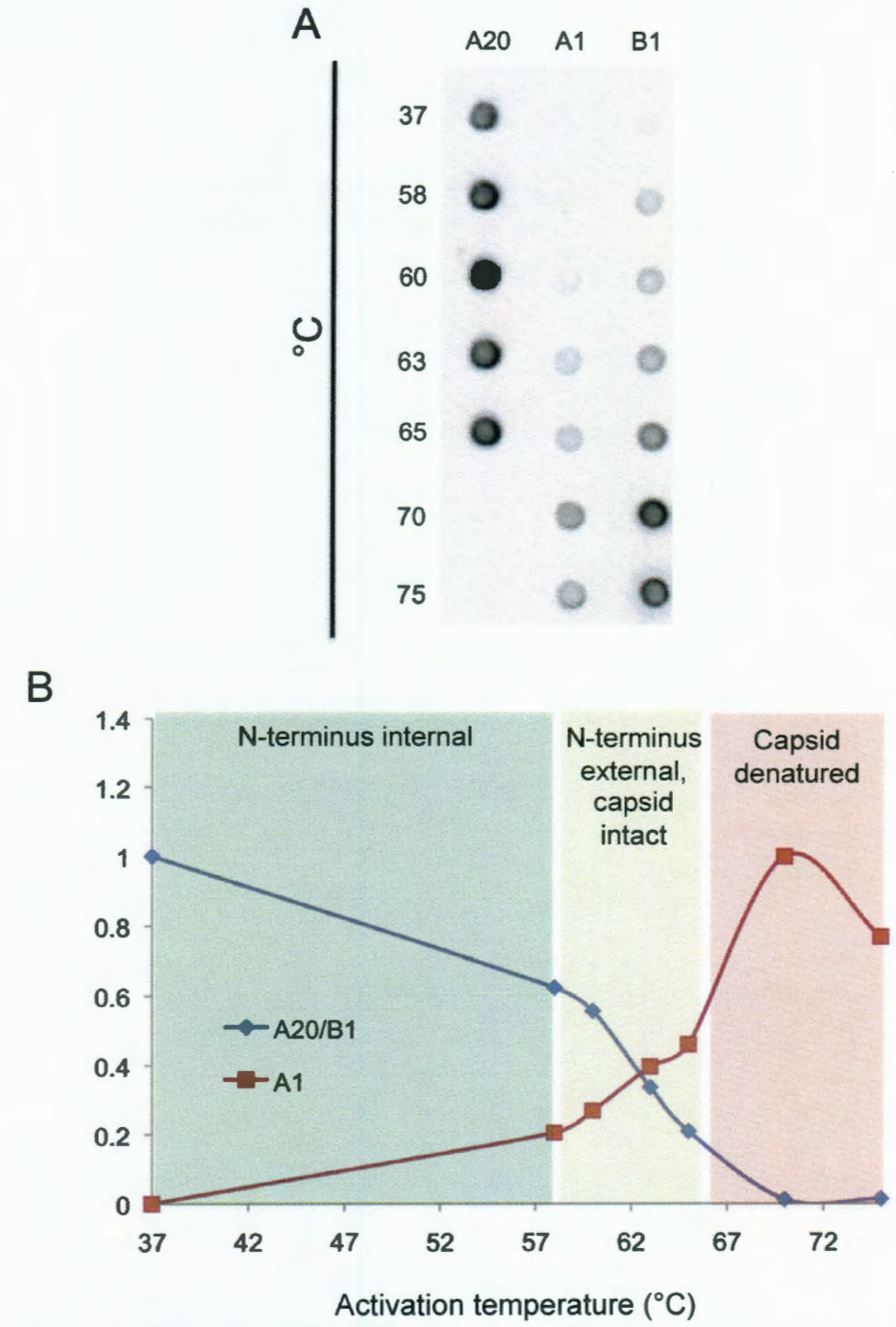

Figure 6.6. Dot blot of ΔP.His. (A) ΔP.His virus was exposed to temperatures ranging from 37-75°C and probed with A20, A1, and B1 antibodies. **(B)** The density values for each antibody signal were determined. The A20/A1 ratio was plotted as a measure of capsid stability. A1 was plotted as a measure of N-terminus externalization.

Density values for each spot were also determined using FluorChem software (Figure 6.6B). Normalized A1 signal was plotted for each temperature, further highlighting the gradual increase in N-terminus externalization that occurs around 60°C. The A20/B1 ratio was also plotted to demonstrate the degradation of capsid integrity that occurs as the supramolecular structure is exposed to heat. N-terminus externalization, without significant denaturation of the capsid, occurs in the 60-65°C region.

Creation and verification of ΔP.His-EP virus libraries. Error-prone PCR libraries were created using Taq polymerase and $MnCl_2$. Mutant ΔP.His *cap* genes were purified on an agarose gel and cloned into a *cap*-free vector containing the remainder of the AAV2 genome. Plasmid library diversity was estimated at 9e5 library members (Table 6.4). After analyzing selected clones, the error rate of the plasmid library was determined to be ~5.8 errors/1000bp. The transition rate was determined to be 48%, while there were 52% transversions. As seen with our AAV2-EP library, there were no insertions or deletions.

Table 6.4 ΔP.His EP Plasmid Library Analysis

Transitions	48%
Transversions	52%
Insertions/deletions	0%
Error rate	5.8bp/1000bp
Diversity	9e5

ΔP.His-EP (EP-PCR library based on ΔPLA-His mutant) virus libraries were created by transfecting 293T cells with 7 ng libray DNA per 15 cm tissue culture dish. Cells were co-transfected with helper plasmid pXX6 and pBluescript. Virus titer was determined to be 5.6e11 vg/mL, a reasonable titer as most are in the range of 1e11-1e12 vg/mL (Table 6.5).

Table 6.5 ΔP.His EP Virus Library Analysis

Transitions	64%
Transversions	36%
Insertions/deletions	0%
Error rate	2.8bp/1000bp
Titer	5.56e11 vg/ml

ΔP.His-EP virus library error rates were determined to be 2.8/1000bp, a 48% decrease from what is observed in the plasmid library. A reduction in error rates for the virus library compared to the plasmid library was also observed with AAV2-EP. In contrast to the plasmid library, the virus library had 64% transitions and 36% transversions, a shift towards more transitions. There were no observed insertions or deletions, as these mutations would be expected to yield incomplete capsids.

Western blot analysis shows that the appropriate virus subunit sizes and ratios are maintained (Figure 6.7). As compared to wt AAV2 and ΔP.His, ΔP.His-EP has the same, shorter VP1 subunit size as ΔP.His, due to the replacement of the PLA2 domain with the shorter hexahistidine tag (Figure 6.7A). The VP2 and VP3 subunits are the same size, as expected. The characteristic stoichiometic 1:1:10 virus subunit ratio is

also preserved. Presence of a band in the α-His blot (Figure 6.7B) for ΔP.His and ΔP.His-EP represent successful His tag insertion.

Figure 6.7. Western blot of wtAAV2, ΔP.His, and ΔP.His-EP. Denaturing western blot of virus samples was probed with B1 (**A**) or α-His (**B**). Decreased band size and the presence of His tag in ΔP.His-EP are as expected.

Temperature selection of ΔP.His-EP library. To select for mutants externalizing N-terminus residues at lower temperatures, we performed a nickel column isolation as in Chapter 5. ΔP.His-EP samples were activated at 58°C and applied to a nickel spin column. Load, wash, and three elution fractions were collected and virus concentration was quantified using QPCR (Figure 6.8). Elution fractions were pooled, capsids lysed, and the contained genomes amplified and subcloned in order to create a new pool of virus mutants.

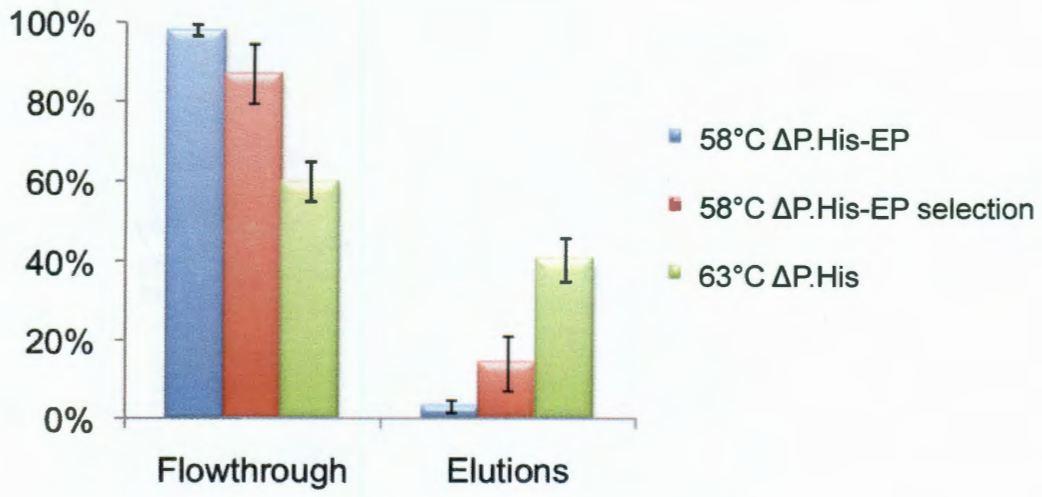

Figure 6.8. Temperature selection of ΔP.His-EP. ΔP.His-EP was exposed to 58°C and run through a nickel affinity spin column. Elution fractions were pooled and *cap* DNA from successful clones was isolated and subcloned to form a new library of selected virus. A modest increase in recovery is observed, but this level does not reach that of 63°C activation.

When activated at 58°C, we observe a 3% recovery with the ΔP.His-EP library. After one round of selection, we re-applied this selected virus pool to the column. When elution fraction were pooled, we observe a 14% recovery of viral genomes within these fractions. This modest increase in recovery suggests the isolation of potentially favorable mutations that allow for the externalization of the AAV2 N-terminus at a slightly suboptimal temperature. This recovery is still dramatically lower than that observed at the 63°C optimal temperature determined in Chapter 5. Additional rounds of selection and mutagenesis could potentially enrich this population, leading to the isolation of one or more mutants capable of increased activity at 58°C.

6.5 Conclusions

Directed evolution holds the potential to create and isolate AAV2 mutants capable of improved functionalities. Many studies have been conducted to modify viral tropism for a range of *in vivo* applications. Isolated mutants have shown improved capability to increase transduction efficiency as well as antibody avoidance. In Chapters 2-5, we have used AAV for surface-immobilized gene delivery and biosensing applications. For these platform technologies to be successful, it is necessary to control the properties of the virus. To address this goal, we have created mutant libraries based on the wild-type AAV2 genome, as well as our ΔP.His mutant virus. Initial studies indicate that we have created diverse, functional libraries of AAV2 variants. Our preliminary selection strategies suggest that we can isolate pools of mutants with increased functionality.

CHAPTER SEVEN

Conclusions and future directions

7.1 Conclusions

In this thesis we have demonstrated that AAV2 can be surface-immobilized and successfully localized while maintaining the integrity of the capsid structure. Successful virus patterning through both microcontact printing and robotic spotting allowed for reverse transduction of HeLa cells. Additionally, we have modified the output of AAV2 by replacing an enzymatic domain necessary for infection with a nickel binding hexahistidine tag. Through these methods we have harnessed the function of AAV2 for novel applications. Optimization through directed evolution could further the efficacy of these platforms.

7.2 Future directions

Microcontact printing. In Chapter 2, we have demonstrated successful patterning of AAV2 for substrate mediated gene delivery by using PDMS stamps and alkanethiol SAMs to localize adhesive protein (HFN) and recombinant AAV. While we are able to demonstrate successful gene expression on these surfaces, we were able to test the versatility of our platform by introducing additional adhesive proteins in Chapter 3. Collagen I, laminin, elastin, and PLL were all capable of facilitating successful HeLa cell localization and AAV2 gene delivery. The dramatic increase in gene expression observed on laminin surfaces was an interesting result from this study. We hypothesized that this increase in gene expression could be due to 1) increased HeLa

cell transcriptional activity on laminin surfaces or 2) favorable binding interactions between AAV2 and laminin. Since BrU incorporation suggests that HeLa cells are not more transcriptionally active when seeded onto laminin coated surfaces, we are exploring additional methods to study AAV-adhesive protein interactions.

Using the platform developed in Chapters 2 and 3, there is a wealth of information still to be generated. First, the protein-AAV interaction information we are developing can be used for *in vitro* virus vector patterning and tissue engineering. As various cell types may require different adhesive proteins for cellular attachment, we may need to further explore the interaction of additional proteins and AAV. Also, there are 11 other naturally occurring AAV serotypes that we have not explored. These serotypes, because they display different amino acids on their capsids, may have completely different adhesive protein binding profiles. As each serotype has different tropism properties, it may be advantageous to use these vectors in our *in vitro* constructs to increase efficiency in different target cells.

One potential method to study the interaction between AAV and ECM proteins is quartz crystal microbalance with dissipation (QCM-D). We have begun promising preliminary studies to investigate virus-protein interactions. We are using gold-coated quartz sensors to perform these studies, a setup that is very similar to the microcontact printing done in Chapters 2 and 3. These coverslips are functionalized by the addition of 2mM $-CH_3$ terminated alkanethiol for 1 h. Samples are rinsed with ethanol and dried with N_2. Using a Q-Sense E4 (Sweden), we are able to observe a frequency shift corresponding to AAV deposition on the SAM as well as AAV deposition directly onto pre-adsorbed HFN (Figure 7.1). Additional experiments can be conducted using other adhesive

proteins, and the amount of AAV adsorbed can be quantified using the Sauerbrey equation, which relates change in frequency to mass.

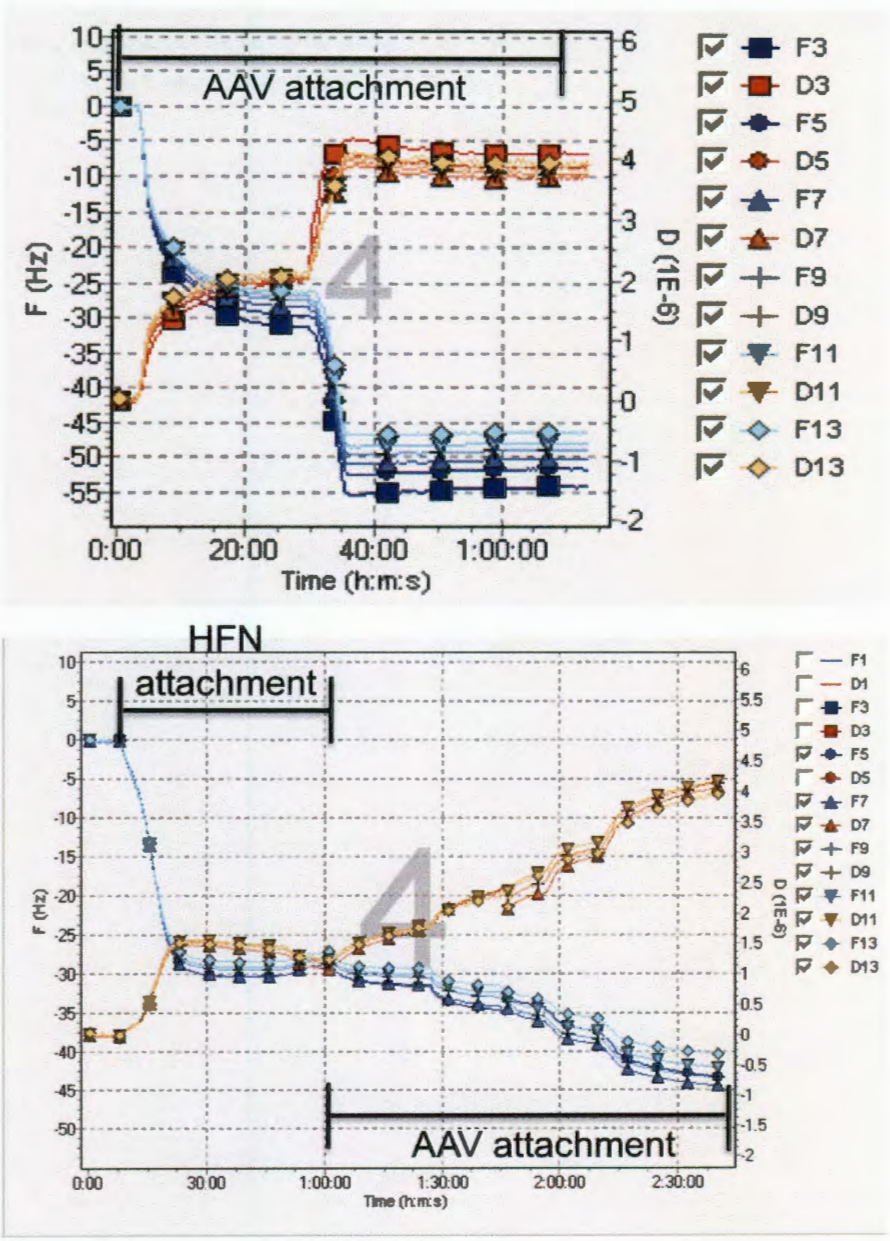

Figure 7.1. QCM analysis of AAV deposition. Using -CH_3 functionalized sensors, we are able to detect the deposition of AAV onto surfaces directly (top) or onto surfaces pre-adsorbed with HFN (bottom).

If more information is determined about specific serotype-adhesive protein interactions, this knowledge could potentially translate to improved *in vivo* gene therapy. While it is known that certain serotypes target different cell types within the human body, little is known about the actual mechanism of targeting. It is widely believed that targeting is primarily due to the interaction of capsid residues with ligands on the outside of cells or possibly intracellular processing of the virus.[10] However, an additional dimension to the story could be that the interaction of AAV with ECM proteins can critically impact what cells are positively transduced. This mechanism appears plausible, as it has previously been shown that co-injection with heparin allows AAV2 to diffuse farther *in vivo*. [65]

Co-injection with an ECM protein that a virus vector has high affinity for could essentially "block" the virus from non-specific adsorption to ECM within the body, allowing the virus to travel further. Since we observe that the interaction of AAV and adhesive proteins does not appear to restrict transduction (the virus is able to desorb from the protein layer), this may not negatively affect the transduction efficiency of the virus once it nears the target cell type. Transduction will still be successful as long as the AAV-cell interaction is stronger than the AAV-ECM interaction. Additionally, once this phenomenon is better understood, it could be possible to modify virus vectors to display desired ECM binding properties. Residues responsible for this interaction could be removed through site-directed mutagenesis in order to block these interactions and allow for increased circulation. If the ECM-virus interaction is desired, it may be possible to increase this interaction, or add this property to mutants isolated through directed evolution.

For *in vitro* patterned gene delivery to be most effective for tissue engineering, we will likely need to control the localization of different AAV vectors delivering different recombinant DNA cassettes. Currently, we are capable of only localizing virus with a single transgene, but there are a number of ways that this technology could be furthered. First, it may be possible to use laser-scanning lithography (LSL) to successively desorb protein resistant alkanethiols and sequentially add adhesive proteins and virus vectors to create more complex 2D patterns.[99] We have begun preliminary testing with AAV2 to determine if this platform is compatible with virus deposition (Figure 7.2). In this sample, a gold coverslip was functionalized with an -OEG terminated protein resistant alkanethiol. Using LSL, nine small areas were desorbed, leaving behind a bare gold layer. HFN and virus were sequentially applied to the sample. When HeLa cells were added, they were localized to eight of the desorbed locations. Both successful cell adhesion and gene expression are observed.

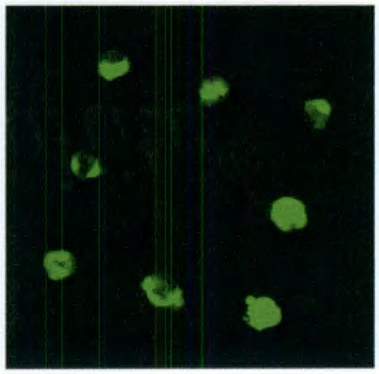

Figure 7.2. LSL patterning of AAV2. Gold-coated coverslips were functionalized with -OEG terminated alkanethiol and desorbed in a nine spot pattern. Samples were incubated with HFN followed by AAV2. Samples were seeded with HeLa cells and imaged for GFP expression at 72 h. (Experiment conducted with Dr. John Slater.)

One bottleneck to this technique is possible deposition of subsequent virus onto previously adsorbed spots. This will disrupt the localization of gene delivery, causing some areas to be transduced by multiple virus vectors. There are a number of possible solutions that can be explored to remedy this problem. First, a variety of blocking agents (BSA, StabilGuard) at different concentrations could be added to the sample between patterning steps, to prevent non-specific adhesion of new protein. Second, wash steps with low levels of salt could be used to disrupt protein-protein interactions. However, caution must be taken not to disassemble the capsid structure of the virus, or remove virus bound to the underlying adhesive protein.

Finally, LSL could be used to pattern different alkanethiols, each with a terminal group specific to a corresponding AAV mutant. Collections of binding pairs could be used to link the SAM to AAV particles in solution (Figure 7.3). Binding domains could be surface exposed on the AAV capsid, allowing specific virus mutants to bind to these alkanethiols. Now, instead of protein being added after each desorption step, a specified alkanethiol could be added. When patterning is complete, a pool of virus vectors could be added, each localizing to its corresponding SAM binding pair.

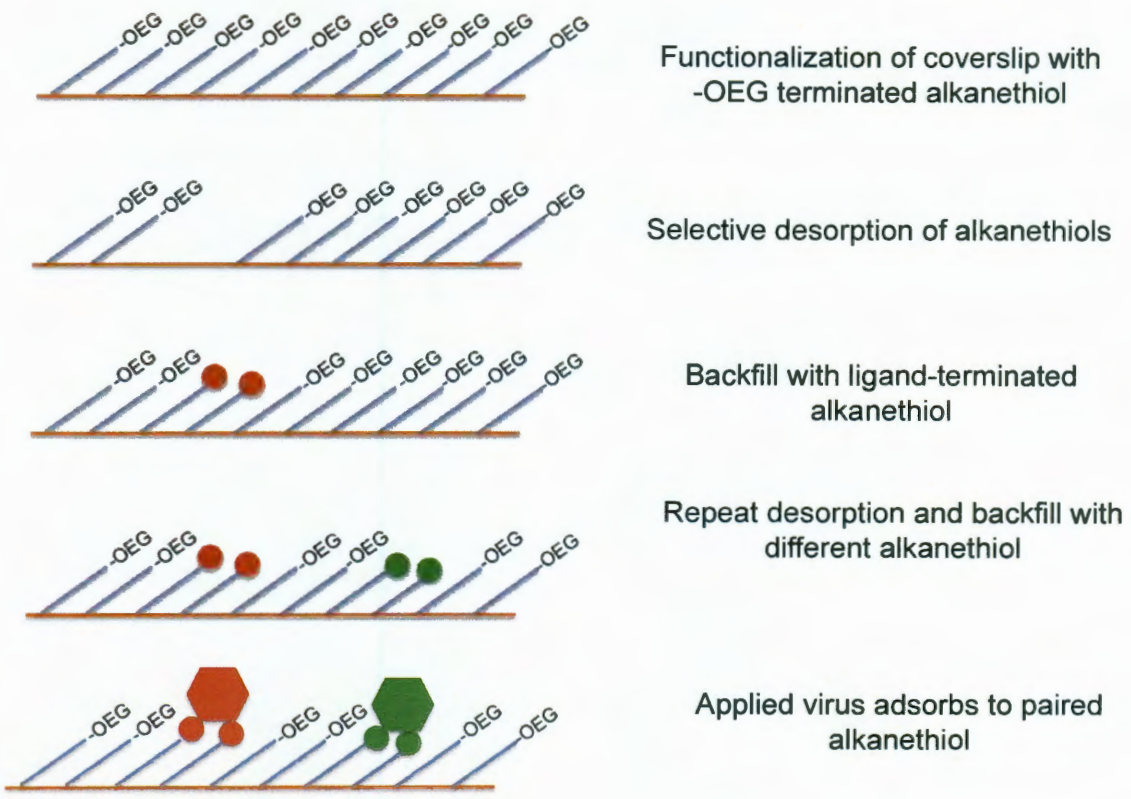

Figure 7.3. LSL using capsid-specific alkanethiols. Using LSL, it may be possible to sequentially desorb an -OEG terminated alkanethiol and backfill with alkanethiol solutions forming capsid-specific SAMs. When patterning is completed, a pool of virus vectors could be added, with vectors self-aligning to the corresponding SAM.

Live cell genetic microarrays using AAV. In Chapter 4, we used AAV and a robotic spotter to create localized islands of transduced cells. We have tested several substrate conditions to isolate a coating that leads to localized expression. Also, we have determined an optimal virus concentration range for efficient gene expression. To further this technology, there are several steps that could be taken. First, cell island formation could potentially be optimized using different pin geometries to create circular cell islands, in contrast to the linear islands we observe with the pin used in these

studies. Also, it should be possible to deposit different combinations of different virus vectors, allowing for high-throughput gene expression studies.

To make our platform more versatile, a number of alterations could be explored. As the goal is to use this platform for high-throughput studies, multiple virus vectors could be patterned by relatively simple robot programming. Virus samples are placed in 384 well plates, and the robotic arm can be moved to the location of different wells. To simply deposit multiple virus vectors in one spot, deposition could be done over multiple rounds. One vector could be patterned, then the arm could return to the supply wells, take up another sample, and deposit that onto the previous spot. Alignment would be preserved as the slide, arm, and well plate would not be moved in between steps.

This system could incorporate different ECM proteins, as these are known to be important in cellular differentiation. As with patterning multiple virus vectors, virus and ECM protein combinations could be patterned by using multiple rounds of spotting. Previous microarray technologies have shown the importance of testing ECM components in a combinatorial fashion to determine their effects on target cells.[100] Combining ECM proteins with gene delivery vectors would allow for an even more complex combinatorial analysis.

One interesting application of our platform would be the study of cellular co-cultures. Within the stem cell niche, supporting cells are also critical to stem cell maintenance and differentiation.[16] Analyzing co-cultures, gene delivery, and ECM effects in a high-throughput manner would allow for a quick, efficient method for analyzing many variables. Additional complexity could be achieved by using virus vectors capable of

targeting only one cell type within the co-culture, thus restricting gene delivery to that cell type. This system could be used to mimic potential changes in supporting cells and their effects on stem cells.

AAV2 as a biosensor. In Chapter 5, we began to explore AAV2 as a biosensor by replacing the wild-type output with a hexahistidine tag. Activated virus particles could be isolated using a nickel affinity column. Preliminary evidence suggests that virus can be patterned using our robotic spotter platform and then activated (Figure 7.4). These results should be verified to ensure proper function of the virus when immobilized to a nitrocellulose coated substrate. While we have discussed these biosensors in the context of immobilization onto a substrate, it is possible for these biosensors to be used intracellularly. As the primary function of AAV is cellular infection, this type of sensing could be uniquely appropriate for this biosensor.

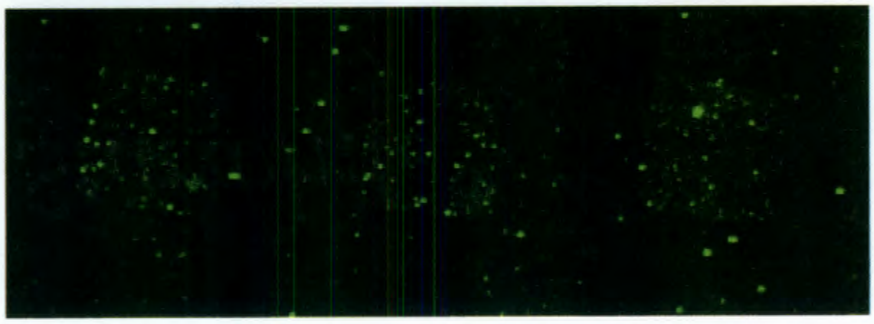

Figure 7.4. Deposition and activation of ΔP.His virus on 3 mg/ml nitrocellulose. Virus was deposited, activated at 63°C, and immunostained using an anti-His antibody and AF532-conjugated secondary antibody. Three virus spots are shown.

While our proof-of-concept studies have set the groundwork for using AAV2 as a biosensor, additional modifications must be explored to evolve these particles into useful sensors. This would involve alterations of both the input and output functionalities of the virus nanoparticles. Current "inputs" of the virus include temperature treatment and intracellular processing. To modify these inputs for a desired stimulus, perhaps a specific biomolecule or target protein, we must make modifications to the dynamic response. Future work to create these changes will likely rest in the further exploration of our directed evolution libraries (Chapter 6), isolating residues crucial in this process.

Appropriate VNP outputs is another avenue that must be addressed to use AAV as a biosensor. Interesting domains could be those that induce viral aggregation or produce a light or color response. Current studies in our lab are exploring the use of leucine zipper domains as a replacement for the PLA2 domain. It is hypothesized that upon activation, these domains would externalize, interact, and allow the virus to aggregate. An alternative to this strategy would be the use of biomolecular fluorescence complementation, where a portion of a fluorescent protein (GFP, for example) would be inserted into the N-terminus. Full GFP protein could not be used in this instance, as the insertion of this protein in the AAV2 N-terminus leads to surface exposed GFP.[101] Upon activation, these fragments would be externalized and capable of interacting with the complementing fragment externalized by another virus particle, producing a fluorescent response.

Directed evolution of AAV. In Chapters 2-5 we explored the use of AAV for substrate mediated gene delivery and biosensing. Optimal performance of the virus in these

applications might depend on altering the capsid properties. We have created virus libraries and verified both sequence diversity and correct protein subunit size.

While we have shown successful virus function using wild-type AAV2, it may be necessary in the future to modify the transduction profiles of the virus to target a cell type with increased efficiency. Depending on the application, AAV2 (or another naturally occurring serotype) may not be sufficient for gene delivery. The libraries developed in this work, or similar libraries modified with higher error rates, could be used to select for clones with increased efficiency. We have also been working to develop additional libraries based on peptide display[29] and DNA shuffling.[32]

Peptide display involves the insertion of a random peptide domain into a specific region of the virus. For AAV2, we have targeted the heparin binding domain as this is a surface exposed, tropism conferring domain. We are developing libraries that display random seven amino acid motifs within this region. This combination of rational (based on insertion location) and combinatorial (large libraries of random insertions) offers a potentially effective method for altering tropism. The development of DNA shuffling libraries is based on recombination of virus *cap* DNA for two or more of the twelve naturally occurring serotypes. As each serotype has different properties, this method allows for the recombination of these domains with the hope of creating new, functional vectors.

Mutations generated through EP-PCR could be used to identify residues responsible for various functionalities of the virus. For example, Maheshri et al used EP-PCR to identify residues responsible for antibody neutralization.[27] For our work, this method could be a

powerful way to identify residues that are responsible for the adhesive protein binding explored in Chapters 2 and 3. One potential selection strategy could be to incubate virus libraries with an adhesive protein, allow virus particles to bind, and then analyze the *cap* DNA of capsids that did not bind. Common mutations could be analyzed to determine any potential trends.

Similar to using EP-PCR to identify residues involved in antibody binding, interesting information could potentially be gained from exploring our ΔP.His-EP libraries. Very little is known about the N-terminus externalization process for AAV2. Specifically, we do not know which domains are important for allowing these residues to externalize when exposed to stimuli. By creating random mutations and selecting for clones that have altered function, we may be able to correlate these protein residues to specific functions. This mapping could be the first step towards modifying AAV2 for an *in vitro* biosensor capable of responding to a novel stimulus.

REFERENCES

1. R. W. Atchison, B. C. Casto and W. M. Hammon, Adenovirus-Associated Defective Virus Particles, *Science*, 1965, **149**, 754-756.

2. R. J. Samulski, K. I. Berns, M. Tan and N. Muzyczka, Cloning of adeno-associated virus into pBR322: rescue of intact virus from the recombinant plasmid in human cells, *Proc Natl Acad Sci U S A*, 1982, **79**, 2077-2081.

3. N. Chirmule, K. Propert, S. Magosin, Y. Qian, R. Qian and J. Wilson, Immune responses to adenovirus and adeno-associated virus in humans, *Gene Ther*, 1999, **6**, 1574-1583.

4. Q. Xie, W. Bu, S. Bhatia, J. Hare, T. Somasundaram, A. Azzi and M. S. Chapman, The atomic structure of adeno-associated virus (AAV-2), a vector for human gene therapy, *Proc Natl Acad Sci U S A*, 2002, **99**, 10405-10410.

5. F. Sonntag, K. Schmidt and J. A. Kleinschmidt, A viral assembly factor promotes AAV2 capsid formation in the nucleolus, *Proc Natl Acad Sci U S A*, 2010, **107**, 10220-10225.

6. M. Schmidt, A. Voutetakis, S. Afione, C. Zheng, D. Mandikian and J. A. Chiorini, Adeno-associated virus type 12 (AAV12): a novel AAV serotype with sialic acid- and heparan sulfate proteoglycan-independent transduction activity, *J Virol*, 2008, **82**, 1399-1406.

7. Z. Wu, A. Asokan and R. J. Samulski, Adeno-associated virus serotypes: vector toolkit for human gene therapy, *Mol Ther*, 2006, **14**, 316-327.

8. C. Summerford and R. J. Samulski, Membrane-associated heparan sulfate proteoglycan is a receptor for adeno-associated virus type 2 virions, *J Virol*, 1998, **72**, 1438-1445.

9. Z. Wu, E. Miller, M. Agbandje-McKenna and R. J. Samulski, Alpha2,3 and alpha2,6 N-linked sialic acids facilitate efficient binding and transduction by adeno-associated virus types 1 and 6, *J Virol*, 2006, **80**, 9093-9103.

10. C. E. Thomas, T. A. Storm, Z. Huang and M. A. Kay, Rapid uncoating of vector genomes is the key to efficient liver transduction with pseudotyped adeno-associated virus vectors, *J Virol*, 2004, **78**, 3110-3122.

11. D. E. Discher, D. J. Mooney and P. W. Zandstra, Growth factors, matrices, and forces combine and control stem cells, *Science*, 2009, **324**, 1673-1677.

12. L. E. Dike, C. S. Chen, M. Mrksich, J. Tien, G. M. Whitesides and D. E. Ingber, Geometric control of switching between growth, apoptosis, and differentiation during angiogenesis using micropatterned substrates, *In vitro cellular & developmental biology*, 1999, **35**, 441-448.

13. R. Singhvi, A. Kumar, G. P. Lopez, G. N. Stephanopoulos, D. I. Wang, G. M. Whitesides and D. E. Ingber, Engineering cell shape and function, *Science*, 1994, **264**, 696-698.

14. C. S. Chen, M. Mrksich, S. Huang, G. M. Whitesides and D. E. Ingber, Geometric control of cell life and death, *Science*, 1997, **276**, 1425-1428.

15. G. H. Underhill and S. N. Bhatia, High-throughput analysis of signals regulating stem cell fate and function, *Curr Opin Chem Biol*, 2007, **11**, 357-366.

16. A. Spradling, D. Drummond-Barbosa and T. Kai, Stem cells find their niche, *Nature*, 2001, **414**, 98-104.

17. T. Yoshikawa, E. Uchimura, M. Kishi, D. P. Funeriu, M. Miyake and J. Miyake, Transfection microarray of human mesenchymal stem cells and on-chip siRNA gene knockdown, *J Control Release*, 2004, **96**, 227-232.

18. S. N. Bailey, S. M. Ali, A. E. Carpenter, C. O. Higgins and D. M. Sabatini, Microarrays of lentiviruses for gene function screens in immortalized and primary cells, *Nat Methods*, 2006, **3**, 117-122.

19. D. M. Pirone, L. Qi, H. Colecraft and C. S. Chen, Spatial patterning of gene expression using surface-immobilized recombinant adenovirus, *Biomed Microdevices*, 2008.

20. J. Ziauddin and D. M. Sabatini, Microarrays of cells expressing defined cDNAs, *Nature*, 2001, **411**, 107-110.

21. L. D. Shea, E. Smiley, J. Bonadio and D. J. Mooney, DNA delivery from polymer matrices for tissue engineering, *Nat Biotechnol*, 1999, **17**, 551-554.

22. T. Houchin-Ray, K. J. Whittlesey and L. D. Shea, Spatially patterned gene delivery for localized neuron survival and neurite extension, *Mol Ther*, 2007, **15**, 705-712.

23. S. Bleker, F. Sonntag and J. A. Kleinschmidt, Mutational analysis of narrow pores at the fivefold symmetry axes of adeno-associated virus type 2 capsids reveals a dual role in genome packaging and activation of phospholipase A2 activity, *J Virol*, 2005, **79**, 2528-2540.

24. S. Kronenberg, B. Bottcher, C. W. von der Lieth, S. Bleker and J. A. Kleinschmidt, A conformational change in the adeno-associated virus type 2 capsid leads to the exposure of hidden VP1 N termini, *J Virol*, 2005, **79**, 5296-5303.

25. J. S. Bartlett, J. Kleinschmidt, R. C. Boucher and R. J. Samulski, Targeted adeno-associated virus vector transduction of nonpermissive cells mediated by a bispecific F(ab'gamma)2 antibody, *Nat Biotechnol*, 1999, **17**, 181-186.

26. W. Shi and J. S. Bartlett, RGD inclusion in VP3 provides adeno-associated virus type 2 (AAV2)-based vectors with a heparan sulfate-independent cell entry mechanism, *Mol Ther*, 2003, **7**, 515-525.

27. N. Maheshri, J. T. Koerber, B. K. Kaspar and D. V. Schaffer, Directed evolution of adeno-associated virus yields enhanced gene delivery vectors, *Nat Biotechnol*, 2006, **24**, 198-204.

28. J. T. Koerber, N. Maheshri, B. K. Kaspar and D. V. Schaffer, Construction of diverse adeno-associated viral libraries for directed evolution of enhanced gene delivery vehicles, *Nat Protoc*, 2006, **1**, 701-706.

29. O. J. Muller, F. Kaul, M. D. Weitzman, R. Pasqualini, W. Arap, J. A. Kleinschmidt and M. Trepel, Random peptide libraries displayed on adeno-associated virus to select for targeted gene therapy vectors, *Nat Biotechnol*, 2003, **21**, 1040-1046.

30. L. Perabo, H. Buning, D. M. Kofler, M. U. Ried, A. Girod, C. M. Wendtner, J. Enssle and M. Hallek, In vitro selection of viral vectors with modified tropism: the adeno-associated virus display, *Mol Ther*, 2003, **8**, 151-157.

31. J. T. Koerber and D. V. Schaffer, Transposon-based mutagenesis generates diverse adeno-associated viral libraries with novel gene delivery properties, *Methods Mol Biol*, 2008, **434**, 161-170.

32. J. T. Koerber, J. H. Jang and D. V. Schaffer, DNA shuffling of adeno-associated virus yields functionally diverse viral progeny, *Mol Ther*, 2008, **16**, 1703-1709.

33. D. Grimm, J. S. Lee, L. Wang, T. Desai, B. Akache, T. A. Storm and M. A. Kay, In vitro and in vivo gene therapy vector evolution via multispecies interbreeding and retargeting of adeno-associated viruses, *J Virol*, 2008, **82**, 5887-5911.

34. W. Li, A. Asokan, Z. Wu, T. Van Dyke, N. Diprimio, S. J. J, L. Govindaswamy, M. Agbandje-McKenna, S. Leichtle, D. Eugene Redmond Jr, T. J. McCown, K. B. Petermann, N. E. Sharpless and R. J. Samulski, Engineering and Selection of Shuffled AAV Genomes: A New Strategy for Producing Targeted Biological Nanoparticles, *Mol Ther*, 2008.

35. K. J. Excoffon, J. T. Koerber, D. D. Dickey, M. Murtha, S. Keshavjee, B. K. Kaspar, J. Zabner and D. V. Schaffer, Directed evolution of adeno-associated virus to an infectious respiratory virus, *Proc Natl Acad Sci U S A*, 2009.

36. J. T. Koerber, R. Klimczak, J. H. Jang, D. Dalkara, J. G. Flannery and D. V. Schaffer, Molecular Evolution of Adeno-associated Virus for Enhanced Glial Gene Delivery, *Mol Ther*, 2009, **17**, 2088-2095.

37. C. A. Gersbach, S. R. Coyer, J. M. Le Doux and A. J. Garcia, Biomaterial-mediated retroviral gene transfer using self-assembled monolayers, *Biomaterials*, 2007, **28**, 5121-5127.

38. C.-W. K. Jau-Ye Shiu, Wha-Tzong Whang and Peilin Chen, Observation of enhanced cell adhesion and transfection efficiency on superhydrophobic surfaces, *Lab on a Chip*, 2010, **10**, 556-558.

39. F. Yamauchi, K. Kato and H. Iwata, Micropatterned, self-assembled monolayers for fabrication of transfected cell microarrays, *Biochimica et biophysica acta*, 2004, **1672**, 138-147.

40. L. A. Chandler, J. Doukas, A. M. Gonzalez, D. K. Hoganson, D. L. Gu, C. Ma, M. Nesbit, T. M. Crombleholme, M. Herlyn, B. A. Sosnowski and G. F. Pierce, FGF2-Targeted adenovirus encoding platelet-derived growth factor-B enhances de novo tissue formation, *Mol Ther*, 2000, **2**, 153-160.

41. I. Fishbein, I. S. Alferiev, O. Nyanguile, R. Gaster, J. M. Vohs, G. S. Wong, H. Felderman, I. W. Chen, H. Choi, R. L. Wilensky and R. J. Levy, Bisphosphonate-mediated gene vector delivery from the metal surfaces of stents, *Proc Natl Acad Sci U S A*, 2006, **103**, 159-164.

42. H. Ito, M. Koefoed, P. Tiyapatanaputi, K. Gromov, J. J. Goater, J. Carmouche, X. Zhang, P. T. Rubery, J. Rabinowitz, R. J. Samulski, T. Nakamura, K. Soballe, R. J. O'Keefe, B. F. Boyce and E. M. Schwarz, Remodeling of cortical bone allografts mediated by adherent rAAV-RANKL and VEGF gene therapy, *Nat Med*, 2005, **11**, 291-297.

43. A. Oehmig, A. Klotzbucher, M. Thomas, F. Weise, U. Hagner, R. Brundiers, D. Waldherr, A. Lingnau, A. Knappik, M. H. Kubbutat, T. O.

Joos and H. Volkmer, A novel reverse transduction adenoviral array for the functional analysis of shRNA libraries, *BMC Genomics*, 2008, **9**, 441.

44. S. D. Raut, P. Lei, R. M. Padmashali and S. T. Andreadis, Fibrin-mediated lentivirus gene transfer: implications for lentivirus microarrays, *J Control Release*, 2010, **144**, 213-220.

45. H. Hanenberg, X. L. Xiao, D. Dilloo, K. Hashino, I. Kato and D. A. Williams, Colocalization of retrovirus and target cells on specific fibronectin fragments increases genetic transduction of mammalian cells, *Nat Med*, 1996, **2**, 876-882.

46. D. V. Schaffer, J. T. Koerber and K. I. Lim, Molecular engineering of viral gene delivery vehicles, *Annu Rev Biomed Eng*, 2008, **10**, 169-194.

47. V. Nair, Retrovirus-induced oncogenesis and safety of retroviral vectors, *Curr Opin Mol Ther*, 2008, **10**, 431-438.

48. A. K. Zaiss and D. A. Muruve, Immune responses to adeno-associated virus vectors, *Curr Gene Ther*, 2005, **5**, 323-331.

49. S. R. Opie, K. H. Warrington, Jr., M. Agbandje-McKenna, S. Zolotukhin and N. Muzyczka, Identification of amino acid residues in the capsid proteins of adeno-associated virus type 2 that contribute to heparan sulfate proteoglycan binding, *J Virol*, 2003, **77**, 6995-7006.

50. R. S. Tomar, H. Matta and P. M. Chaudhary, Use of adeno-associated viral vector for delivery of small interfering RNA, *Oncogene*, 2003, **22**, 5712-5715.

51. D. Grimm, K. Pandey and M. A. Kay, Adeno-associated virus vectors for short hairpin RNA expression, *Methods Enzymol*, 2005, **392**, 381-405.

52. Y. N. Xia and G. M. Whitesides, Soft lithography, *Angew. Chem.-Int. Edit.*, 1998, **37**, 551-575.

53. H. Hamilton, J. Gomos, K. I. Berns and E. Falck-Pedersen, Adeno-associated virus site-specific integration and AAVS1 disruption, *J Virol*, 2004, **78**, 7874-7882.

54. X. Xiao, J. Li and R. J. Samulski, Production of high-titer recombinant adeno-associated virus vectors in the absence of helper adenovirus, *J Virol*, 1998, **72**, 2224-2232.

55. B. G. Keselowsky, D. M. Collard and A. J. Garcia, Surface chemistry modulates fibronectin conformation and directs integrin binding and

specificity to control cell adhesion, *Journal of biomedical materials research*, 2003, **66**, 247-259.

56. L. M. Work, S. A. Nicklin, N. J. Brain, K. L. Dishart, D. J. Von Seggern, M. Hallek, H. Buning and A. H. Baker, Development of efficient viral vectors selective for vascular smooth muscle cells, *Mol Ther*, 2004, **9**, 198-208.

57. L. Perabo, D. Goldnau, K. White, J. Endell, J. Boucas, S. Humme, L. M. Work, H. Janicki, M. Hallek, A. H. Baker and H. Buning, Heparan sulfate proteoglycan binding properties of adeno-associated virus retargeting mutants and consequences for their in vivo tropism, *J Virol*, 2006, **80**, 7265-7269.

58. W. S. Hu and V. K. Pathak, Design of retroviral vectors and helper cells for gene therapy, *Pharmacol Rev*, 2000, **52**, 493-511.

59. E. Verhoeyen and F. L. Cosset, Surface-engineering of lentiviral vectors, *Journal of Gene Medicine*, 2004, **6**, S83-S94.

60. A. P. Ngankam, G. Mao and P. R. Van Tassel, Fibronectin adsorption onto polyelectrolyte multilayer films, *Langmuir*, 2004, **20**, 3362-3370.

61. C. R. Wittmer, J. A. Phelps, W. M. Saltzman and P. R. Van Tassel, Fibronectin terminated multilayer films: protein adsorption and cell attachment studies, *Biomaterials*, 2007, **28**, 851-860.

62. M. A. Lan, C. A. Gersbach, K. E. Michael, B. G. Keselowsky and A. J. Garcia, Myoblast proliferation and differentiation on fibronectin-coated self assembled monolayers presenting different surface chemistries, *Biomaterials*, 2005, **26**, 4523-4531.

63. V. Vogel and G. Baneyx, The tissue engineeting puzzle: a molecular perspective, *Annu Rev Biomed Eng*, 2003, **5**, 441-463.

64. Z. Wu, A. Asokan, J. C. Grieger, L. Govindasamy, M. Agbandje-McKenna and R. J. Samulski, Single amino acid changes can influence titer, heparin binding, and tissue tropism in different adeno-associated virus serotypes, *J Virol*, 2006, **80**, 11393-11397.

65. J. B. Nguyen, R. Sanchez-Pernaute, J. Cunningham and K. S. Bankiewicz, Convection-enhanced delivery of AAV-2 combined with heparin increases TK gene transfer in the rat brain, *Neuroreport*, 2001, **12**, 1961-1964.

66. D. Dalkara, K. D. Kolstad, N. Caporale, M. Visel, R. R. Klimczak, D. V. Schaffer and J. G. Flannery, Inner limiting membrane barriers to AAV-

mediated retinal transduction from the vitreous, *Mol Ther*, 2009, **17**, 2096-2102.

67. D. Carstanjen, P. Dutt and T. Moritz, Heparin inhibits retrovirus binding to fibronectin as well as retrovirus gene transfer on fibronectin fragments, *J Virol*, 2001, **75**, 6218-6222.

68. S. Shin, D. M. Salvay and L. D. Shea, Lentivirus delivery by adsorption to tissue engineering scaffolds, *J Biomed Mater Res A*, 2010, **93**, 1252-1259.

69. H. J. Lee, Y. S. Lee, H. S. Kim, Y. K. Kim, J. H. Kim, S. H. Jeon, H. W. Lee, S. Kim, H. Miyoshi, H. M. Chung and D. K. Kim, Retronectin enhances lentivirus-mediated gene delivery into hematopoietic progenitor cells, *Biologicals*, 2009, **37**, 203-209.

70. M. L. Yarmush and K. R. King, Living-cell microarrays, *Annu Rev Biomed Eng*, 2009, **11**, 235-257.

71. J. Tian, S. Alimperti, P. Lei and S. T. Andreadis, Lentiviral microarrays for real-time monitoring of gene expression dynamics, *Lab Chip*, 2010, **10**, 1967-1975.

72. S. Rajan, H. Djambazian, H. C. Dang, R. Sladek and T. J. Hudson, The living microarray: a high-throughput platform for measuring transcription dynamics in single cells, *BMC Genomics*, 2011, **12**, 115.

73. S. Mousses, N. J. Caplen, R. Cornelison, D. Weaver, M. Basik, S. Hautaniemi, A. G. Elkahloun, R. A. Lotufo, A. Choudary, E. R. Dougherty, E. Suh and O. Kallioniemi, RNAi microarray analysis in cultured mammalian cells, *Genome Res*, 2003, **13**, 2341-2347.

74. P. Lei, R. M. Padmashali and S. T. Andreadis, Cell-controlled and spatially arrayed gene delivery from fibrin hydrogels, *Biomaterials*, 2009, **30**, 3790-3799.

75. K. J. Excoffon, J. T. Koerber, D. D. Dickey, M. Murtha, S. Keshavjee, B. K. Kaspar, J. Zabner and D. V. Schaffer, Directed evolution of adeno-associated virus to an infectious respiratory virus, *Proc Natl Acad Sci U S A*, 2009, **106**, 3865-3870.

76. K. I. McConnell, J. H. Slater, A. Han, J. L. West and J. Suh, Microcontact printing for co-patterning cells and viruses for spatially controlled substrate-mediated gene delivery, *Soft Matter, DOI:10.1039/C0SM01209B*.

77. A. Girod, M. Ried, C. Wobus, H. Lahm, K. Leike, J. Kleinschmidt, G. Deleage and M. Hallek, Genetic capsid modifications allow efficient re-targeting of adeno-associated virus type 2, *Nat Med*, 1999, **5**, 1438.

78. M. Wernig, A. Meissner, R. Foreman, T. Brambrink, M. Ku, K. Hochedlinger, B. E. Bernstein and R. Jaenisch, In vitro reprogramming of fibroblasts into a pluripotent ES-cell-like state, *Nature*, 2007, **448**, 318-324.

79. A. Chatterji, W. F. Ochoa, T. Ueno, T. W. Lin and J. E. Johnson, A virus-based nanoblock with tunable electrostatic properties, *Nano Letters*, 2005, **5**, 597-602.

80. C. Mao, D. J. Solis, B. D. Reiss, S. T. Kottmann, R. Y. Sweeney, A. Hayhurst, G. Georgiou, B. Iverson and A. M. Belcher, Virus-based toolkit for the directed synthesis of magnetic and semiconducting nanowires, *Science*, 2004, **303**, 213-217.

81. A. Merzlyak, S. Indrakanti and S. W. Lee, Genetically Engineered Nanofiber-Like Viruses For Tissue Regenerating Materials, *Nano Letters*, 2009, **9**, 846-852.

82. W. Wu, S. C. Hsiao, Z. M. Carrico and M. B. Francis, Genome-free viral capsids as multivalent carriers for taxol delivery, *Angew Chem Int Ed Engl*, 2009, **48**, 9493-9497.

83. J. C. Falkner, M. E. Turner, J. K. Bosworth, T. J. Trentler, J. E. Johnson, T. Lin and V. L. Colvin, Virus crystals as nanocomposite scaffolds, *J Am Chem Soc*, 2005, **127**, 5274-5275.

84. T. Douglas and M. Young, Host-guest encapsulation of materials by assembled virus protein cages, *Nature*, 1998, **393**, 152-155.

85. J. D. Lewis, G. Destito, A. Zijlstra, M. J. Gonzalez, J. P. Quigley, M. Manchester and H. Stuhlmann, Viral nanoparticles as tools for intravital vascular imaging, *Nat Med*, 2006, **12**, 354-360.

86. D. E. Prasuhn, Jr., R. M. Yeh, A. Obenaus, M. Manchester and M. G. Finn, Viral MRI contrast agents: coordination of Gd by native virions and attachment of Gd complexes by azide-alkyne cycloaddition, *Chem Commun (Camb)*, 2007, 1269-1271.

87. N. F. Steinmetz, G. P. Lomonossoff and D. J. Evans, Decoration of Cowpea mosaic virus with multiple, redox-active, organometallic complexes, *Small*, 2006, **2**, 530-533.

88. B. Dragnea, C. Chen, E. S. Kwak, B. Stein and C. C. Kao, Gold nanoparticles as spectroscopic enhancers for in vitro studies on single viruses, *Journal of the American Chemical Society*, 2003, **125**, 6374-6375.

89. X. L. Huang, L. M. Bronstein, J. Retrum, C. Dufort, I. Tsvetkova, S. Aniagyei, B. Stein, G. Stucky, B. McKenna, N. Remmes, D. Baxter, C. C. Kao and B. Dragnea, Self-assembled virus-like particles with magnetic cores, *Nano Letters*, 2007, **7**, 2407-2416.

90. M. A. Bruckman, J. Liu, G. Koley, Y. Li, B. Benicewicz, Z. W. Niu and Q. A. Wang, Tobacco mosaic virus based thin film sensor for detection of volatile organic compounds, *J Mater Chem*, 2010, **20**, 5715-5719.

91. F. Sonntag, S. Bleker, B. Leuchs, R. Fischer and J. A. Kleinschmidt, Adeno-associated virus type 2 capsids with externalized VP1/VP2 trafficking domains are generated prior to passage through the cytoplasm and are maintained until uncoating occurs in the nucleus, *Journal of Virology*, 2006, **80**, 11040-11054.

92. J. T. Koerber, J. H. Jang, J. H. Yu, R. S. Kane and D. V. Schaffer, Engineering adeno-associated virus for one-step purification via immobilized metal affinity chromatography, *Hum Gene Ther*, 2007, **18**, 367-378.

93. H. G. Zhang, J. F. Xie, I. Dmitriev, E. Kashentseva, D. T. Curiel, H. C. Hsu and J. D. Mountz, Addition of six-His-tagged peptide to the C terminus of adeno-associated virus VP3 does not affect viral tropism or production, *Journal of Virology*, 2002, **76**, 12023-12031.

94. P. Keohavong and W. G. Thilly, Fidelity of DNA polymerases in DNA amplification, *Proc Natl Acad Sci U S A*, 1989, **86**, 9253-9257.

95. R. C. Cadwell and G. F. Joyce, Randomization of genes by PCR mutagenesis, *PCR Methods Appl*, 1992, **2**, 28-33.

96. P. C. Cirino, K. M. Mayer and D. Umeno, Generating mutant libraries using error-prone PCR, *Methods Mol Biol*, 2003, **231**, 3-9.

97. R. A. Beckman, A. S. Mildvan and L. A. Loeb, On the fidelity of DNA replication: manganese mutagenesis in vitro, *Biochemistry*, 1985, **24**, 5810-5817.

98. J. C. Grieger, S. Snowdy and R. J. Samulski, Separate basic region motifs within the adeno-associated virus capsid proteins are essential for infectivity and assembly, *J Virol*, 2006, **80**, 5199-5210.

99. J. S. Miller, M. I. Bethencourt, M. Hahn, T. R. Lee and J. L. West, Laser-scanning lithography (LSL) for the soft lithographic patterning of cell-adhesive self-assembled monolayers, *Biotechnol Bioeng*, 2006, **93**, 1060-1068.

100. C. J. Flaim, S. Chien and S. N. Bhatia, An extracellular matrix microarray for probing cellular differentiation, *Nat Methods*, 2005, **2**, 119-125.

101. K. H. Warrington, Jr., O. S. Gorbatyuk, J. K. Harrison, S. R. Opie, S. Zolotukhin and N. Muzyczka, Adeno-associated virus type 2 VP2 capsid protein is nonessential and can tolerate large peptide insertions at its N terminus, *J Virol*, 2004, **78**, 6595-6609.